

HIGHER-ORDER FIELD EFFECTS ON STORED IONS
IN A QUADRUPOLE ION TRAP

By

DONALD M. EADES

A DISSERTATION PRESENTED TO THE GRADUATE SCHOOL
OF THE UNIVERSITY OF FLORIDA IN PARTIAL FULFILLMENT
OF THE REQUIREMENTS FOR THE DEGREE OF
DOCTOR OF PHILOSOPHY

UNIVERSITY OF FLORIDA

1994

LD
1780
1994
.E11

To my future family.

ACKNOWLEDGEMENTS

I would like to extend my thanks to my advisor Dr. Richard A. Yost for everything (both personal and professional) he taught me throughout my graduate career. I also would like to thank my committee members, Dr. Willard W. Harrison, Dr. David H. Powell, Dr. James M. Boncella, and Dr. Barbara A. Purdy, and acknowledge the U.S. EPA/EMSL for funding this research.

I want to thank all of my fellow group members for their friendship and assistance over the past four years. Special thanks go to Nathan A. Yates and Jodie V. Johnson for taking the time to help me become a better investigator and a better person. Thanks also go to Brad I. Coopersmith, James L. Stephenson, Jon A. Jones, Matthew M. Booth, and Timothy P. Griffin for their friendship and willingness to be team players. Very special thanks go to my good friend, Lawrence A. Villanueva, for making the last four years nothing less than enjoyable. I will be forever indebted to my very close friend, Geoffre A. Seelbach, for his generosity and for the computer on which this dissertation was prepared.

I wish to thank my entire family (all 19 of them) for all of their support and fun times throughout my life. There is nothing like Sunday afternoon at Mom and Dad's house. I especially want to thank my oldest and newly discovered brother, Mark, for all the heart-to-heart talks and for teaching me to say what I mean and

mean what I say. Special heartfelt thanks go to my dear sister Mary Kay for the encouragement and closeness over the years. Although I missed the chance to thank them directly, I am indebted to my Uncle Norman for the inspiration to go to college and become a chemist, to my Grandma Lynch for partial financing of my education, and to my Grandma Eades for many afternoon visits and meals.

I thank my mother and father for their unconditional support, guidance, and acceptance throughout my entire life. I especially appreciate the weekly dose of encouragement, the plane tickets home, and the special times we shared every morning. Early morning chats over a fresh brewed pot of coffee will always be my favorite time spent with my parents.

Lastly, I want to thank my partner in life to whom this dissertation is partially dedicated. I will be forever indebted to Julia L. Malham for her encouragement, support, and assistance throughout my graduate career and with the preparation of this dissertation. I cannot imagine my life without her and words alone cannot fully express my gratitude; perhaps my actions on July 2, 1994, will speak for me.

TABLE OF CONTENTS

ACKNOWLEDGEMENTS	iii
ABSTRACT	viii
CHAPTERS	
1 INTRODUCTION	1
Historical Development of the Quadrupole Ion Trap	2
Fundamental Principles of Quadrupole Ion Trap Operation	8
The Finnigan MAT Ion Trap Mass Spectrometer (ITMS™)	13
Mode of Operation	13
Resonance Excitation	19
Mass-Selective Isolation	21
User-Defined Scanning Strategies	25
Practical Equations	25
Scope of Dissertation	27
2 HIGHER-ORDER FIELDS	28
Introduction	28
"Ideal" Quadrupole Ion Traps	29
Practical Quadrupole Ion Traps	35
Theoretical Treatment	47
Previously Reported Higher-Order Field Effects	57
Early Development of the Quadrupole Ion Trap	57
Ion Injection Experiments	59
Resonance Excitation Experiments	61
Mass Range Extension Experiments	64
EI Spectra	65
Alternative Scanning Modes	66
Conclusions	67

3	CHARACTERIZATION OF HIGHER-ORDER FIELD EFFECTS	69
	Introduction	69
	Ion Displacement from the Center of the Quadrupole Ion Trap	70
	Experimental	73
	$C_2H_5^+$ as a Chemical Probe	76
	Parameters Influencing Observation of Higher-Order Field Effects	84
	Storage Conditions (q_z , a_z Parameters)	84
	Ion Population	92
	Storage Time	96
	Mass-to-Charge Ratio	98
	Field Penetration	101
	Endcap Electrode Spacing	104
	Conclusions	109
4	HIGHER-ORDER FIELD EFFECTS ON CHEMICAL IONIZATION	112
	Introduction	112
	Chemical Ionization with the Quadrupole Ion Trap	112
	Experimental	119
	The Experimental Stability Region for $C_2H_5^+$	122
	Effects on CI Reagent Ions	134
	Collision-Induced Dissociation	134
	Ion Ejection	137
	Effects on CI Quantitation	140
	Effects on CI Spectral Quality	147
	Conclusions	156
5	HIGHER-ORDER FIELD EFFECTS ON ION MOTION	159
	Introduction	159
	Ion Motion Under Resonance Excitation	160
	Previously Reported Simulation Results	163
	Previously Reported Experimental Results	168
	Experimental	170
	Instrumentation and Chemicals	170
	Experimental Considerations	173
	Probing Ion Frequencies Near the $\beta_z=0$ Boundary	181
	Dipolar Excitation	182
	Quadrupolar Excitation	186

Probing Ion Frequencies Along the $a_z=0$ Line	189
Dipolar Excitation	190
Quadrupolar Excitation	195
Probing Ion Frequencies Near the Apex	203
Dipolar Excitation	204
Quadrupolar Excitation	206
Conclusions	210
6 CONCLUSIONS AND FUTURE WORK	213
REFERENCE LIST	225
BIOGRAPHICAL SKETCH	235

Abstract of Dissertation Presented to the Graduate School
of the University of Florida in Partial Fulfillment of the
Requirements for the Degree of Doctor of Philosophy

HIGHER-ORDER FIELD EFFECTS ON STORED IONS
IN A QUADRUPOLE ION TRAP

By

Donald M. Eades

April 1994

Chairperson: Dr. Richard A. Yost
Major Department: Chemistry

This dissertation presents a series of fundamental investigations of higher-order field effects on trapped ions. Due to electrode truncation, holes in the endcap electrodes, and deviations from the theoretically predicted electrode geometry and spacing, a nonideal quadrupolar trapping field results. Consequently, hexapolar, octopolar, and other higher-order fields are superimposed on the quadrupolar trapping field. At specific storage conditions corresponding to higher field resonances, stored ions can absorb power and undergo ejection or dissociation.

Higher-order field effects are characterized with regard to the following instrumental parameters: storage conditions (RF and DC potentials, as reflected in the Mathieu stability parameters, q_z , a_z), number of trapped ions, storage time, mass-to-charge ratio (m/z), field penetration, and endcap electrode spacing. Increases in

ion losses due to higher-order fields were observed with increasingly negative a_z values (increasingly positive applied DC voltage), increasingly higher number of trapped ions, and increasingly longer storage times. An asymmetrical displacement of the endcap electrodes produced substantial ion losses due to the increased contribution of the hexapolar field.

A detailed investigation of higher-order field effects on the mass-selected chemical ionization (CI) mode of operation is presented. Due to higher-order field resonances, low m/z CI reagent ions underwent both ejection and dissociation. Acquisition of CI spectra at storage conditions near these resonances resulted in reduced sensitivity and altered CI spectra. Examples of these effects are presented for several compounds.

A qualitative investigation of higher-order field effects on ion motion is presented. Dipolar and quadrupolar resonance excitation was employed to probe frequency components of ion motion for ions stored throughout the Mathieu stability diagram. Higher-order field induced frequency components are identified and discussed.

CHAPTER 1 INTRODUCTION

The quadrupole ion trap is currently undergoing rapid development both as a mass spectrometer and as a chemical problem solving tool. In the last decade, the quadrupole ion trap has evolved from a simple benchtop detector for a gas chromatograph / mass spectrometer (GC/MS) to potentially one of the most versatile and powerful mass spectrometers available. Researchers now are utilizing the quadrupole ion trap in much more sophisticated experiments and in more complex instrumentation than when first introduced. Due to the rapid advances in quadrupole ion trap technology and application, thoroughly understanding the theoretical basis and fundamental aspects of this device becomes increasingly critical. Indeed, many of the major advances in quadrupole ion trap technology have come directly from a better understanding of the fundamental operation of the storage device. A full comprehension of both the theory and fundamental aspects becomes increasingly crucial in order to implement the full potential of the quadrupole ion trap. This dissertation presents fundamental investigations of trapping field distortions due to contributions of higher-order fields (i.e. hexapolar, octopolar). The introduction of higher-order fields to the quadrupolar trapping field can be attributed to the nonideal characteristics of the quadrupole ion trap electrodes. Deviations from the "ideal" electrodes can be due to electrode truncation, geometry,

and assembly. The relationship between higher-order field effects and instrumental parameters is of particular importance, especially the degree to which higher-order field effects are manifested during the more complex experiments now being conducted with this instrument. Presented in this dissertation is the characterization of higher-order field effects in relation to instrumental parameters. The implications of these effects on different types of experiments will be discussed; more specifically, a detailed discussion of the implications of higher-order fields with regards to chemical ionization will be presented.

This introductory chapter will begin with a brief historical review of quadrupole ion trap development along with the principles of basic operation. A detailed description of the Finnigan MAT instrument used for these studies will be presented together with details regarding the operational modes. A description of the recent developments in quadrupole ion trap technology achieved with this type of instrument also will be included.

Historical Development of the Quadrupole Ion Trap

The three-dimensional rotationally symmetric quadrupole ion trap was first described simultaneously by Paul and Steinwedel (1953) and by Post and Henrich (1953). In 1956, Paul and Steinwedel patented both the quadrupole ion trap and the quadrupole mass filter (the two-dimensional analog of the quadrupole ion trap), the latter of which is presently the most common analyzer employed for mass spectrometry.

Early research with the quadrupole ion trap utilized its capabilities to store ions for relatively long periods of time; its use as a mass analyzer was not realized until much later. Paul *et al.* (1958) first used a resonance detection method to detect stored ions. This procedure was accomplished by applying a small radio frequency (RF) voltage between the endcaps and measuring the power absorption by the stored ions. Also in 1959, Fischer first showed the mass-selective detection of ions by a power-measuring circuit; a unit-mass-resolved spectrum of krypton isotopes demonstrated the applicability of this method. Also noted was the first description of adverse effects due to ion-ion interactions caused by the high ion populations (i.e. space charge). In 1967, Rettinghaus described mass-selective detection which was accomplished by ramping the RF voltage until the frequency of motion of the stored ions matched the resonance detection circuit. Although the 1 Da/s scan speed employed (Rettinghaus, 1967) was very slow compared to today's mass spectrometry time scale, the first mass spectrum of residual gas components was acquired. The influence of space charge effects and the first description of ion-molecule reactions within the quadrupole ion trap also were noted in that report. During the mid 1960s, gas-phase spectroscopic studies of atomic and molecular ions stored in the quadrupole ion trap were pursued (Dehmelt, 1967, 1969). This work continues to be an active field of research in ion trap mass spectrometry, especially in the physics community.

In the late 1960s, Dawson and Whetten (1968ab, 1969ab, 1971) evaluated the ability of the quadrupole ion trap to discriminate between masses, thus investigating

its use as a true mass spectrometer. A significant advancement brought forth during these studies was the ability to eject ions from the quadrupole ion trap through holes in the electrodes for detection by an external device such as an electron multiplier. This capability alleviated many of the problems associated with the earlier detection circuits. Investigations into the quadrupole ion trap for use as a mass spectrometer led to the development of mass-selective storage (Dawson and Whetten, 1971) in which ions of only a single m/z were allowed to attain stable storage conditions. This mode of operation is analogous to the operational mode of the linear quadrupole mass filter employed today. Mass-selective storage with the quadrupole ion trap was accomplished by applying appropriate combinations of RF and direct current (DC) voltages such that the storage conditions were represented by the upper or lower apex of the stability diagram (see section on fundamental principles). The operation of the quadrupole ion trap consisted of an ionization pulse, followed by a storage period, and then detection by ejecting the ions towards an electron multiplier by means of a DC pulse on the opposite endcap. A mass spectrum was acquired by repeating this process throughout the m/z range of interest by ramping the applied RF and DC voltages at a constant RF-to-DC ratio. This work was the foundation for the continued research towards the practical employment of the quadrupole ion trap as a mass spectrometer.

During the 1970s, the quadrupole ion trap was utilized as an ion source for a quadrupole mass filter instrument (Todd *et al.*, 1972, 1978; Lawson *et al.*, 1976) as well as a sector instrument (Mather *et al.*, 1978). The goal of this research was to

investigate both the fragmentation behavior of metastable ions and ion/molecule reactions. Employing the quadrupole ion trap as an ion source for the linear quadrupole was later found to be very useful in characterizing the quadrupole ion trap (Todd *et al.*, 1978). The so-called QUISTOR (QUadrupole Ion STORe) was operated with RF and DC voltages on the ring; the endcaps were grounded. Ions were created internally by pulsing electrons into the quadrupole ion trap through a hole in the ring electrode; ion detection was accomplished by pulsing a DC voltage to one (or both) endcap in order to extract the ions out the opposite endcap towards a detector. This mode was similar to the detection scheme used by Dawson *et al.* (1971). Investigations into ion/molecule reactions and charge exchange reactions led to a better understanding of the processes occurring within the trapping volume (Todd *et al.*, 1978; Bonner *et al.*, 1974, 1976; Lawson *et al.*, 1976). Towards the late 1970s, practical applications of and investigations with the quadrupole ion trap led to the two very significant advances; the use of resonant excitation (Fulford *et al.*, 1980; Armitage *et al.*, 1979) and mass-selective isolation (Fulford and March, 1978). Resonant excitation was accomplished by applying a supplemental AC signal on each endcap at a frequency corresponding to a component of ion motion. The ion would then absorb power, increase its trajectory amplitude, and either undergo collision-induced dissociation (CID) or be ejected from the ion trap. Mass-selective isolation was used to eject all unwanted m/z ions while selectively storing only the m/z of interest. This allowed for kinetic studies under more controlled conditions. The advanced experiments that followed from these two important advances

demonstrated multiple stages of mass spectrometry (Fulford and March, 1978) and simultaneous positive / negative chemical ionization (CI) studies (Mather and Todd, 1980).

Although the quadrupole ion trap was quickly developing in all of the aforementioned areas, no practical ion trap mass spectrometer was available, instead only research grade and in-lab manufactured ion traps were being employed. The first commercially available quadrupole ion trap was delivered by Finnigan MAT in 1983 (Stafford *et al.*, 1983ab) as an inexpensive yet sensitive mass analyzer for a dedicated GC/MS system (i.e. the Ion Trap Detector, ITD™). The operational mode of the ITD™ was drastically different from the modes previously described; this instrument employed mass-selective instability (Stafford *et al.*, 1983ab). In general terms, this process consists of the storage of all m/z ions followed by a linear ramp of the applied RF voltage. Upon increasing the RF amplitude, ions of increasingly higher m/z are sequentially ejected from the quadrupole ion trap (see the section on fundamental principles of operation). Since mass-selective ion ejection is linear with respect to RF voltage and the RF voltage ramp is linear in time, a mass spectrum can be acquired by detecting increasingly higher m/z ions which reach the detector sequentially in time.

The Finnigan MAT ITD™ system was a dramatic improvement over the mass-selective storage/DC pulse extraction method used with the QUISTOR. The ITD™ offered unprecedented resolution and sensitivity. The ease of operation and improved scan speed allowed for the acquisition of EI spectra with unit mass

resolution up to 650 Da (Stafford *et al.*, 1983ab). With a 10^3 dynamic range, the ITD™ gained popularity as a sensitive, inexpensive benchtop GC-MS system.

Further improvements in performance of the ITD™ were observed with the presence of a low molecular weight gas (i.e. hydrogen or helium) at a pressure of approximately one millitorr (Stafford *et al.*, 1984). The presence of the gas causes frequent collisions between the ions and the neutral gas species, which in effect, cause viscous damping of the ion's amplitude of motion and thus focus the ion cloud towards the center of the trap. The collisional damping improved the resolution, dynamic range, and sensitivity of the ITD™.

In 1985, Finnigan MAT offered a limited number of full-size research grade Ion Trap Mass Spectrometers (ITMS™) which possessed advanced capabilities (Kelley *et al.*, 1985, 1986ab). This instrument offered a number of options unavailable on the benchtop ITD™. The ITMS™ offered user-designed scanning strategies, supplemental waveforms for mass-selective excitation or ejection, acquisition of electron ionization (EI) or chemical ionization (CI) mass spectra, and MSⁿ capabilities. In the last ten years, research with this instrument has pushed the capabilities of the quadrupole ion trap to the forefront of mass spectrometry. Since most of the research described in this dissertation was performed on an ITMS™ system, more details of its operational modes and recent advancements will be discussed below. Several reviews of recent advances in quadrupole ion trap technology can be found in the literature (March, 1992; Todd, 1991; Nourse and Cooks, 1990; Cooks and Kaiser, 1990; Cooks *et al.*, 1991). A comprehensive book

on the theory and fundamental principles of quadrupole ion traps is offered by March and Hughes (1989). A two-volume set describing practical applications of quadrupole ion traps is currently in development (March and Todd, 1994).

Fundamental Principles of Quadrupole Ion Trap Operation

The quadrupole ion trap consists of two endcap electrodes on either side of a ring electrode, all of which possess hyperbolic surfaces. The electrode surfaces and positions within the trapping volume are expressed in terms of the cylindrical coordinates (r, z, ϕ) and not the common Cartesian coordinates (x, y, z) . Due to the rotational symmetry about the z -axis, ϕ can be neglected. The z coordinate is the endcap-to-endcap position (axial) and r , defined as $(x^2 + y^2)^{1/2}$, is the position in the ring direction (radial). Construction of the hyperbolic electrodes is based upon the general mathematical equations for hyperbolae; traditionally, the following equations, written in terms of the cylindrical coordinates r and z , are used for construction of the ring and endcap electrodes, respectively (March and Hughes, 1989):

$$\frac{1}{r_0^2}(r^2 - 2z^2) = 1 \quad (1-1)$$

$$\frac{1}{2z_0^2}(r^2 - 2z^2) = -1 \quad (1-2)$$

where r_0 is the radius of the ring electrode and z_0 is the center-to-endcap distance. The relationship between the ring radius and the endcap distance for a pure

quadrupolar field is typically defined by the equation $r_o^2 = 2z_o^2$ (Knight, 1983). It is important to note, however, that this is not the only geometry that can be used. Deviations from this equation can still lead to a quadrupolar field; the electrodes simply need to be constructed with surfaces which obey the proper equations (Knight, 1983). Further details on this topic are included in chapter 2. A three-dimensional quadrupolar field is created within the electrode volume by applying combined RF, $V\cos\Omega t$, and DC, U , potentials between the ring and endcap electrodes (March and Hughes, 1989). Note that V is the zero-to-peak amplitude of the applied RF; $\Omega/2\pi$ is the frequency (Hz). The resulting potential, Φ , is of the form $U - V\cos\Omega t$ and can be generated by three different modes (March and Hughes, 1989): in mode I the potential $+\Phi$ is applied to the ring electrode and $-\Phi$ is applied to the endcap electrodes; in mode II, $+\Phi$ is applied to the ring electrode while endcap electrodes are grounded; in mode III the DC component (U) is applied to both endcaps and the RF component, $V\cos\Omega t$, is applied to the ring. The ITMS™, and all commercially available quadrupole ion traps, are operated in mode II. The potential at the center of an ion trap (Φ_o) becomes (March and Hughes, 1989):

$$\Phi_o = \frac{U - V\cos\Omega t}{2} \quad (1-3)$$

where U is the DC voltage, V is the RF peak voltage, Ω is the RF drive frequency, and t is time. The potential distribution within an ion trap employing an "ideal" quadrupolar trapping field, Φ_o , can be expressed by the following equation (March and Hughes, 1989):

$$\Phi_2 = \Phi_0 + \frac{\Phi_0}{r_0^2}(r^2 - 2z^2) \quad (1-4)$$

The field potential equation above must satisfy Laplace's equation, that is, the field strength at the exact center of the ion trap must be equal to zero. These conditions allow the equations of ion motion to be derived as shown below (March and Hughes, 1989):

$$\frac{d^2r}{dt^2} + \frac{2e}{2mr_0^2}(U - V\cos\Omega t)r = 0 \quad (1-5)$$

$$\frac{d^2z}{dt^2} + \frac{4e}{2mr_0^2}(U - V\cos\Omega t)z = 0 \quad (1-6)$$

These equations are of the form of linear second-order differential equations which conform to that of the Mathieu equation. The solution to the Mathieu equation is well known, and from that, the stability parameters, a_u and q_u , can be obtained. Here, u represents either r or z . For Mode II, a_u and q_u are (March and Hughes, 1989)

$$a_z = -2a_r = \frac{-8eU}{m(r_0^2 + 2z_0^2)\Omega^2} \quad (1-7)$$

$$q_z = -2q_r = \frac{4eV}{m(r_0^2 + 2z_0^2)\Omega^2} \quad (1-8)$$

The Mathieu stability parameters (q_u, a_u) are proportional to the applied RF and DC voltages, respectively; therefore the Mathieu stability diagram also can be expressed in terms of the applied RF and DC voltages. Both of the Mathieu stability parameters are inversely proportional to the m/z of the ion of interest; therefore, all ions can be expressed in terms of q_u, a_u parameters. The range of q_u and a_u values that give rise to stable ion trajectories in both the z and r directions can be expressed in terms of Mathieu stability diagrams. Two stability regions exist, that is, two areas where the z stability and r stability overlap. These regions allow the ions to be stable in all directions and thus storage for long periods of time is possible. All commercially available quadrupole ion traps utilize the first stability region, and, therefore, this will be the only region discussed. A plot of the Mathieu stability region q_z, a_z space is shown in Figure 1-1. Ions of higher m/z values appear at lower q_z due to the inverse relationship described in Equation 1-8; lower m/z ions, therefore, are stored closer to the stability edge labelled $\beta_z=1$ (where β is described below). The stable solutions to the Mathieu equation are of the form (March and Hughes, 1989):

$$u(\xi) = A \sum C_{2n} \cos(2n + \beta)\xi + B \sum C_{2n} \sin(2n + \beta)\xi \quad (1-9)$$

where ξ is the phase interval of the RF field, C_{2n} represents the relative contribution of each frequency to the total ion motion, and β_u is related to the ion frequency ($\omega_{n,u}$) by the following equation (March and Hughes, 1989):

$$\omega_{n,u} = (2n + \beta_u) \frac{\Omega}{2} \quad (1-10)$$

where $0 \leq \beta_u \leq 1$ and $n = 0, 1, 2, \dots$. The secular (main) frequency ($n=0$) is therefore calculated by $\beta_u \Omega/2$. The stability edges are defined by the limits of the allowable ion frequency. A β_u value equal to zero is the lowest allowable frequency (0 kHz) in that direction (r or z); a value equal to one is the highest allowable secular frequency (one-half of the RF driving frequency, $\Omega/2$). The accuracy of the calculated secular frequency is dependent on the accuracy of the calculated β_u value. There are several ways to calculate β_u ; increasing the complexity of the equation increases the accuracy. The simplest approximation (Wuerker *et al.*, 1959; Dehmelt, 1967) is given by the following equation:

$$\beta_u = \left[a_u + \frac{q_u^2}{2} \right]^{\frac{1}{2}} \quad (1-11)$$

which is valid for $q_u < 0.4$. A more accurate approximation (Carrico, 1972) is

$$\beta = \left[a_u - \frac{(a_u - 1)q_u^2}{2(a_u - 1)^2 - q_u^2} - \frac{(5a_u + 7)q_u^4}{32(a_u - 1)^3(a_u - 4)} - \frac{(9a_u^2 + 58a_u + 29)q_u^6}{64(a_u - 1)^5(a_u - 4)(a_u - 9)} \right]^{1/2} \quad (1-12)$$

which is valid for $q_u < 0.8$; however, the most accurate method of calculating β_u is by the continued fraction given below (McLachlan, 1947):

$$\begin{aligned}
 \beta_u^2 = a_u + & \frac{q_u^2}{(2+\beta_u)^2 - a_u - \frac{q_u^2}{(4+\beta_u)^2 - a_u - \frac{q_u^2}{(6+\beta_u)^2 - a_u - \dots \text{etc}}}} \\
 + a_u + & \frac{q_u^2}{(\beta_u - 2)^2 - a_u - \frac{q_u^2}{(\beta_u - 4)^2 - a_u - \frac{q_u^2}{(\beta_u - 6)^2 - a_u - \dots \text{etc}}}} \quad (1-13)
 \end{aligned}$$

The calculation of β_u by the continued fraction given above is accurate to 1 part in 10^6 and is the preferred method. All values of β_u presented in this dissertation were calculated based on equation 1-13. As displayed in Figure 1-2, the Mathieu stability diagram can be gridded with corresponding iso- β_u lines. Along a given iso- β_u resonance line, an ion will possess a constant frequency in that particular direction (i.e. r or z depending on whether it is a β_z or β_r line). This allows for the prediction of the ion frequency in both directions regardless of its location within the stability diagram.

The Finnigan MAT Ion Trap Mass Spectrometer (ITMS™)

Mode of Operation

The Finnigan MAT Ion Trap Mass Spectrometer (ITMS™) (Kelley *et al.*, 1985, 1986ab) was used for all studies in this dissertation and was operated in Mode II (March and Hughes, 1989) using mass-selective instability (Stafford *et al.*, 1983ab).

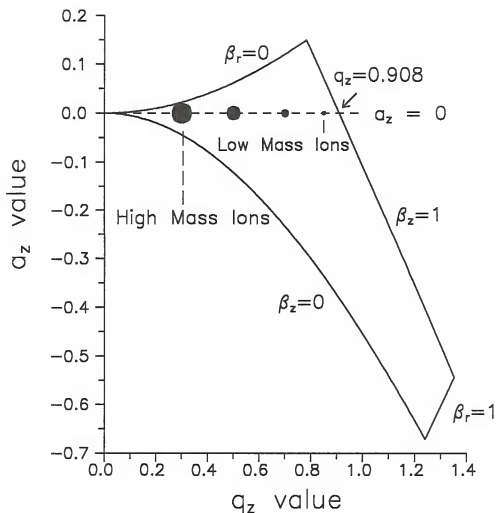


Figure 1-1: A Mathieu stability diagram plotted in q_z , a_z space. The q_z parameter is directly proportional to the applied RF voltage; the a_z parameter is directly proportional to the applied DC voltage. In the RF only mode ($a_z=0$) all ions $q_z < 0.908$ will be stored. The $\beta_z=0,1$ and $\beta_r=0,1$ lines define the stability boundary.

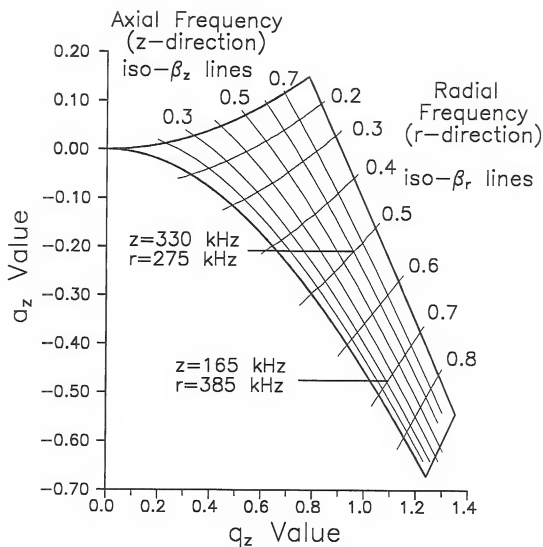


Figure 1-2: The Mathieu stability diagram, in q_z , a_z space, plotted with corresponding iso- β_u lines which relate to ion frequency.

Fundamental research with this instrument is responsible for much of the development in quadrupole ion trap technology during the last decade. Several of the new advancements developed on the ITMS™ have been incorporated into a new series of benchtop instruments; the Finnigan MAT ITS-40™. Another family of benchtop instruments, currently under development, certainly will offer the user even more capabilities than the ITS-40™.

The quadrupole ion trap electrodes used in the ITMS™ are constructed from stainless steel. The ring electrode radius (r_o) of 1 cm; the endcap electrode surfaces have been constructed based on the traditional relationship where $r_o^2 = 2z_o^2$. The center-to-endcap distance (z_o), predicted by the above equation, is 0.7071 cm; however, a recent report by Finnigan MAT (Louris *et al.*, 1992) revealed that the center-to-endcap distance of all ITMS™ ion traps was actually 0.783 cm. Further details regarding electrode spacing can be found in chapter 2.

A schematic of the Finnigan MAT ITMS™ instrument is shown in Figure 1-3. The RF is applied to the ring electrode; the endcap electrodes are held at ground unless the supplemental RF signal is applied. Electrons are gated with a gate electrode (± 180 V) into the quadrupole ion trap through a hole (1/16") drilled in the apex of the hyperbolic surface of the entrance endcap. The internally created ions are stored due to presence of the quadrupolar trapping field. Detection is accomplished by ejecting the ions out the exit endcap towards an electron multiplier. The exit endcap has 6 holes (1/16" each) centered about an equally sized hole.

ION TRAP MASS SPECTROMETER (ITMS™)

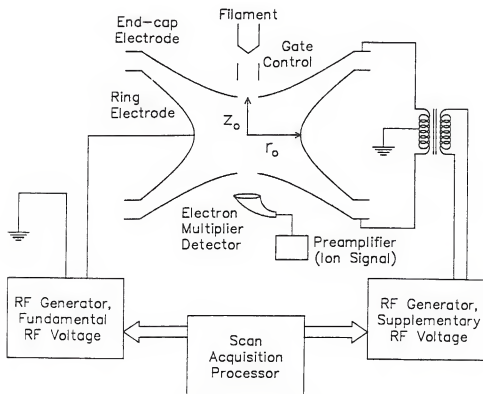


Figure 1-3: Schematic of the Finnigan MAT ion trap mass spectrometer (ITMS™). The ring electrode radius, r_o , is 1 cm; endcap distance, z_o , is 0.783 cm. The RF trapping potential, 1.1 MHz, and the DC potential are applied to the ring; the endcaps are grounded unless a supplemental AC signal is employed for resonance excitation (March and Hughes, 1989).

Since ion detection occurs through the exit endcap (z-direction), the Mathieu stability parameters in the z-direction are commonly the parameters of interest. The RF trapping frequency is 1.1 MHz thus the maximum allowable ion secular frequency is 550 kHz (i.e. $\beta_z=1$).

Mass-selective instability (Stafford *et al.*, 1983ab) is accomplished by linearly ramping the amplitude of the applied RF potential from approximately 100 $V_{0,p}$ to 7,500 $V_{0,p}$. The scan rate is 5550 Da/s. Each mass/charge (m/z) unit is represented by approximately 11.5 $V_{0,p}$ per Da or, in terms of digital-to-analog converter units (DACs), approximately 6.31 DACs/amu. The finest control of the RF voltage is therefore limited to one DAC unit or 1.8 $V_{0,p}$. During the linear RF voltage ramp, an ion's q_z value increases until the stability limit is reached near the $\beta_z=1$ boundary. At this point, $q_z=0.908$, the ion is unstable in the z-direction (axially). Ions of sequentially higher m/z are detected upon ejection from the quadrupole ion trap. Due to the relationship between RF amplitude and m/z stability, the RF level can be expressed in terms voltage, m/z (low-mass-cutoff), or the Mathieu stability parameter q_z . The ITMS™ software expresses the RF voltage in terms of low-mass-cutoff; an instrumental parameter information page also offers the DAC value. The user, in turn, must then calculate both the applied RF voltage defined by the requested low-mass-cutoff (LMCO) and the Mathieu stability parameter q_z . The accuracy of these calculations depends on the stability of the RF voltage and the slope of the RF linear ramp which is reported in the software (approximately 6.3 DAC/amu).

Recently, increased resolution has been demonstrated by altering the scan rate of the applied RF voltage (Schwartz *et al.*, 1991). In theory, the resolution can be affected by controlling the interaction of the ion and the auxiliary excitation field (i.e. resonance ejection which is discussed below). Decreasing the RF amplitude ramping rate so that the ion is influenced by the excitation signal for a longer period of time results in higher resolution. The current ramping rate of the RF used in the ITMS™ is 5550 Da/s; this rate generates slightly better than unit mass resolution. A decrease in the ramping rate to 27.8 Da/s reportedly generated a resolution equal to 33,000 (Schwartz *et al.*, 1991). The highest resolution has been reported to be over 1 million (Williams *et al.*, 1991a).

Resonance Excitation

One of the most powerful capabilities of the ITMS™ is resonance excitation (Kelley *et al.*, 1985, 1986ab; Louris *et al.*, 1987). An ion can be resonantly excited by applying a low voltage supplemental RF signal on the endcap electrodes. When the RF is applied to both endcaps so that the signals on the endcap are 180° out of phase, an approximate dipolar field results; when the RF is applied in phase to each endcap, a quadrupolar field results. Applying the supplemental signal to one endcap results in monopolar excitation. Most of the applications utilizing resonance excitation employ the commercially available dipolar mode. An ion will be resonantly excited if the applied signal matches an axial frequency component of its motion. The ion absorbs power from the applied signal resulting in an increase in

the amplitude of its axial trajectory. This increase in ion trajectory may result in either instability and thus ejection or energetic collisions with background gases thus causing collision-induced dissociation (CID).

Resonance excitation is utilized in several modes of ion trap operation including CID, ion ejection (Kelley *et al.*, 1985), axial modulation (Weber-Grabau *et al.*, 1988; Tucker *et al.*, 1988), high resolution (Schwartz *et al.*, 1991), mass-range extension (Kaiser *et al.*, 1991), and ion isolation (Schwartz and Jardine, 1992). As discussed above, resonance excitation can be employed to induce fragmentation for MSⁿ studies. By varying the duration (typically 0-20 ms) and amplitude (typically 50-500 mV) or the excitation signal, energy deposition can be controlled. Resonance excitation CID has been the focus of several reports (Louris *et al.*, 1987; Johnson *et al.*, 1990ab).

Application of a much higher voltage (typically 1000-6000 mV) resonance excitation can cause ion ejection. Selective ion ejection, known as notch filter (Kelley *et al.*, 1985), can cause the ejection of ions of a single m/z while all other ions remain efficiently stored. This principle is the premise for axial modulation (Weber-Grabau *et al.*, 1988; Tucker *et al.*, 1988). By applying a dipolar resonance excitation of relatively high voltage at a frequency just below the $\beta_z=1$ boundary (i.e. <550 kHz), ions can be ejected earlier during the mass-selective instability scan. This method is known as axial modulation and allows for improved resolution and peak shape. These results are believed to be due to the fact that the $\beta_z=1$ boundary is not very sharp; when the ions approach the boundary, instability is not

instantaneous. By applying axial modulation, the boundary becomes very well defined and ions are promptly ejected during the mass-selective instability scan. This mode of operation has been applied to increase the mass-range (Kaiser *et al.*, 1991). By applying axial modulation at much lower frequencies, ions become unstable and are ejected towards the detector much sooner during the mass-selective instability scan. In essence this increases the scan range that was once limited by the maximum RF amplitude available. High mass capabilities approaching 70,000 Da have been reported (Kaiser *et al.*, 1991).

Mass-Selective Isolation

Ion isolation can be achieved by two basic methods: RF/DC isolation of the desired ion via "apex" (Weber-Grabau *et al.*, 1987; Todd *et al.*, 1987) or "two-step" isolation (Gronowska *et al.*, 1990; Yates *et al.*, 1991a), or resonant ejection via single frequency (Kelley *et al.*, 1985) or broadband ejection of all unwanted ions (Kelley *et al.*, 1993; Julian and Cooks, 1993; Yates *et al.*, 1991b; Eades *et al.*, 1991). The basic premise of both methods is to selectively store only the ions of interest. The RF/DC isolation methods utilize the stability boundaries to define the stable and unstable conditions. The RF/DC isolation methods are shown graphically on the Mathieu stability diagram in Figure 1-4. "Apex isolation" (Weber-Grabau *et al.*, 1987; Todd *et al.*, 1987) is accomplished by initially positioning the ion of interest at $q_z=0.78$, $a_z=0$ which is located directly beneath the upper apex of the Mathieu stability diagram (see Figure 1-1).

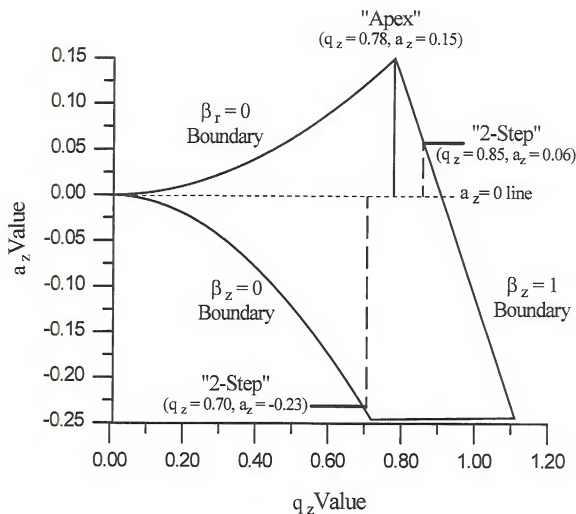


Figure 1-4: Expanded view of the upper portion of the Mathieu stability diagram showing points used for RF/DC isolation. "Apex" isolation employs the point where the $\beta_r=0$ and $\beta_z=1$ boundaries meet. The "2-step" method sequentially employs the $\beta_z=0$ and $\beta_z=1$ boundaries.

Upon application of a sufficiently negative DC voltage (i.e. $a_z=0.15$), the ion of interest remains within the stability diagram; ions of lower m/z are axially unstable (due to $\beta_z=1$ boundary) while ions of higher m/z are radially unstable (due to $\beta_r=0$ boundary), both of which lead to ejection of the unwanted ions. "Two-step isolation" (Gronowska *et al.*, 1990; Yates *et al.*, 1991a) also utilizes stability boundaries for mass isolation. This method is accomplished by first storing the ions near $q_z=0.5$. Upon application of a sufficiently positive DC voltage (to approach the $\beta_z=0$ boundary), ions of higher m/z than the ion of interest will become axially unstable and undergo ejection. Next, the ion is stored near $q_z=0.85$. Upon application of sufficiently negative DC voltage (to approach the $\beta_z=1$ boundary), ions of lower m/z than the ion of interest become axially unstable and are ejected. The "two step" isolation method has been reported to be more efficient than the apex isolation method (Yates *et al.*, 1991a).

Resonance excitation also can be employed for mass-selective isolation. These methods utilize specific frequencies to define the stable and unstable regions. The single frequency method (Schwartz and Jardine, 1992) is accomplished by applying a high frequency dipolar resonance excitation signal of relatively high amplitude (1000-6000 mV) while the RF amplitude is ramped upward; this brings unwanted low m/z ions into resonance thus inducing ejection. The excitation frequency is then lowered and the RF amplitude is ramp downward in order to bring unwanted high m/z ions into resonance thus causing ejection. The desired single mass or mass range is then isolated from all other ions.

Recently, broadband resonance ejection of unwanted ions has been employed for mass isolation (Julian and Cooks, 1993; Eades *et al.*, 1991; Kelley *et al.*, 1993). This method can be accomplished by using a signal derived from multiple single discrete frequencies (Eades *et al.*, 1991), stored waveform inverse Fourier transform (SWIFT) (Julian and Cooks, 1993; Yates *et al.*, 1993), or random noise (McLucky *et al.*, 1992; Kelley *et al.*, 1993). By using a broadband signal in which single frequencies are applied sequentially in time, ions of varying m/z (i.e. various frequencies) can be resonantly excited to the point of ejection. This technique can be efficient if only a few m/z ions need to be ejected; a wide m/z range requires constant power for each m/z for uniform ejection efficiency. Due to constraints in both the signal amplitude and duration, multiple single frequency broadband ejection typically is most efficient when employed for a relatively narrow mass range or for a few target ions. The most effective broadband technique for ejection of a wide m/z range is either SWIFT (Julian and Cooks, 1993; Yates *et al.*, 1993) or random noise (McLucky *et al.*, 1992; Kelley *et al.*, 1993), due, in part, to the ability to apply hundreds of discrete signals simultaneously. This technique has proven to be very effective for ejection of a wide m/z range (Julian and Cooks, 1993) and for efficient CID over a GC peak (Yates *et al.*, 1993). Application of random noise during ion formation (Kelley *et al.*, 1993) allows for the efficient ejection of a wide range of unwanted ions; consequently, the quadrupole ion trap selectively stores only the ions of interest. This has increased the sensitivity by selectively "filling" the ion trap with

only analyte ions while simultaneously discriminating against matrix or background ions.

User-Defined Scanning Strategies

Due to the tandem-in-time nature of the quadrupole ion trap, the ITMS™ has the capability of performing a variety of experiments simply by altering the sequence of events of the amplitude and duration of the applied RF and DC signals. This sequence of applied signals is known as a scan function. The software intensive mode of operation allows the rapid interchange of experiments without the need for hardware modifications. For example, the instrument can be programmed to acquire EI and/or CI and/or MSⁿ spectra during consecutive scans (Strife *et al.*, 1990). Controlling the signal sequence allows the user to create experiment-specific scan functions which further increase the potential of this instrument.

Practical Equations

Many of the complicated equations presented in this chapter can be simplified by incorporating parameters which are relevant to the specific quadrupole ion trap employed. Given Equations 1-7 and 1-8 for the Mathieu parameters a_z and q_z , the following values apply for the Finnigan MAT ITMS™ (Johnson *et al.*, 1992):

U	= DC voltage	r_o	= 0.01000 m
$V_{o,p}$	= RF voltage (zero-to-peak)	z_o	= 0.00783 m

$$e = 1.60219 \times 10^{-19} \text{ C}$$

$$\Omega = 2\pi f$$

$$z = +1$$

$$f = 1.1 \times 10^6 \text{ s}^{-1}$$

$$m_u = \text{mass (in Da)} \times (10^{-3} \text{ kg/mol}) / 6.02205 \times 10^{23} \text{ mol}^{-1}$$

Using the above values and substituting into Equations 1-7 and 1-8, the practical equations for a_z and q_z become

$$q_z = \frac{0.072584(V)}{m_u} \quad (1-14)$$

$$a_z = \frac{-0.14517(U)}{m_u} \quad (1-15)$$

If the equations are rearranged, the RF and DC voltages can be calculated as follows:

$$V_{o-p} = -13.777(q_z)(m_u) \quad (1-16)$$

$$U = -6.8885(a_z)(m_u) \quad (1-17)$$

Since the ITMS™ software expresses the RF voltage in terms of DACS or low-mass-cutoff (LMCO), the user must first calculate q_z in order to calculate V_{o-p} . By knowing the q_z of ejection, a simple ratio can be generated in order to calculate the q_z value for any RF level. The $\beta_z=1$ stability boundary corresponds to $q_z=0.908$; if axial modulation is employed in order to eject the ions just prior to the $\beta_z=1$ edge, the q_z of ejection can be calculated based upon the frequency of the axial modulation signal by using Equation 1-13 (i.e. $q_z=0.9065$ for 530 kHz). Using the simple ratio below, the q_z value at any point can be calculated by:

$$q_z = (\text{LMCO} \times q_{z,\text{ejection}}) / m/z \quad (1-18)$$

Scope of Dissertation

This dissertation presents the experimental results from characterization studies of higher-order field effects on stored ions in the quadrupole ion trap. Chapter 1 has provided both a historical and a fundamental summary of the quadrupole ion trap along with details regarding specific capabilities of the ITMS™. Chapter 2 will present a theoretical treatment of higher-order field contributions to the quadrupolar trapping field. Sources of higher-order fields specific to the ITMS™ will be presented; their relation to higher field resonance conditions will be discussed. Chapter 3 will present detailed characterization studies with regards to instrumental parameters. The influence of such factors as storage condition, ion population, and storage time will be presented in detail. Chapter 4 will describe the implications of higher-order field effects on chemical ionization. Examples of reduced CI sensitivity and altered CI spectra resulting from the influence of higher field resonances will be offered. The experimentally determined stability region for the CI reagent ion, $C_2H_5^+$, also will be presented. Chapter 5 will discuss the implications of higher-order fields on ion motion in the quadrupole ion trap. Both dipolar and quadrupolar resonant excitation of stored ions will be employed to probe ion frequencies. Evidence for higher-order field-induced frequency components of motion will be presented. The final chapter, Chapter 6, will summarize the characterization studies and the observed implications of higher-order fields. The chapter will conclude with suggestions for future studies in the area of fundamental aspects and implications of higher-order fields.

CHAPTER 2 HIGHER-ORDER FIELDS

Introduction

This chapter provides a detailed introduction to the fundamental principles of higher-order fields. The basic premise of an "ideal" quadrupole ion trap is presented along with the predicted properties of such a device. The geometry and properties of all commercially available quadrupole ion traps significantly deviate from those of the "ideal" quadrupole ion trap. A technical description of practical quadrupole ion traps will be given along with the expected properties. Sources of higher-order fields in the commercial quadrupole ion trap will be identified and discussed.

A theoretical treatment of higher-order fields will be given. Specifically, equations allowing the calculation of the storage field potential throughout the quadrupole ion trap for any amount of contribution from higher-order fields ranging from third-order (hexapolar) to sixth-order (dodecapolar) will be given. Calculation and identification of the resulting higher-order field resonance lines will be offered and placed in context with the Mathieu stability diagram. The chapter will conclude with a brief description of previously observed higher-order field effects.

"Ideal" Quadrupole Ion Traps

The endcap and ring electrodes of the quadrupole ion trap are typically constructed of stainless steel. Many of the early investigations utilized wire mesh constructed out of stainless steel (Dawson *et al.*, 1969a) and copper (Bonner *et al.*, 1972); however, the construction of the electrodes to conform to the exact theoretical surface geometry is extremely difficult with wire mesh. Stainless steel offers a relatively pure material which can be machined to precise tolerances (± 0.0001 cm). This material also exhibits sufficient rigidity and temperature independent properties necessary for use with a rugged, versatile mass spectrometer. The surfaces of the electrodes are constructed to follow the equations of hyperbolae; the exact geometry for the electrode surface is dependent on the radius of the ring electrode (r_o) and the endcap distance from the center of the quadrupole ion trap (z_o). Traditionally, the endcap distance (from the exact center of the trap to the apex of the endcap) has been dictated by the equation (Knight, 1983)

$$r_o^2 = 2z_o^2 \quad (2-1)$$

Rearranging the equation to solve for z_o gives

$$z_o = \frac{r_o}{\sqrt{2}} \quad (2-2)$$

Note that the equations are expressed in terms of the cylindrical coordinates (r, z, ϕ) and not the familiar Cartesian coordinates (x, y, z). Due to the rotational symmetry, ϕ is neglected; r is defined as $(x^2 + y^2)^{1/2}$. Apparently, the constraint given in Equation

2-1 (or 2-2) resulted from the original form of the equations for the electrode surface geometries. These electrode surfaces were defined by (Knight, 1983)

$$\frac{r^2}{r_o^2} - \frac{z^2}{z_o^2} = 1 \quad (2-3)$$

$$\frac{r^2}{r_o^2} - \frac{z^2}{z_o^2} = -1 \quad (2-4)$$

for the ring and endcap electrode, respectively. The constraint shown in Equations 2-1 and 2-2 originates from the required constant potential of $r^2 - 2z^2$ along the entire electrode surface. The general equation for hyperboloids of revolution intersecting the point z_o, r_o , however, allow a number of surfaces to be generated. Constraining the ring and endcap electrodes to follow the same asymptotes reduces the number of possible surfaces. The slope of the most commonly chosen asymptote, $1/\sqrt{2}$, is independent of both r_o and z_o and bisects the gap between the ring and endcap electrode. This constraint results in the following surface equations (Knight, 1983):

$$\frac{r^2}{2r_o^2} - \frac{2z^2}{r_o^2} = 1 \quad (2-5)$$

$$\frac{r^2}{2z_o^2} - \frac{z^2}{z_o^2} = -1 \quad (2-6)$$

for the ring and endcap electrodes, respectively. The resulting endcap surfaces are not restricted by r_0 and the ring electrode is not restricted by z_0 as in Equations 2-3 and 2-4.

For convenience, the ring electrode commonly has been constructed with $r_0=1\text{cm}$; the endcap distance, as defined by Equation 2-1, has been $1/\sqrt{2}$ or 0.7071 cm. Given these dimensions (i.e. $r_0=1$ cm, $z_0=0.7071$), Figure 2-1 shows the electrode surfaces calculated with Equations 2-5 and 2-6. According to theory, the surfaces follow the hyperbolic shape infinitely; the ring and endcap electrodes follow asymptotes that bisect the center of the trap at an angle of 35.26° (Knight, 1983). Given that the quadrupole ion trap is operated with RF and DC potentials applied to the ring and ground applied to the endcaps (i.e. Mode II of March and Hughes, 1989), and the applied potentials are free of fluctuations, an "ideal" quadrupole trapping field is created. Figure 2-2a shows the equipotential contours of such a quadrupole ion trap; the contours are expressed in terms of percent applied potential. The center of the trapping volume exhibits 50% of the applied potential; the potential increases towards the ring surface and decreases towards the endcap surface. A more practical manner of inspecting the trapping field is to consider the field strength. The strength of the trapping field is defined as the change in potential per change in distance (dV/du , $u = r$ or z) from the center of the trap to an electrode. A plot of field strength versus distance for an "ideal" quadrupole ion trap is shown in Figure 2-2b. This particular graph shows the field strength from the center to an endcap electrode.

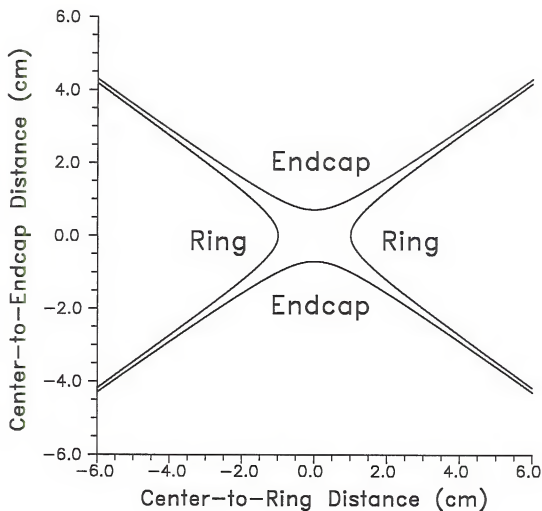
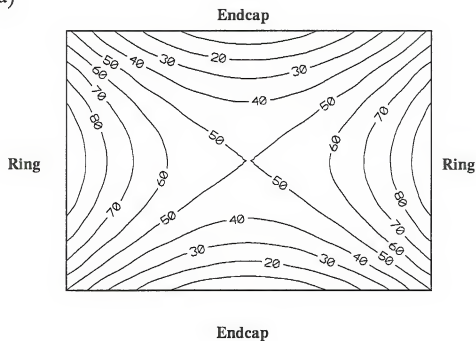


Figure 2-1: "Ideal" theoretical electrode surfaces calculated with Equations 2-5 and 2-6 for the ring and endcap electrodes, respectively.

a)



b)

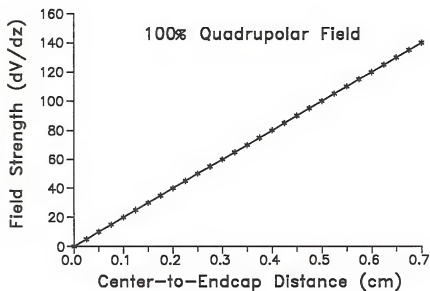


Figure 2-2: "Ideal" quadrupole ion trap a) storage field and b) field strength. Calculations based on Equation 2-8.

Note that at the center of the trap the field strength is zero and linearly increases towards the outer regions. This relationship is true in all directions outward from the exact center of the device. One characteristic of ion motion in a quadrupole ion trap is that once the ion is outside the stability region defined by Mathieu stability diagram, the amplitude of the ion oscillation increases linearly with time. This relationship, combined with the linearly increasing field strength, results in a linear resonance. Due to the mathematical properties of the Mathieu equations, the frequency of ion motion is predicted to be independent of the ion's amplitude (Wang *et al.*, 1992).

Recall that ion motion in an "ideal" quadrupole ion trap follows the Mathieu equations discussed in Chapter 1. The ion secular (main) frequency (ω_u) is required to be less than half of the RF trapping frequency (Ω) and is defined by the trapping parameters a_u and q_u by the equation for β_u . Within the stability diagram, ions exhibit constant frequency along iso- β_u lines (see Figure 1-3). The frequency components defining the total motion of an ion are defined by: $(n+\beta_u/2)\Omega$ where $n=0, \pm 1, \pm 2, \pm 3 \dots$ (March and Hughes, 1989). The ion trajectory displays mainly the secular frequency, defined by $n=0$, but also exhibits a higher-order ripple defined by $n \neq 0$. The main component of the higher frequency motion is due to $\Omega - \omega_u$ and $\Omega + \omega_u$ for $n = -1$ and $+1$, respectively. With increasing absolute value of n , the contribution of each frequency component to the total ion motion decreases (Wang *et al.*, 1992). The contribution of each component can be calculated by the C_{2n} equation discussed in Chapter 1 and is dependent on the a_u and q_u parameters.

Relative contributions of each higher component frequency to the total ion motion have been calculated previously (Bonner, 1974). Due to the mathematical properties of the Mathieu equations, the ion's motion in the z-direction is predicted to be completely decoupled from the motion in the r-direction.

Consideration of the "ideal" quadrupole ion trap discussed above, reveals several properties which are summarized below (Wang, 1992):

1. All electrode surfaces are flawlessly constructed
2. The electrode surfaces extend hyperbolically to infinity
3. The endcap and ring electrodes share a common asymptote
4. The field strength is linear in both the r and z directions
5. Ion motion is decoupled in r- and z-direction
6. Ion frequency of motion is independent of amplitude of motion

Practical Quadrupole Ion Traps

Construction of practical quadrupole ion traps requires deviation from the "ideal" quadrupole ion trap discussed above. Any deviation will result in quadrupolar field perturbations due to the introduction of higher-order fields superimposed on the trapping field. In general, higher-order even fields are introduced by a symmetrical deviation from the "ideal" geometry; higher-order odd fields are introduced by an asymmetrical deviation from the "ideal" geometry (Beatty, 1986). The symmetry is respective to the $z=0$ plane of the quadrupole ion trap (the plane bisecting the trap through the center of ring electrode).

The most significant deviation of the practical quadrupole ion trap from the "ideal" ion trap is electrode truncation. Obviously the electrodes cannot be infinitely long; therefore, all practical quadrupole ion traps employ truncated electrodes. Besides the ease of construction, truncation is required to avoid a voltage arc from the applied RF on the ring (which can approach 15000 V_{p-p} on Finnigan MAT ion trap instruments) to the grounded endcaps. Since these practical electrodes do not follow the expected theoretical geometry, a nonideal quadrupolar field exists; higher-order fields are superimposed on top of the quadrupolar field. Since electrode truncation is symmetrical about the $z=0$ plane (Beatty, 1986), even fields are introduced (i.e. octopolar, dodecapolar, etc.). Of particular importance is that the higher-order fields which are introduced due to truncation contribute to the overall field with opposite sign to that of the quadrupolar trapping field (Franzen, 1993). As discussed below, this "destructive" contribution (opposite sign) causes poor overall performance (Franzen, 1993). Shown in Figure 2-3 are the electrode surfaces of the quadrupole ion trap used in the Finnigan MAT Ion Trap Mass Spectrometer (ITMS™). The electrodes have been truncated so that the surfaces extend only 2.0 cm from the center of the trap. Note that the entire electrode has not been shown, only the electrode surface. The introduction of higher-order fields to the quadrupolar trapping field alters the trapping conditions. Shown in Figure 2-4a is a comparison of the equipotential contours for an "ideal" quadrupolar field to that of one superimposed with a 5% octopolar field.

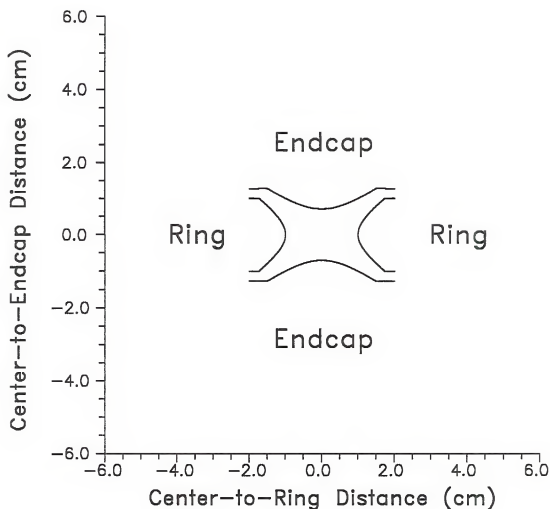


Figure 2-3: Electrode surfaces showing the more practical "real" quadrupole ion trap. Electrodes are truncated such that the surface extends 2 cm from either side of the origin.

a)

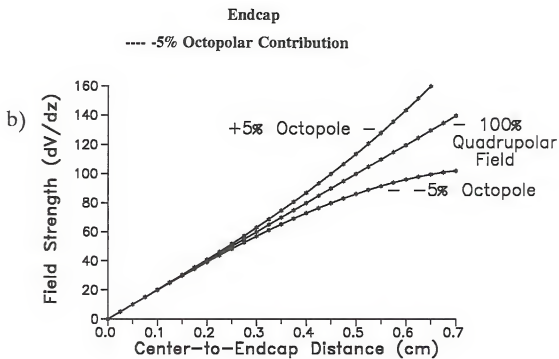
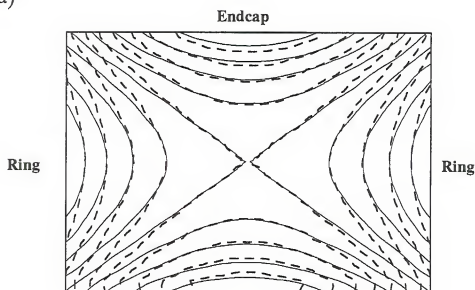


Figure 2-4: Comparison of "ideal" quadrupolar ion trap with one superimposed with 5% octopole field: a) storage field and b) field strength. Calculated based on Equations 2-8 through 2-13.

In this specific case, the superimposed octopolar field has the opposite sign ("destructive") as the quadrupolar field (as in the case of electrode truncation). Note that the two fields deviate only in the outer regions of the trap; an "ideal" quadrupolar field remains in the very center for the 5% octopolar case.

An ion stored near the center of a nonideal quadrupole ion trap continues to experience an "ideal" quadrupolar field; an ion stored in the outer regions, however, is influenced by the higher-order fields present. Shown in Figure 2-4b is a comparison of the field strength for three different trapping fields; a pure quadrupolar field, a quadrupolar field superimposed with a 5% octopolar field of the same sign as that of the quadrupolar field ("constructive"), and one superimposed with a 5% octopolar field of the opposite sign as that of the quadrupolar trapping field ("destructive"). Of particular importance is that the addition of the octopolar field results in a field strength that no longer is linearly related to distance from the center of the trap. This results in a non-linear resonance. Specific storage conditions (q_z, a_z values) resulting in ion frequencies of motion corresponding to higher-order field resonances can cause stored ions to absorb power and undergo altered ion trajectories.

The addition of a "constructive" octopolar contribution causes the field strength, beyond a certain distance, to increase more quickly than the "ideal" case; addition of a "destructive" octopolar contribution causes the field strength, beyond a certain distance, to be less than the "ideal" quadrupolar field. The importance of this observation can be seen in the performance of a quadrupole ion trap as a mass

spectrometer when employing mass-selective instability (Stafford *et al.*, 1983ab). An ion trap with "destructive" octopolar contributions (opposite sign) has been observed to exhibit poor resolution and broad mass peaks; an ion trap with a "constructive" (similar sign) octopolar contribution has been observed to exhibit improved resolution and narrower mass peaks (Franzen, 1993). This behavior can be explained by considering the field strength shown in Figure 2-4b. With a "destructive" octopolar contribution, the total field strength increases less than linearly causing the ion to absorb power from the trapping field more slowly compared to the "ideal" case. This deviation causes the ions to be ejected more slowly than the "ideal" case thus resulting in broad mass peaks and poor resolution. With a "constructive" octopolar contribution, the total field strength increases more than linearly causing the ion to absorb power more quickly than the "ideal" case. This causes the ion to be ejected more quickly thus resulting in narrower mass peaks and improved resolution (Franzen, 1993). The contributions of hexapolar fields show less of an effect on the total field strength as compared to the octopolar field (i.e. less deviation from "ideal" for 5% and 10% hexapolar field contributions). This can be attributed to only 3rd-order terms contributed by the hexapolar field as opposed to 4th-order terms contributed by the octopolar field (Beaty, 1986).

The introduction of higher-order even fields of opposite sign than the quadrupolar trapping field caused by the need to truncate the electrodes presumably justified the current design of the Finnigan MAT quadrupole ion traps. All quadrupole ion traps delivered by Finnigan MAT possess a "stretched" design (Louris

et al., 1992). The distance from the center of the trap to the endcap is somewhat longer than predicted by theoretical equations. The ring electrode radius is 1 cm; the endcap distance is reportedly 0.783 cm (Louris *et al.*, 1992). The hyperbolic electrode surfaces, however, are constructed based on Equation 2-1 which predicts $z_0=0.7071$ cm. The resulting "stretch" is approximately 10.7%. Experimental measurements of another quadrupole ion trap assembly reported $z_0=0.7811$ (Julian *et al.*, 1992); the ion trap used for the studies in this dissertation exhibited $z_0=0.785$ cm. Interestingly, recent measurements of the Finnigan MAT ion traps employed in the ITS-40™ benchtop instruments report $z_0=0.790$ cm (Timothy P. Griffin, private communication); a "stretch" of approximately 11.7%. Figure 2-5a compares the predicted electrode surfaces ($z_0=0.7071$ cm) calculated by equations 2-3 and 2-4 to that of the "stretched" design of the Finnigan MAT ITMS™ ($z_0=0.783$ cm). Although the surfaces do not appear to deviate greatly from the theoretical spacing, the displaced endcaps significantly contribute higher-order even fields. Shown in Figure 2-5b is an expanded view of the top endcap surface. Also included on the graph is the calculated surface using equations 2-5 and 2-6 (i.e. $r_0=1$ cm, $z_0=0.783$ cm) (Knight, 1983). Comparing the two surfaces employing $z_0=0.783$ cm reveals that both endcap surfaces converge at the apex; the outer regions, however, deviate significantly. The "stretched" endcap, which is parallel to the theoretical surface ($z_0=0.7071$ cm), displays a surface in which the terminal ends are farther from the center of the quadrupole ion trap than with the calculated surface for $z_0=0.783$ cm. This deviation in the surface geometry is the source of the higher-order fields.

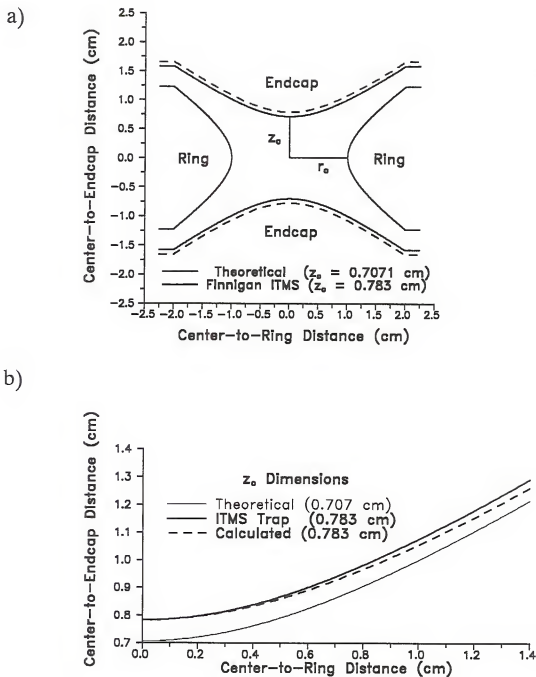


Figure 2-5: Comparison of electrode surfaces for theoretical endcap spacing ($z_o=0.7071$ cm) with a) that employed with the Finnigan MAT ITMS™ ($z_o=0.783$ cm) and b) expanded view of upper right quadrant of top graph.

The "stretched" design reportedly improved the performance of the quadrupole ion trap in terms of mass resolution (Louris *et al.*, 1992). This can be understood based on field strength as shown in Figure 2-4b. By symmetrically displacing the endcap electrodes, higher-order even fields are introduced with the same sign as that of the quadrupolar trapping field (constructive contribution). This "stretch", in effect, compensates for the detrimental effects of electrode truncation. During ejection, the ion absorbs power more quickly than with the un-stretched trap and thus exhibits narrower peak widths (i.e. improved mass resolution).

Other deviations from that of the "ideal" electrode can be identified in the Finnigan MAT ITMS™; the major contributions include holes in electrodes, field penetration, and machining flaws during construction. Each deviation from the "ideal" case will introduce field distortions in the quadrupolar trapping field by contributing higher-order fields. Higher-order odd field resonances are introduced due to the inherent differences between the entrance and exit endcaps (Beaty, 1986). This axially asymmetric distortion may arise from machining flaws or differences in the number or size of holes in each endcap. The exit endcap of Finnigan quadrupole ion traps has 6 holes (1/16") symmetrically positioned around a center hole of equal size located at the endcap apex. These holes are used for the ion extraction to the detector. The entrance endcap of Finnigan quadrupole ion traps has one center hole (the same size as each of the exit holes) at its apex and is used for the introduction of electrons. Holes in the electrodes introduce distortions in the pure quadrupolar field due to a discontinuous equipotential electrode surface. Consequently, the

distortion will be asymmetric with respect to the $z=0$ plane due to the differences in the number of holes in each endcap. The degree of distortion is expected to be less near the entrance endcap due to the fewer number of holes.

Another source of higher-order fields (which is caused directly from the holes in the endcaps) is field penetration. Due to the holes, potentials which exist behind each endcap (i.e. ± 180 V behind the entrance endcap; multiplier and dynode voltages behind the exit endcap), can penetrate the storage field thus causing perturbations. Also due to the holes, the storage field can essentially "spill" out of the trapping volume. Furthermore, the degree of penetration or withdrawal of each field will vary with the phase of the RF trapping field. When the RF is essentially zero, penetration from either the ± 180 V gate or from the dynode or multiplier will penetrate the storage field; when the RF is either positive or negative, the trapping field can "spill" out of the trapping volume causing the endcaps to no longer "appear" to be at ground potential. With the differences in the applied potentials behind each endcap, field penetrations may differ, resulting in axially asymmetric field distortions. Indeed, higher-order odd field effects (e.g. hexapolar) in the ITMS™ previously have been attributed to field penetration (Louris *et al.*, 1992). Investigations into field distortions due to holes in the endcaps of a non-commercial quadrupole ion trap (Griffiths and Heesterman, 1990) reported effects from octopolar resonance lines. Since the endcaps were identical in geometry and potential (axially symmetric), it follows that a higher-order even field resonance would be observed. It should be noted that the field penetration due to the dynode and/or multiplier potentials will

depend on their distance from the endcap electrode; furthermore, the presence of a grounded shield between the endcap and dynode / multiplier assembly in some Finnigan MAT ion trap instruments will significantly reduce field penetration.

Bruker-Franzen Analytik has patented (Franzen *et al.*, 1989) a quadrupole ion trap device in which higher-order fields also have been introduced purposely. Besides the contribution of higher-order even fields due to electrode truncation and higher-order odd fields due to differences in the endcaps, higher-order even fields are introduced into this device by altering the ion trap shape parameter, Θ , which is defined as $\Theta = r_o^2/z_o^2$. This parameter represents the angle of the common asymptote shared by the ring and endcap electrode; the "ideal" geometry predicts that $\Theta = 1/\sqrt{2}$ or 0.7071. Employing the dimensions discussed above, a purely quadrupolar field would yield $\Theta = (1 \text{ cm})^2/(0.7071 \text{ cm})^2 = 2.0$; the Bruker-Franzen quadrupole ion trap shape parameter is reportedly $\Theta = 1.9$ (Franzen *et al.*, 1989). The asymptotic angle produced by this geometry would be 0.7255 or $1/\sqrt{1.9}$. In the patent, the following equation is used to define the electrode geometry of the Bruker-Franzen quadrupole ion trap:

$$Q = \frac{R_e}{R_r} \times \frac{r_o}{z_o} \quad (2-7)$$

where r_o and z_o have the same definition as above and R_e and R_r represent the inscribed radii required to generate the spherical portion of the hyperbolic endcap and ring electrode, respectively (i.e. the portion of the electrodes closest to the center of the ion trap can be described by an equation of a circle). The value of Q

for the Bruker-Franzen ion tap is $(1.9)^2$ or 3.61. The ring radius is reportedly 1 cm; the z_0 dimension would, therefore, be $z_0=0.7255$.

Operation of the Bruker-Franzen Analytik quadrupole ion trap employs mass-selective instability (Stafford *et al.*, 1983ab); however, the octopolar resonance, $\beta_z+\beta_t=1$, is used for ejection instead of the $\beta_z=1$ stability edge or the axial modulation edge (Weber-Grabau *et al.*, 1988; Tucker *et al.*, 1988). Simulated ejection analyses (Wang, 1992) at various points along the $a_z=0$ line showed that ions can be efficiently ejected at the octopolar sum resonance; however, an energy threshold exists, therefore, the ion needs to be initiated (e.g. dipole resonance) just prior to the resonance line. No ejection was observed near $q_z=0.635$, the octopolar resonance at $\beta_z=1/2$. Reportedly, this was due to the fact that the quadrupole ion trap shape parameter, Θ , was close enough to the theoretical value of 2.0.

A recent report (Wang and Wanczek, 1993) describes the procedure for generating an exact three-dimensional quadrupolar field with superposition of a homogeneous dipolar field. This is accomplished by the design of new electrodes possessing linearly varied potentials along the electrode surfaces. Generation of linearly varied potentials can be achieved by using a series of parallel plates which have circular holes which form the inner surface of a cone. The sheets are equally spaced and the potential is applied to the top ($-\Phi$) and bottom ($+\Phi$) plate. Practical applications with this type of quadrupole ion trap have not been reported.

Theoretical Treatment

Ideally, the quadrupolar field applied to the ion trap can essentially be described by two harmonic oscillators, one in the z-direction and one in the r-direction. As shown in Figure 2-2b, the strength of each oscillator is predicted to increase linearly with distance from the center of the ion trap. Contributions from higher-order fields distort this relationship between the field strength and displacement from the center, as shown Figure 2-4b. When the applied quadrupolar field is such that ion secular frequencies (in z-direction or r-direction) correspond to those of higher-order field resonances, trapped ions may absorb power and undergo altered trajectories.

Recall that the potential at the center of an "ideal" quadrupole ion trap operated in Mode II is 50% of the applied potential whose distribution can be expressed as (March and Hughes, 1989):

$$\Phi_z = \Phi_o + \frac{\Phi_o}{r_o^2} (r^2 - 2z^2) \quad (2-8)$$

where

$$\Phi_o = \frac{U - V \cos \Omega t}{2} \quad (2-9)$$

If contributions of all fields (dipolar, quadrupolar, and higher-order fields) are considered, a power-series can be written to describe the field potential about the point ($z=0$, $r=0$) as follows (Beatty, 1986):

$$\Phi_{\text{Total}} = \Phi_o + \Phi_o (A_1 \Phi_1 + A_2 \Phi_2 + A_3 \Phi_3 + A_4 \Phi_4 + \dots) \quad (2-10)$$

where the A_N terms are weighting factors dependent on the relative contribution of each field and the subscripts represent the field order; the field = $2N$ where $N=1,2,3,\dots$ (i.e. dipolar=1, quadrupolar=2, hexapolar=3, octopolar=4). When N is odd, a higher-order odd field is described; when N is even, a higher-order even field is described. The equation for the dipolar field potential (Beatty, 1986) is

$$\Phi_1 = \frac{z}{r_o} \quad (2-11)$$

and the equations for the higher-order field potentials are (Beatty, 1986):

$$\Phi_3 = \frac{(2z^3 - 3zr^2)}{r_o^3} \quad (2-12)$$

$$\Phi_4 = \frac{(8z^4 - 24z^2r^2 + 3z^4)}{r_o^4} \quad (2-13)$$

$$\Phi_5 = \frac{(8z^5 - 40z^3r^2 + 15zr^4)}{r_o^5} \quad (2-14)$$

$$\Phi_6 = \frac{(16z^6 - 120z^4r^2 + 90z^2r^4 - 5r^6)}{r_o^6} \quad (2-15)$$

where the Φ_N functions (spherical harmonics) have numerical coefficients chosen to satisfy the Laplace equation. Note that the Φ_o terms have been factored out of each of the Φ_N terms. No contribution from higher-order terms (i.e. $A_{N>2} = 0$) and no

application of a dipolar field yields the "ideal" quadrupolar field equation expressed in Equation 2-8.

Construction of theoretically correct electrodes yields zero contribution from higher-order even terms (i.e. octopolar, dodecapolar). Higher-order odd terms (i.e. hexapolar, decapolar) can be eliminated by making both the electrode surfaces and the applied potentials with reflection symmetry in the $z=0$ plane (Beaty, 1986). Although the relationship between r_0 and z_0 (center-to-endcap distance) for a pure quadrupolar field is typically $r_0^2=2z_0^2$ (Knight, 1983), other dimensions can be used provided the electrodes conform to equipotential surfaces of a pure quadrupolar field according to Equations 2-5 and 2-6 (Knight, 1983).

Although the amount of contribution of each higher-order field is difficult to determine, the locations of higher resonances within the stability region can be predicted. In general, higher-order even (e.g. octopolar, dodecapolar) field resonances can be predicted with solutions for the harmonic oscillator as described by the following equation (Dawson and Whetten, 1969c; Dawson, 1976):

$$\frac{1}{2}K\beta_r + \frac{1}{2}(N-K)\beta_z = 1 \quad (2-16)$$

where N is the field order and K can have the values $N, N-2, N-4$, etc., with a maximum of N number of resonances (i.e. octopolar yields a maximum of 4 resonances). The parameters β_z and β_r yield values between 0 and 1 and are related to the ion's secular frequencies in the radial (ω_r) and axial (ω_z) directions, with $\beta_r=2\omega_r/\Omega$ and $\beta_z=2\omega_z/\Omega$. Higher-order even fields are introduced by axially

symmetric field distortions which are caused by any deviation from the theoretical dimension in which the departures from "ideal" are equal on either side of the $z=0$ plane. As stated above, sources of higher-order even fields can be caused by identical electrode truncation or equal deviations in each endcap-to-ring distance, as in the "stretched" quadrupole ion trap (Louris *et al.*, 1992).

Higher-order odd field resonances (e.g. hexapolar, decapolar) are described by the following equation (Wang *et al.*, 1993):

$$\frac{1}{2}(N-K)\beta_z + \frac{1}{2}K\beta_z = 1 \quad (2-17)$$

where N , K , β_z , and β_z have the same definitions as given above. Again, a maximum number of N resonances exist. Higher-order odd fields are introduced by axially asymmetric field distortions which are caused by any deviation from the theoretical dimension in which the departures from "ideal" are different on each side of the $z=0$ plane. As stated above, sources of higher-order odd fields can be caused by employing two endcaps differing in endcap-to-ring distances, geometries, or potentials.

The higher field resonances which can be calculated from equations 2-16 and 2-17 above are listed in Table 2-1. Note that only fields less than eighth-order are listed and that resonances possessing positive terms (i.e. $K \geq 0$) only are included. The higher field resonances which are marked in the table have been observed experimentally and will be discussed throughout the research chapters. Shown in Figure 2-6 is the Mathieu stability diagram along with the higher resonances for

hexapole, octopole, and dodecapole fields. When higher-fields are considered, the Mathieu stability diagram becomes very complex. Note that several resonances converge at each apex of the stability diagram. Early operation of the quadrupole ion trap (Dawson and Whetten, 1968b, 1969ab) employed the lower apex for mass-selective detection. The observation of split mass peaks can be explained by this convergence of several higher field resonances.

Recently, a more direct approach for the determination of higher-order field resonances have been reported (Wang *et al.*, 1993). The authors stressed that the equation previously used by Dawson and Whetten (1969b, 1976), Equation 2-16, is not the general formula but only describes higher-order even fields. Furthermore, the equation is valid only for the two-dimensional potential field (i.e. linear quadrupole). A quadrupole ion trap with a three-dimensional potential field exhibits rotational symmetry; field forces on the ions occur only in two directions, r and z . The forces in the ϕ direction are zero, thus the initial velocity in that direction can be assumed to be equal to zero. Consideration of the ion motion in only the r and z directions leads to a "degenerated" two-dimensional case which can be solved for the higher resonance conditions. The following equation describes all higher-order field resonances (Wang *et al.*, 1993):

$$\frac{\beta_r}{2}n_1 + \frac{\beta_z}{2}n_2 = \nu \quad (2-18)$$

where $|n_1| + |n_2| = N$ (N is the field order) and ν is an integer.

Table 2-1: Higher-order Field ($N = 3$ to $N = 8$) Resonances[†], Positive and Sum Resonances Only ($K \geq 0$)

Third Order (Hexapolar)	Fourth Order (Octopolar)	Fifth Order (Decapolar)	Sixth Order (Dodecapolar)	Seventh Order (Tetradecapolar)	Eighth Order (Hexadecapolar)
$\beta_z = 2/3^\dagger$	$\beta_z = 1/2^\dagger$	$\beta_z = 2/5$	$\beta_z = 1/3^\dagger$	$\beta_z = 2/7$	$\beta_z = 1/4$
$\beta_z/2 + \beta_r = 1$	$\beta_r = 1/2^\dagger$	$3/2\beta_z + \beta_r = 1$	$\beta_r = 1/3$	$1/2\beta_z + 3\beta_r = 1$	$\beta_r = 1/4$
	$\beta_z + \beta_r = 1^\dagger$	$1/2\beta_z + 2\beta_r = 1$	$\beta_z + 2\beta_r = 1^\dagger$	$3/2\beta_z + 2\beta_r = 1$	$1\beta_z + 3\beta_r = 1$
			$2\beta_z + \beta_r = 1$	$5/2\beta_z + \beta_r = 1$	$2\beta_z + 2\beta_r = 1$
					$3\beta_z + \beta_r = 1$

[†] Calculated using Equations 2-16 and 2-17.[‡] Observed experimentally (see research chapters).

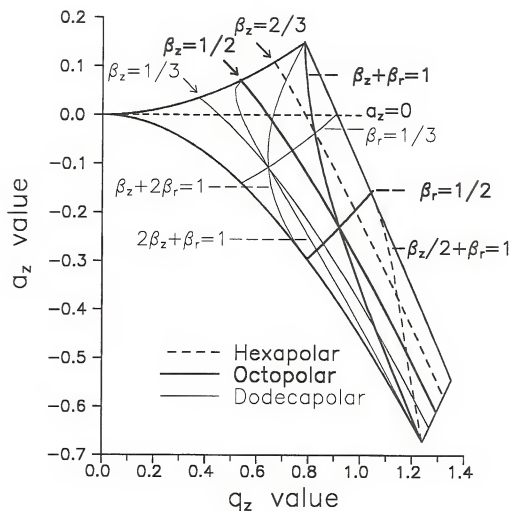


Figure 2-6: Mathieu stability diagram, plotted in q_z , a_z space, together with higher field resonances for hexapolar, octopolar, and dodecapolar fields. Resonances are those calculated using Equations 2-16 and 2-17.

Based on this equation, two types of resonances exist, coupled and un-coupled. Un-coupled resonances consist of z-type ($n_1=0, n_2 \neq 0$) and r-type ($n_1 \neq 0, n_2=0$); coupled resonances consist of sum resonances ($n_1, n_2 \neq 0$; n_1 and n_2 have same sign) and difference resonances ($n_1, n_2 \neq 0$; n_1 and n_2 have opposite sign).

Several properties based on the above equations exist (Wang *et al.*, 1993):

1. A maximum of $2N$ resonances exist for each N (i.e. octopolar exhibits 8 resonances).
2. Only resonances of $N, N-2, N-4$, etc.. exist (similar to the parameter K in the above equation).
3. The intensity of the resonance line of order N decrease with increasing order.
4. Un-coupled resonances are of the z-type (which absorb power only in the z-direction) and the r-type (which absorb power in only the r-direction).
5. Coupled resonances include sum resonances (which absorb power in both the r- and z-directions) and difference resonances (which exchange power between r and z oscillations).

The properties listed above give insight into the nature of higher-field resonances. Based on properties 1 and 2 and Equations 2-16 through 2-18, the number of higher field resonances and their location within the stability region can be determined. Due to property 3, the strength of each higher-order field decreases with increasing order; therefore only the lower fields (i.e. $N \leq 6$) significantly contribute to the quadrupolar trapping field. The resonances which have the potential of leading to unstable ion trajectories include the non-coupled resonances

(both the r- and z-type) and the sum resonance; difference resonances do not cause instability due to the exchange of energy between r and z oscillations.

The frequency relationship for higher field resonances can be determined for a nonideal quadrupole ion trap operated in Mode II in the first stability region by the following equation (Wang *et al.*, 1993):

$$\frac{\beta_r}{2}n_r + \frac{\beta_z}{2}n_z = 1 \quad (2-19)$$

Rewriting the equation in terms of ion secular frequency (ω_u) and RF trapping frequency (Ω) and recalling that $\omega_u = (\beta_u/2)\Omega$, the frequency relationship for higher field resonances can be expressed as (Wang *et al.*, 1993):

$$n_r\omega_r + n_z\omega_z = \Omega \quad (2-20)$$

where n_r and n_z are positive integers. Visual inspection of Equation 2-20 reveals that a higher resonance will exist only if the sum of the whole number multiples of the secular frequencies in the z- and r-directions equal that of the drive frequency. The restriction of rotational symmetry, however, reduces the number of allowed resonances predicted by the above equation. Odd powers of r (i.e. r^3 or z^2r) in the field equations do not exist due to restrictions in the Hamiltonian function used to describe the system. The restriction results in the forbidden resonances for higher-order even fields for the cases when both n_r and n_z are odd and for higher-order odd fields for the cases when n_r is odd (Wang *et al.*, 1993). Shown in Tables 2-2 through 2-4 are the resonances for the hexapolar, octopolar, and dodecapolar fields predicted by Equation 2-20.

Table 2-2: Hexapolar Resonance Lines Calculated Using Equation 2-20.

n_z Parameter	n_r Parameter	Third Order (Hexapolar)	
3	0	$\beta_z = 2/3$	Forbidden
2	1	$\beta_z + 1/2\beta_r = 1$	
1	2	$1/2\beta_z + \beta_r = 1$	
0	3	$\beta_r = 2/3$	Forbidden

Table 2-3: Octopolar Resonance Lines Calculated Using Equation 2-20.

n_z Parameter	n_r Parameter	Fourth-Order (Octopolar)	
4	0	$\beta_z = 1/2$	Forbidden
3	1	$3/2\beta_z + 1/2\beta_r = 1$	
2	2	$\beta_z + \beta_r = 1$	
1	3	$1/2\beta_z + 3/2\beta_r = 1$	Forbidden
0	4	$\beta_r = 1/2$	

Table 2-4: Dodecapolar Resonance Lines Calculated Using Equation 2-20.

n_z Parameter	n_r Parameter	Sixth-Order (Dodecapolar)	
6	0	$\beta_z = 1/3$	Forbidden
5	1	$5/2\beta_z + 1/2\beta_r = 1$	
4	2	$2\beta_z + 1\beta_r = 1$	
3	3	$3/2\beta_z + 3/2\beta_r = 1$	Forbidden
2	4	$1\beta_z + 2\beta_r = 1$	
1	5	$1/2\beta_z + 5/2\beta_r = 1$	Forbidden
0	6	$\beta_r = 1/3$	

Previously Reported Higher-Order Field Effects

Early Development of the Quadrupole Ion Trap

During the earliest development of the quadrupole ion trap, several observations of higher field resonance effects were reported. Although von Busch and Paul first discussed the effects of field distortions in the quadrupole mass filter as early as 1961, Dawson and Whetten (1969ab, 1976) were the first to discuss these effects with regards to the quadrupole ion trap. During the early evaluation of the ion trap as a mass spectrometer, Dawson and Whetten (1968b) reported both asymmetric and split mass peaks, the magnitude of which increased with increasing storage time. Of particular relevance to these observations was the operational mode of the quadrupole ion trap employed. During the early development, the ion trap operation was similar to that of the quadrupole mass filter (i.e. mass-selective storage, Dawson and Whetten, 1971). Both the RF and DC voltages were applied to the ring electrode with the endcap electrodes grounded; however, the ratio was held constant so that the scan line would pass through the bottom apex of the Mathieu stability diagram. The lower apex of the stability diagram, however, is the convergence point of several higher resonances (as shown in Figure 2-6); therefore the observation of asymmetric and split mass peaks is not surprising.

Further investigations by Dawson and Whetten (1969b) verified that the peak splitting was due to higher field resonances. The authors applied non-linear resonance theory to the case of the quadrupole ion trap and offered equations to

describe the potential distribution of a distorted quadrupolar field. From the equations, the authors were able to derive peak shapes for various degrees of higher-order field contribution as well as the location in the Mathieu stability diagram where higher field resonances could be predicted for each higher-order field. By plotting the experimentally observed splits in the mass peaks in terms of q_z , a_z , the authors were able to confirm the existence of the theoretically predicted higher field resonances due to the $\beta_r + \beta_z/2 = 1$ and $\beta_r = 2/3$ (both hexapolar) and the $\beta_r + \beta_z = 1$ (octopolar). Although much of this work was the foundation for higher field resonance theory, some extrapolations from the linear quadrupole were incorrectly applied to the quadrupole ion trap. Specifically, the existence of the higher resonance along $\beta_r = 2/3$ is not predicted for the quadrupole ion trap according to their theory. Their work employed Equation 2-16 for predicting all higher field resonances; however, as was later demonstrated (Wang *et al.*, 1993), this equation is valid only for the higher-order even fields.

Since the work reported by the early pioneers, relatively few reports of higher field effects have appeared in the literature. Recently, however, several publications have described anomalous behavior due to higher field resonances. The recent surge of reported effects is due, in part, to both the increased popularity of the quadrupole ion trap and the rapid development of the instrument during the last decade. Researchers are now utilizing the ion trap in more sophisticated experiments and in more sophisticated instrumentation. Pushing the performance of the instrument

beyond that afforded by its original operational mode has revealed many of the reported anomalies.

Ion Injection Experiments

Within the last decade, the first indications of higher-order field effects were observed during the development and characterization of ion injection systems (Schwartz and Cooks, 1988; Louris *et al.*, 1989; Pedder *et al.*, 1989; Williams *et al.*, 1991) on the ITMS™. Schwartz *et al.* (1988) first showed the dependence of injected ion intensity on the q_z of injection. No DC was applied to the ring electrode for these experiments (i.e. $a_z=0$). For ion energies ranging from 20 eV to 60 eV, the ion signal minimum was reportedly near $q_z=0.64$ ($\beta_z=1/2$, octopolar resonance). The authors attributed these observations to the power absorption by the ion due to its coincidental oscillation to that of 1/4 of the driving RF frequency (i.e. while stored at $q_z=0.635$ an ion's fundamental frequency is exactly 1/4 the drive frequency).

Louris *et al.* (1989) also showed the dependence of injected ion intensity on the RF trapping voltage. The minimum RF voltage (low-mass-cutoff) required for efficient trapping of injected perfluorotributylamine (PFTBA) ions increased with increasing mass of the injected ion; the minimum q_z required decreased with increasing mass. Interestingly, the ion signal for m/z 69 maximized near $q_z=0.65$; higher m/z ions did not exhibit this behavior. No explanation for this observation was offered. Apparently, the same ion injection system was used for studies by both Louris *et al.* and Schwartz *et al.*, however, no ion minima near $q_z=0.64$ was reported

by Louris *et al.* Note that no DC was applied to the ring electrode for these experiments (i.e. $a_z=0$); therefore only the dependence of q_z along the $a_z=0$ line was evaluated.

Pedder *et al.* (1989) reported that the ion intensity from off-axis ion formation and subsequent injection also was dependent on the RF amplitude. While injecting ions along the $a_z=0$ line (0V DC), ion signal minima were reportedly caused by higher field resonances due to third- and forth-order distortions in the quadrupolar trapping field. Inspection of the plot of ion intensity versus RF voltage, however, revealed a large increase in the injected ion intensity signal near RF levels corresponding to $q_z=0.63$ (octopolar resonance at $\beta_z=1/2$). The exact assignment of the q_z value inhibited the determination of whether this maximum occurs directly on a higher resonance or just off-resonance. These results were similar to that of Louris *et al.* (1989). While applying a negative DC to the ring electrode (i.e. $a_z>0$), investigations of q_z dependence were repeated for the upper portion of the stability diagram. Presenting the data in terms of a topographical plot revealed evidence of other higher field resonances (Randall E. Pedder, private communication). The resonances corresponding to $\beta_z=1/2$ and $2/3$ were observed throughout the upper portion of the stability diagram. Of particular interest, was the evidence of the octopolar sum resonance $\beta_z+\beta_r=1$.

Williams *et al.* (1991) reported resonance effects during ion injection into the quadrupole ion trap. Again, no DC voltage was applied to the ring electrode (i.e. $a_z=0$); therefore only the q_z dependence along the $a_z=0$ line was investigated.

Apparently, the same ion injection system used in these studies was used also in the above studies by Louris *et al.* and Schwartz *et al.*. A plot of injected ion intensity (10 eV) versus β_z of injection revealed maxima near $\beta_z=0.1, 0.32$, and 0.5 . Injecting higher energy ions caused a loss in resolution of the observed resonances. Nevertheless, increased trapping efficiency apparently occurred near RF levels corresponding to β_z values of $1/3$ (dodecapolar) and $1/2$ (octopolar) as evidenced by the increase in ion intensity. To investigate further the observed resonance effects, a supplemental resonance excitation frequency ($6V_{p-p}$) was applied to the endcaps (dipolar mode) while injecting ions into the trap at RF levels corresponding to the various maxima described above (e.g. $\beta_z=1/3, 1/2$). Results from these studies revealed ion losses when the resonance excitation frequency corresponded to $\omega_z/2$, ω_z , $2\omega_z$, $3\omega_z$, and $\Omega-\omega_z$. The frequencies corresponding to ω_z and $\Omega-\omega_z$ were attributed to the well known fundamental and first harmonic of ion motion. The power absorption observed for the $\omega_z/2$ frequency component was attributed to the second harmonic of the supplemental excitation signal; power absorption observed for the $2\omega_z$ and $3\omega_z$ frequencies was attributed to the higher-order hexapolar field superimposed on the supplementary excitation signal.

Resonance Excitation Experiments

Within the last two years, higher-order field effects have been observed during resonance excitation collision-induced dissociation (CID) experiments (Guidugli and Traldi, 1991; Morand *et al.*, 1991; Guidugli *et al.*, 1992; Louris *et al.*, 1992). Guidugli

and Traldi (1991) first reported anomalous behavior during CID experiments; the phenomenon was termed a "black hole". Reportedly, if a CID product ion was created when its q_z during formation was near 0.78, the ion intensity dropped to zero. This was observed for various product ions of two different compounds. Ions created by EI and stored near $q_z=0.78$ for the same amount of time did not show any detectable loss of ion signal. Instrumental parameters such as helium buffer gas pressure and resonance excitation voltage and time reportedly did not influence the CID product ion intensity.

Following the report by Guidugli and Traldi, Morand *et al.* (1991) verified the results near $q_z=0.78$ and identified another "black hole" near $q_z=0.635$. The authors correlated the q_z values to β_z values equal to 0.50 and 0.67. The authors attributed the ion losses to ejection due to overtones of the fundamental drive frequency; at β_z values of 0.5 and 0.67, ion secular frequencies correspond to 1/2 and 1/3 the RF driving frequency, respectively. The authors point out that the ion population may need to be displaced from the center of the trap (i.e. resonance excitation or ion injection) in order to observe these effects.

In a subsequent paper, Guidugli *et al.* (1992) reported further details pertaining to "black holes". A more thorough search for "black holes" lead to the description of "black canyons" along portions of $\beta_z=1/2$ (octopolar) and $2/3$ (hexapolar). To investigate the need to displace the ions from the center in order to observe these effects, CID produced ions were compared to EI produced ions undergoing resonance excitation. The premise for the experiment was to test the

theory that only displacement from the center was needed to observe the effects. The CID product ion displayed ion losses when formed near $q_z=0.78$ with 55 mV excitation for 15 ms; when the same ion (produced by EI) underwent resonance excitation near $q_z=0.78$ with 55 mV for 15 ms, no ion loss was observed. The authors concluded that the extent of ion loss must be different for each mode of ion displacement from the center of the trap. The authors reported also that exciting the ion in the radial direction (quadrupolar excitation at ω_z) did not result in loss of ion signal; excitation in the axial direction (quadrupolar excitation at $2\omega_z$) exhibited the "black hole" phenomenon. To investigate this further, the parent ion was stored near the $\beta_z=0$ stability edge in order to induce fragmentation via radial excitation by the border-induced dissociation (BID, Paradisi *et al.*, 1992) method. Performing this experiment so that the product ion was formed near $\beta_z=2/3$ failed to yield ion losses due to higher field resonances. The authors concluded that the ions need to be displaced in the axial direction in order to observe the higher field resonance.

Louris *et al.* (1992) recently presented ion losses during resonance excitation CID experiments which agreed with those of Guidugli *et al.* (1991, 1992). Interestingly, hexapolar effects at $\beta_z=2/3$ ($q_z=0.78$) during CID experiments were reported to be reduced with the "stretched" quadrupole ion trap geometry as compared to traps with theoretical dimensions. This effect was believed to be due to reduced field penetration through the holes of the endcaps of the "stretched" design.

Mass Range Extension Experiments

Kaiser *et al.* (1991) investigated mass range extension on the quadrupole ion trap. One method examined was to physically reduce the size of the ion trap (i.e. 1/2, 1/3, and 1/4 size) electrodes. Standard sized holes (1/16") were drilled into the vertex of the endcap electrodes for ion introduction and detection. A single hole was drilled in all of the entrance endcaps; seven holes were drilled in the exit endcap of the half-sized trap (similar to the normal sized endcap) and a single hole was drilled in the exit endcap of the third-sized and quarter-sized endcaps. Spectra acquired using these reduced sized quadrupole ion traps exhibited "artifact" peaks of low intensity. The authors attributed the anomalous peaks to prematurely ejected ions due to field imperfections caused by the abnormally large endcap holes. Visual inspection of the published spectra obtained with the half-sized quadrupole ion trap reveal that the ions are ejected at RF levels of approximately 87% to 92% for ejection RF level of the real peak. This could be evidence for ion ejection caused by the $\beta_z=2/3$ resonance line. Spectra obtained with the quarter-sized quadrupole ion trap exhibit more pronounced artifact peaks. When performing mass range extension by resonance ejection on a standard sized quadrupole ion trap, no anomalous peaks were reported (Kaiser *et al.*, 1991).

Higher-order field effects during mass range extension experiments also were observed in our laboratory (Jodie V. Johnson, private communication). During investigations with a $6V_{p-p}$ axial modulation signal at frequencies ranging from 20 kHz to 530 kHz, several characteristics of ion ejection for the m/z ions of PFTBA

(m/z 131, 219, 414, 502, 614) were revealed. At any given q_z of ejection, high m/z ions were detected at higher-than-predicted m/z values; low m/z ions were detected at lower-than-predicted m/z values. In other words, ions of higher m/z appeared to be ejected "more slowly" than low m/z ions. Near q_z of ejection equal to 0.65, however, all ions were detected at lower-than-predicted m/z values (i.e. all ions were ejected "more quickly"). Also, higher m/z ions appeared to be ejected more quickly than the low m/z ions. This observation may be explained assuming that high m/z ions are located in the outer regions of the ion cloud. As q_z of ejection approaches 0.65 (octopolar resonance of the z -type), the ions in the most outer regions of the trapping volume will be influenced to a greater degree than ions near the center.

EI Spectra

Cameron *et al.* (1990) have reported the appearance of anomalous peaks in EI mass spectra of low m/z ions while employing a commercially available quadrupole ion trap. Their studies involved the use of air as a buffer gas for the real-time detection of organic air pollutants. At relatively moderate pressures (1×10^{-5} torr - 1.2×10^{-4} torr) of air ($N_2=28$ Da, $O_2=32$ Da), an anomalous peak at m/z 25 was observed. This was investigated further by employing other buffer gases. Argon (m/z 40) exhibited an anomalous peak at m/z 35, carbon dioxide (m/z 44) exhibited a peak at m/z 38, and krypton (m/z 84) exhibited a peak at 72. Although the authors did not offer an explanation, the anomalous peaks intensities were observed to be pressure dependent. Inspection of the m/z ratios of the anomalous

peak to the parent peak reveals that the anomalous peaks occur at RF levels of approximately 86% to 89% percent of the RF level for ejection of the real peak. This suggests that the anomalous peaks correspond to ejection of the parent ions near the $\beta_z=2/3$ hexapolar resonance line. The q_z value corresponding to the $\beta_z=2/3$ line ($a_z=0$) is 0.79; the ratio of this q_z of ejection to the expected q_z of ejection (0.9065) is: $0.7900/0.9065 = 0.8715$ or approximately 87%.

Lammert *et al.* (1993) recently reported higher-order field effects during acquisition of EI spectra. The authors investigated ion losses near $\beta_z=1/2$ by promoting ion displacement from the center via a short (ns) DC pulse to an endcap electrode. Although EI produced ions were used in the investigation, storage times of between 5 ms and 20 ms were required to observe such effects. They reported that ions formed at $\beta_z=1/2$ showed appreciable ion loss and additional displacement with the DC pulse did not influence the effect. Ions created under stable conditions (away from $\beta_z=1/2$) and then placed near the higher field resonance did not show ion losses unless displaced from the center with the DC pulse.

Alternative Scanning Modes

Todd *et al.* (1991) have investigated alternative scanning modes with the quadrupole ion trap. Instead of the normal mass-selective instability mode (Stafford *et al.*, 1983ab) in which a linear RF voltage ramp (DC=0) causes ions of successively higher m/z to become unstable via the $\beta_z=0$ boundary, the authors examined mass-selective instability via DC voltages and other stability boundaries. During "reverse"

scans, in which the RF and DC voltages were reduced (keeping the ratio constant) forcing the scan line to intersect the $\beta_z=0$ boundary, the authors observed ion ejection due to the octopolar resonance line at $\beta_z=1/2$. During "down" scans, in which the DC voltage was increased at constant RF voltage causing the scan line to intersect the $\beta_z=0$ boundary, ion ejection at $\beta_z=1/2$ also was observed.

Higher-order field resonance effects have been observed (Timothy P. Griffin, private communication) while scanning ions out of the lower portion of the stability diagram. Following a simultaneous RF and DC ramp in order to place ions in the lower portion of the stability diagram, ions were scanned out of the device by mass-selective instability along the $a_z=-0.54$ line (instead of the $a_z=0$ line for normal mass-selective instability). Anomalous peaks were observed which corresponded to ion ejection due to the octopolar resonance line at $\beta_z=1/2$ and the hexapolar resonance line at $\beta_z=2/3$. Employing the simultaneous RF and DC ramp in order to probe the lower portion of the stability diagram, Griffin observed ion losses due to higher-field resonances at $\beta_z=1/3$, $1/2$, and $2/3$. Ion losses in the lower portion of the stability diagram were observed when storing ions for as short as 200 μ s.

Conclusions

This chapter has provided a detailed introduction to the fundamental principles of higher-order fields. The basic premise of an ideally quadrupolar ion trap is investigated as well as the more practical quadrupole ion traps. The geometry and properties of each were discussed and deviations from "ideal" quadrupole ion

trap were presented. Sources of higher-order fields in the quadrupole ion trap employed for all studies in this dissertation were identified. The primary sources of higher-order even fields were electrode truncation and symmetric displacement of each endcap (i.e. "stretched" geometry); sources of higher-order odd fields are holes in the endcaps and field penetration.

A theoretical treatment of higher-order fields was given. Equations for calculating the storage field potential throughout the quadrupole ion trap for any contribution of higher-order fields were discussed. "Constructive" contributions of higher-order fields (i.e. with the same sign as the quadrupolar field) cause the trapping field strength to increase more than linearly with distance from the center of the ion trap; "destructive" contributions (i.e. opposite sign as the quadrupolar field) cause the field strength to increase less than linearly. The observed field strength is assumed to be the cause of improved resolution obtained with a quadrupole ion trap superimposed with a small percent of "constructive" octopolar fields (Louis *et al.*, 1992; Franzen *et al.*, 1989).

Higher-order field resonance lines were identified on the Mathieu stability diagram. Several resonances exist for each higher-order field. The contribution of even and odd higher-order fields decreases with increasing order; therefore, hexapolar (3rd-order) and octopolar (4th-order) fields are primarily responsible for the influence of stored ions.

CHAPTER 3 CHARACTERIZATION OF HIGHER-ORDER FIELD EFFECTS

Introduction

This chapter will present characterization studies of higher-order field effects on stored ions in the quadrupole ion trap. The $C_2H_5^+$ ion, derived from ion/molecule reactions of methane, will be used as a chemical probe for the majority of the characterization studies; the molecular ion of n-butylbenzene also will be used. Higher-order field effects will be investigated with regards to the influence of several instrumental factors. Due to the capability of user-defined scanning strategies, the user can control several instrumental parameters which define the type of experiment to be performed with the quadrupole ion trap (i.e. acquisition of EI, CI, or MSⁿ spectra). Therefore, understanding the influence of each parameter in relation to higher-order field effects is of particular concern. The following parameters were investigated and will be discussed in this chapter: ion displacement, storage conditions (q_z , a_z values), ion population, storage time, multiplier/dynode voltage (field penetration), and endcap electrode spacing.

Ion Displacement from the Center of the Quadrupole Ion Trap

The most significant factor contributing to the observation of higher-order field effects is ion displacement from the center of the trap. As discussed in Chapter 2, and shown in Figure 2-4a, higher-order field contributions are insignificant near the center of the ion trap where a purely quadrupolar field exists. Higher-order field potentials increasingly deviate from the "ideal" quadrupolar field with increasing distance from the center of the trap; therefore, ions displaced from the center will be influenced to a higher degree than ions stored in the center of the device. In fact, the majority of the previously reported observations of higher-order field effects can be attributed directly to the displacement of the ions from the center of the ion trap. In general, ion displacement from the center of the trap can be caused by:

1. high ion population
2. absence of buffer gas
3. resonance excitation
4. ion injection
5. ion formation near electrodes
6. ion storage near stability boundaries

High ion populations result in ion-ion repulsions causing the stored ions to be displaced from the center. This is further enhanced by the absence of buffer gas due to longer times required for the ion trajectories to damp down towards the

center of the trap following ionization. This increased damping time allows the ions more time to be influenced by the nonideal field in the outer regions.

Resonance excitation, by design, displaces the ions from the center due to the increased axial (and possibly radial) trajectories of the excited ion. Excitation times can approach 10-50 ms allowing time for the ions to be influenced by the higher-order fields. As discussed in Chapter 2, several groups have reported higher-order field effects during resonance excitation MS/MS experiments (Guidugli and Traldi, 1991; Morand *et al.*, 1991; Guidugli *et al.*, 1992; Louriis *et al.*, 1992).

Ion injection experiments will be influenced by higher-order field effects. Injected ions first experience the trapping field while in the extreme outer regions of the trapping volume. Also discussed in Chapter 2 are several reports of higher-order field effects during ion injection experiments (Schwartz and Cooks, 1988; Louriis *et al.*, 1989; Pedder *et al.*, 1989; Williams *et al.*, 1991b). Another form of ion displacement, which is similar to ion injection, is ion formation in the outer regions. Electrons (or CI reagent ions) can form ions anywhere in the trapping volume. Electron trajectory simulations (Pedder and Yost, 1988) show that electrons will strike the ring electrode when entering the trapping volume during a positive phase of the RF; electrons strike the endcap electrodes when entering the trapping volume during a negative phase of the RF. Consequently, ions can be created near any one of the three electrodes when employing internal electron ionization. Additionally, ions can be formed near the electrodes by other ionization techniques such as internal laser desorption.

Ion displacement also can be caused by the storage conditions (i.e. q_z , a_z values). The amplitude of the ion trajectories is dependent on the q_z , a_z values. Storage at very high q_z values cause increased axial trajectory amplitudes. Indeed, the mass-selective instability scan mode (Stafford *et al.*, 1983ab) exploits this phenomenon in order to eject the ions out of the ion trap towards a detector. During the instability scan, the q_z value of the ion approaches the $\beta_z=1$ stability edge causing the amplitude of the ion trajectory in the axial direction to exceed the limits of the trapping volume. Operating under $a_z \neq 0$ condition (i.e. RF/DC mode) also alters the ion trajectories. Simulations (Reiser *et al.*, 1992; March *et al.*, 1992) suggest that application of a positive DC voltage results in an increase in the ion trajectory amplitude in the z-direction and decrease in the r-direction; alternately, the application of a negative DC voltage causes increased radial amplitudes and decreased axial amplitudes.

The majority of the previously reported higher-order field effects have been observed as a direct result of ion displacement from the center. Others can be attributed to alternative scanning modes in which the ion trap was operated in regions of the stability diagram where higher field resonances converge or are enhanced (see characterization studies below). Until now, no effects have been observed during ion storage without the prerequisite of ion displacement. This chapter will identify higher-order field effects observed during normal ion storage. These effects will be characterized with regards to several instrumental parameters.

Experimental

Experiments were performed on a Finnigan MAT (San Jose, CA, USA) ion trap mass spectrometer (ITMS™) maintained at 100° C. Field penetration studies were performed on a modified Finnigan MAT ITS-40™ benchtop instrument (Yates *et al.*, 1993). Careful measurements of each ion trap assembly produced z_0 distances of 0.785 cm for the ITMS™ ion trap and 0.793 cm (Timothy P. Griffin, private communication) for the ITS-40™ ion trap. Helium (Liquid Air, Walnut Creek, CA) was used as the buffer gas in both instruments. Methane (Matheson Gas Products, Morrow, GA) was introduced into both the ITMS™ and the ITS-40™ via a fine metering valve (Negretti, Southampton, England). The n-alkylbenzenes (Eastman Kodak, Rochester, NY) were introduced into the ITMS™ via a Granville-Phillips (Boulder, CO) variable leak valve mounted directly on a 1/2" O.D. stainless steel probe. Pressures on the ITMS™ were read directly off a Bayard-Alpert ionization gauge (Granville-Phillips, Boulder, CO) and are reported with no correction factors. An ion gauge was added onto the vacuum chamber (Yates *et al.*, 1993) of the ITS-40™ instrument. Due to the high population of ions created by the ion gauge, the ITS-40™ instrument could not be operated while obtaining pressure readings. Typical indicated pressures for all experiments were 1.1×10^{-4} Torr for helium (corresponding to a corrected pressure of approximately 9×10^{-4} Torr), 1.0×10^{-5} Torr for methane and 2.0×10^{-6} torr for the n-alkylbenzenes. It should be noted that gases are introduced directly into the ion trap of the ITS-40™, thus, the pressure is approximately ten fold higher in the ITS-40™ than in the ITMS™.

The instrument software, ICMS© (developed by Nathan A. Yates, University of Florida), was used for all experiments on the ITMS™. The software allowed data acquisition while incrementing the RF amplitude by the RF digital-to-analog converter (DAC) step or by incrementing the low mass cutoff (LMCO). For these experiments, a FORTH procedure was used to increment the RF amplitude by a user-defined ΔLMCO value, typically 0.2 Da. The scan function used for these experiments employed a 1 ms ionization time at $q_z=0.3$ followed by a variable ion/molecule reaction period. The ion of interest was mass-selected by RF/DC "apex" isolation at $q_z=0.78$, $a_z=0.15$ (Weber-Grabau *et al.*, 1987; Todd *et al.*, 1987). The RF amplitude was then ramped to the desired q_z value for ion storage for up to a maximum of 100 ms.

The instrument software, GATORWARE (developed by Timothy P. Griffin, University of Florida), was used for all experiments on the ITS-40™. The software allows the creation of user-defined scan functions, a feature not available from the manufacturer of this instrument. A scan function, similar to that used with the ITMS™, was used with the ITS-40™. The software also allows data acquisition while incrementing the RF amplitude by a user-defined Δq_z value. The relevant procedure language code required to increment the RF on the ITS-40™ is shown below:

```

FORTH 150 PROCEDURE <TIMES> FORTH / loop 150 times
      1 . SCN-COUNTER . / set scan counter
      9 DUP -> CRNT-TABLE GET-TABLE / identify scan table
      002. D+ TABLE-END-Q / increment  $q_z$  by 0.002
      CALC-SAP-VALUES TABLE-FILE / set sap value
      LOAD-SCAN GET-NEXT-SCAN / load new scan function
PROCEDURE <LOOP> / and take scan

```


All calculations were performed according to the corrected equations for the "stretched" ion trap design (Johnson *et al.*, 1992). All ITMS™ data reduction was performed using the BASIC program, CHROLIST (written by Randall E. Pedder and Nathan A. Yates, University of Florida), which retrieved original ITMS™ data files, averaged selected mass intensities, and wrote the data into a tabular ASCII format. ITS-40™ data reduction was performed using the C++ program, ITCRUNCH (written by Timothy P. Griffin, University of Florida), which retrieved the ASCII file created by the procedure code used above, averaged selected mass intensities, and wrote the data into a tabular ASCII format. All data manipulation was performed with the commercial spreadsheet program QUATTRO (Borland International, Inc., Scotts Valley, CA). The q_z values were calculated by first determining the low mass cutoff by multiplying the corresponding DAC value by the experimentally determined slope of the calibration curve for low m/z ions (e.g. 6.314 DACS/amu). The low mass cutoff was then used in the equation below to calculate the q_z value:

$$q_z = \frac{\text{LowMassCutoff} * q_{z,\text{ejection}}}{m/z} \quad (3-1)$$

All β_u values and ion frequency determinations were calculated by the BASIC program AQFORM (written by Donald M. Eades and Matthew Booth, University of Florida). This program uses the continued fraction method (McLachlan, 1947) for β_u calculations (see Equation 1-13 of Chapter 1).

The RF trapping frequency was 1.1 MHz for the ITMS™ and 1.05 MHz for the ITS-40™. A $6V_{pp}$ axial modulation (Weber-Grabau *et al.*, 1988; Tucker *et al.*, 1988) signal was employed at 530 kHz (resonance ejection at $q_z=0.906$) for the ITMS™ and 485 kHz for the ITS-40™ (ejection at $q_z=0.8922$), each applied during the mass-selective instability scan (Stafford *et al.*, 1983ab). The electron multiplier (EM) voltage was set to yield 10^5 gain on each instrument and no conversion dynode voltage was used. A grounded shield was present in front of the dynode/EM assembly of the ITMS™. The multiplier (no dynode) of the ITS-40™ was located directly behind the exit endcap of the ion trap assembly.

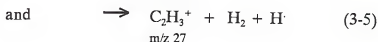
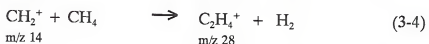
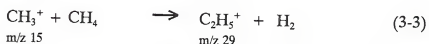
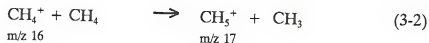
The endcap distances were varied by constructing new spacers for the ion trap assembly. The spacers delivered by Finnigan MAT have a width of 1.040 cm which produced a z_0 of 0.785 cm. To construct spacers to yield $z_0=0.7071$ cm, the width of the spacers were machined to 1.000 cm (i.e. decreased by 0.040 cm); this amount corresponds to $(0.785 \text{ cm} - 0.7071 \text{ cm}) / 2 = 0.040 \text{ cm}$. The difference is divided by two for displacement of each endcap electrode.

$C_2H_5^+$ as a Chemical Probe

To characterize higher-order field effects on stored ions, a sensitive chemical probe is required; furthermore, changes in the probe ion need to be observed easily. An ion that readily absorbs power, for example, can be monitored by observing ion ejection, the collision-induced dissociation (CID) product ions, or ion/molecule reaction products. Some chemical species, however, do not readily undergo any of

these obvious observable changes; these species are unlikely candidates as sensitive probes to higher field resonances. For example, due to their unreactivity or inability to undergo CID, ions such as Ar^+ , m/z 40, and the benzene molecular ion, m/z 78, are unlikely candidates for probe ions. In order to be truly sensitive to the resonances, subtle changes in the probe ion need to be observed easily (i.e. ejection, CID, or ion/molecule reactions).

The probe ion employed for the characterization studies was the ion/molecule reaction product of methane, C_2H_5^+ . This ion is created in the following manner: upon electron ionization (EI) of neutral methane, the major ions formed are CH_4^+ , CH_3^+ , and CH_2^+ which, in turn, react with neutral methane according to the following reactions (Harrison, 1992):



with



Following EI, all of the above listed ions are present, the ratios of which are dependent on the methane pressure and duration of ion storage. If these reactions

are allowed to continue, $C_2H_5^+$ will increase for a period of time until the final product ion, $C_3H_5^+$, eventually dominates. Storage times required for the optimum production of $C_2H_5^+$ can be determined for any pressure of methane; typical reaction times employed throughout this dissertation are between 5 and 20 ms.

Once the $C_2H_5^+$ ion population was maximized, all other m/z ions were removed from the ion trap by the selectively isolating $C_2H_5^+$, m/z 29. Although all other m/z ions have been removed, $C_2H_5^+$ can continue to react with any neutral species within the trapping volume (e.g. methane, water). This process ultimately depletes the total number of probe ions available for the experiment. Indeed, increasing the storage time of $C_2H_5^+$ while storing at a low mass cutoff below m/z 19, exhibits a continual increase in the H_3O^+ ion and a decrease in the $C_2H_5^+$ ion due to proton transfer to the neutral water molecules.

To monitor the effects from higher-order fields, $C_2H_5^+$ was stored for a relatively long period of time (e.g. 100 ms). Following the storage period the ions are detected and the intensity is recorded. Taking in to account all of the ions present, the resulting ion intensity can be used as an indication of storage efficiency; a reduction in the ion intensity corresponds to reduced storage efficiency and an increase in the ion intensity corresponds to an improved storage efficiency. Figure 3-1 shows the intensity of the $C_2H_5^+$ probe ion versus the RF level in terms of both its Mathieu stability parameter, q_z , and its low mass cutoff. In this particular experiment the ion was stored for 50 ms and no DC was applied; therefore, the data was acquired only along the $a_z=0$ line.

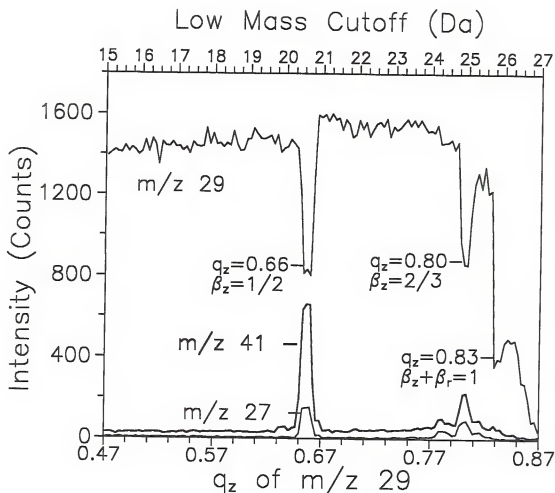
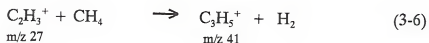
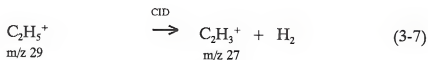


Figure 3-1: Intensities of $C_2H_5^+$ (m/z 29) and CID product ions, $C_2H_3^+$ (m/z 27) and $C_3H_5^+$ (m/z 41) versus q_z of m/z 29 for 50 ms storage ($a_z=0$) of mass-selected m/z 29 ions. Intensity losses correspond to $\beta_z=1/2$ (octopolar), $\beta_z=2/3$ (hexapolar), and $\beta_z+\beta_r=1$ (octopolar).

Although the ion intensity was relatively constant for $q_z < 0.60$, near $q_z = 0.65$ and $q_z = 0.80$ signal minima for m/z 29 were observed along with corresponding increases in m/z 27 and 41. The loss of ion signal beyond $q_z = 0.85$ was due to inefficient storage near the ejection edge ($q_z = 0.906$ with axial modulation). The ion signal minima at $q_z = 0.65$, $q_z = 0.80$, and $q_z = 0.83$ correspond to the higher-order field resonance lines which are plotted on the Mathieu stability diagram shown in Figure 3-2. The q_z values associated with the signal minima correspond to the $\beta_z = 1/2$ (octopolar), $\beta_z = 2/3$ (hexapolar), and $\beta_z + \beta_1 = 1$ (octopolar) resonances, respectively. At these q_z values, the $C_2H_5^+$ ion of methane absorbed power from the higher-order fields and underwent energetic collisions with the helium buffer gas molecules which caused dissociation to form m/z 27, which can then react with neutral methane to form m/z 41 as follows (Harrison, 1992):



The reaction pathway was confirmed by resonance excitation CID of m/z 29 at q_z values free of higher field resonances (i.e. $q_z = 0.50$, $a_z = 0$). The inefficient storage near $q_z = 0.65$ and 0.80 agrees with the q_z values observed for loss of product ion signal from previously reported MS/MS experiments (Guidugli and Traldi, 1991; Morand *et al.*, 1991; Guidugli *et al.*, 1992; Louris *et al.*, 1992).

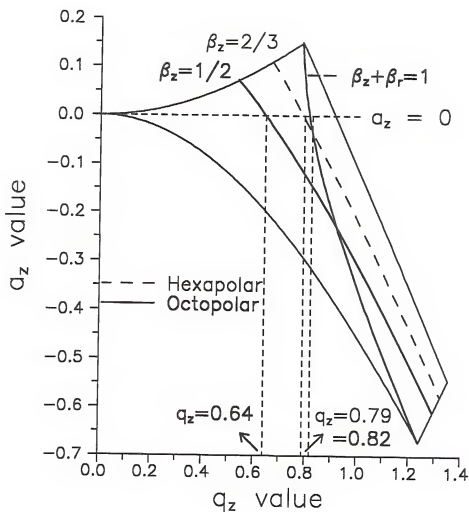


Figure 3-2: Mathieu stability diagram along with higher field resonances corresponding to the experimentally observed losses of $C_2H_5^+$ (m/z 29) ion intensity. The resonances correspond to $\beta_z = 1/2$ (octopolar), $\beta_z = 2/3$, and $\beta_z + \beta_r = 1$ (octopolar).

In the present study, however, no ion displacement was required in order to observe higher-order field effects. It should be noted that higher-order field effects can be observed without mass-isolating the ion of interest; with isolation, however, the effects become more apparent by simplifying the mass spectrum to the selected m/z ion and its associated product ions. Although the loss of ion signal for m/z 29 at $q_z=0.8$ was comparable to the loss at $q_z=0.66$, the corresponding increase in the product ions, m/z 27 and 41, was less due to the fact that the low mass cutoff is approaching m/z 27. Since m/z 41 is produced via the m/z 27 intermediate and the storage conditions are not as favorable for m/z 27, the production of m/z 41 is lower at $q_z=0.80$. As demonstrated in Figure 3-1, both the ion loss of m/z 29 and the production of m/z 41 is, therefore, easier to observe for the octopolar resonance at $\beta_z=1/2$ ($q_z=0.65$) than the hexapolar resonance at $\beta_z=2/3$ ($q_z=0.80$) and the octopolar resonance at $\beta_z+\beta_r=1$ ($q_z=0.83$).

The $C_2H_5^+$ probe ion is very sensitive to the effects of the higher field resonances due to its ability to easily undergo CID and ion ejection; therefore, monitoring the effects is easily accomplished by detecting either the loss of m/z 29 or the increase in the ion signals for m/z 27 and/or 41. Figure 3-3 shows the conversion of m/z 29 to its CID and ion/molecule reaction products while stored near the octopolar resonance at $q_z=0.65$, $a_z=0$ ($\beta_z=1/2$). The m/z 27 ion reached a pseudo steady state as it was created from the CID of m/z 29 and reacted with neutral methane to form m/z 41. The m/z 41 ion signal increased linearly with storage time while the m/z 29 ion linearly decreased with reaction time.

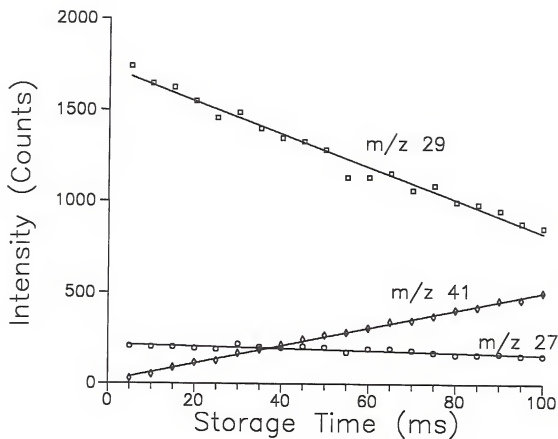


Figure 3-3: Intensities of $C_2H_5^+$ (m/z 29) and CID product ions, $C_2H_3^+$ (m/z 27) and $C_3H_5^+$ (m/z 41) versus storage time near the $\beta_z=1/2$ (octopolar) resonance ($q_z=0.65$, $a_z=0$).

Parameters Influencing Observation of Higher-Order Field Effects

Storage Conditions (q_z , a_z Parameters)

To characterize the influence of storage conditions on higher-order field effects, experiments similar to that described for Figure 3-1 were repeated along other a_z lines (various applied DC voltages) as shown in Figure 3-4. The experimental results corresponding to ion storage along the $a_z = +0.023$ line (-5 V DC) and the $a_z = -0.047$ line ($+10$ V DC) are shown in Figures 3-5a and 3-5b respectively. Although not shown in the figures, an increase in m/z 27 and 41 mirror each loss of intensity of m/z 29. Note that the intensity minima appeared at different q_z values for each a_z line as predicted by Figure 3-4.

Comparison of results for the $a_z = +0.023$ line (-5 V DC) and the $a_z = -0.047$ line ($+10$ V DC), reveals an increased intensity loss for $a_z < 0$ ($+DC$). Note that in this context, loss of $C_2H_5^+$ ion signal refers to both ion ejection and conversion to m/z 27 and 41 via CID and subsequent ion/molecule reactions. Furthermore, an increased affected mass range (i.e. greater width of loss band at 10% maximum loss) also occurred for $a_z < 0$ ($+DC$). In general, effects of higher-order field resonances on stored ions were observed to be increasingly more pronounced with increasingly negative $a_z = 0$ values (i.e. increasingly positive DC voltages). This can be seen more clearly in Figures 3-6a and 3-6b where the results from a similar study are plotted in terms of % $C_2H_5^+$ remaining (Figure 3-6a) and affected mass range (Figure 3-6b) versus the a_z value during storage (applied DC voltage).

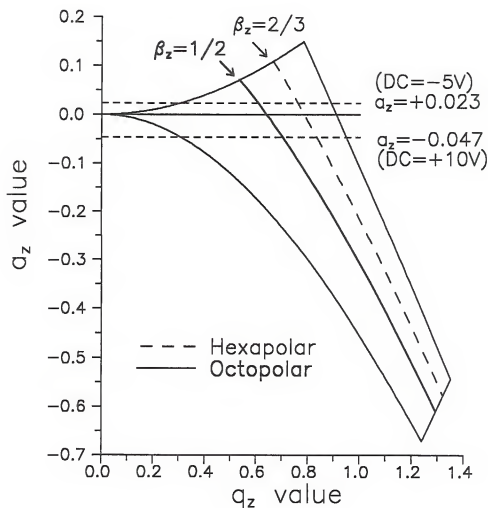


Figure 3-4: Mathieu stability diagram showing the storage lines used to compare the influence of a_z (DC voltage) storage conditions on higher-order field effects.

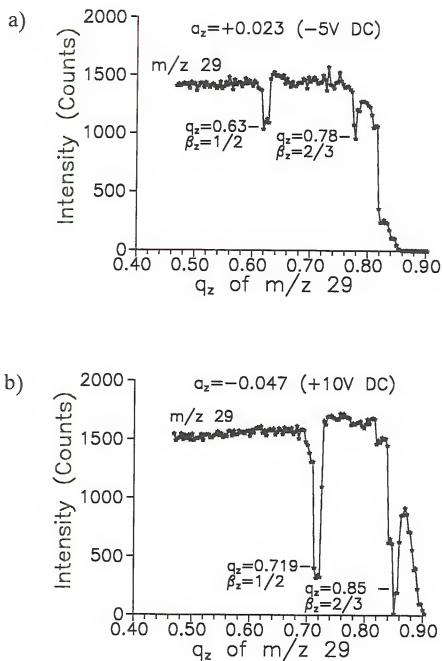


Figure 3-5: Intensity of $C_2H_5^+$ (m/z 29) versus q_z of m/z 29 following 50 ms storage at a) $a_z = +0.023$ (DC = $-5V$) and b) $a_z = -0.047$ (DC = $+10V$). Intensity losses correspond to $\beta_z = 1/2$ (octopolar) and $\beta_z = 2/3$ (hexapolar).

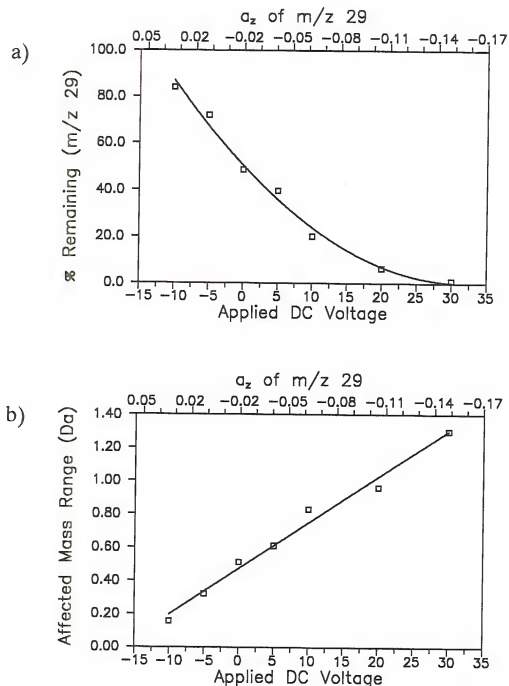


Figure 3-6: Influence of the a_z stability parameter (DC voltage) on higher-order field effects in terms of a) magnitude of ion loss and b) magnitude of affected mass range (ΔDa).

Note that the data used for Figures 3-6a and 3-6b were acquired along an iso- β_z resonance line as opposed to an iso- q_z line. In essence, these plots represent a gauge for the "width" and "depth" of the ion signal loss bands. With application of increasingly negative a_z values (positive DC voltage), the $C_2H_5^+$ ion signal exhibited a linear decrease until approximately 80% had been lost (Figure 3-6a). The relationship indeed may be completely linear; however, the deviation from linearity observed with low ion signals may be a result of inaccurate ion signal measurements and ion/molecule reactions. The relationship between the affected mass range and the a_z value used for storage (Figure 3-6b) was linear over the range studied. In this particular case, the affected mass range is 0.5 Da along the $a_z=0$ line and over 1.0 Da near the $a_z=-0.15$ line (DC = +25 V). As demonstrated in other sections below, the mass range can be affected additionally by the influence of other parameters (i.e. ion population and storage time).

The influence of the a_z stability parameter can be attributed to the changes in the amplitude of the ion trajectory in the z-direction as a result of the applied DC potential. Published simulation studies (March *et al.*, 1992) of RF/DC apex isolation have shown that radial amplitudes increase and axial amplitudes decrease with increasingly negative applied DC voltages. When the DC voltage was returned to 0V DC, simulated axial motions were observed to increase until reaching the same amplitude of motion as before the application of DC. Indeed, this trend also was observed in simulation studies employing both the ITSIM (Reiser *et al.*, 1992) and HYPERION (Pedder and Yost, 1988) programs. Upon application of a +DC

voltage to the ring electrode, simulated axial amplitudes increased and radial amplitudes decreased; application of -DC to the ring caused increased radial and decreased axial amplitudes. Since the higher field resonances observed during this experiment are all of the z-type and thus absorb power only in the z-direction (Wang *et al.*, 1993), it follows that the effects become more apparent with increased axial motion. Indeed, this agrees with the results by Guidugli *et al.* (1992) in which ion displacement via axial resonant excitation resulted in the observation of higher-order field effects while displacement via radial resonant excitation did not.

The influence of the a_z stability parameter (applied DC voltage) was investigated further by using a higher m/z probe ion. The advantage of using a higher m/z ion is two-fold: not only can a higher applied DC voltage be investigated, but also the effects of higher-order fields on a more complex organic molecule. The compound chosen for these studies was n-butylbenzene; the molecular ion ($M^+ = 134$) was chosen as the probe ion for its ease of fragmentation upon resonant excitation. The main CID fragment ions are $C_6H_5CH_2^+$, m/z 91, and the lower energy fragment $C_6H_5CH_3^+$, m/z 92. This compound has been used extensively to characterize resonance excitation CID on the quadrupole ion trap (Harrison and Lin, 1983; Johnson *et al.*, 1990a).

Figure 3-7a shows the effects of varying the q_z value for 50 ms storage of the M^+ ion (m/z 134) along the $a_z = 0.041$ line (-40V DC). Near $q_z = 0.60$, the ion undergoes ejection and CID. Note that the CID product ions at m/z 91 and 92 can not be observed due to the high value of the low mass cutoff (i.e. $q_z = 0.65$

corresponds to a low mass cutoff of 96 Da). The product ion, m/z 92, near the left edge of Figure 3-7a represents evidence of boundary-induced dissociation (Paradisi *et al.*, 1992), a similar process to resonance excitation CID. However, the excitation source arises from increased ion amplitudes near the stability boundary, and thus is not directly related to higher-order field effects.

Figure 3-7b shows the effects of varying the q_z value of the n-butylbenzene M^+ ion (m/z 134) while storing for 50 ms in the lower portion of the stability diagram along the $a_z = -0.204$ line (DC = +200V). Note that the three minima correspond to β_z values of 1/3 (dodecapolar, not typically observed at $a_z \geq 0$), 1/2 (octopolar) and 2/3 (hexapolar). This is the first report for the evidence of contributions from the dodecapolar field. The effects of the dodecapolar ($\beta_z = 1/3$) and hexapolar ($\beta_z = 2/3$) resonance lines are not observed in the upper portion of the stability diagram (e.g. $a_z < 0.041$, DC = -40 V) for n-butylbenzene in the above case. Again, this is due to the reduced axial motion caused by the applied -DC potential. Both the magnitude of the loss of ion signal and the affected mass range (i.e. the width of the intensity loss band at 10% maximum loss) are increased significantly when storing ions in the lower portion of the stability region. Storage of the M^+ ion of n-butylbenzene coincidental with the application of +200V DC demonstrates that 90% of the ion signal is lost due to the octopolar resonance at $q_z = 0.894$ and that over 50% of the ion signal is lost beyond $q_z = 0.92$.

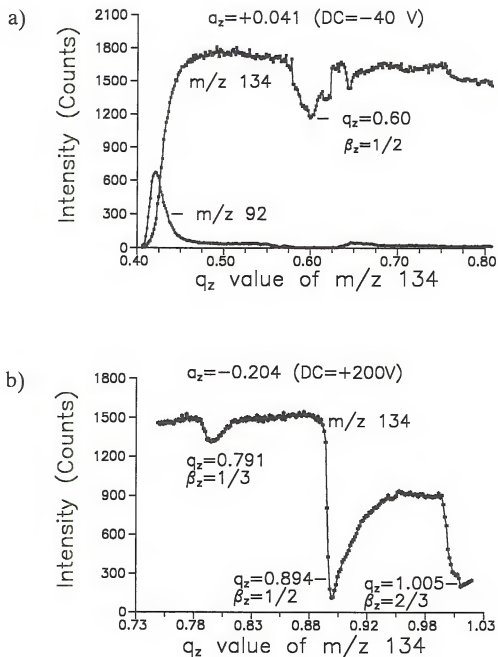


Figure 3-7: Intensity of the mass-selected M^+ ion (m/z 134) of *n*-butylbenzene and fragment ion, m/z 92, versus q_z following 50 ms storage at a) $a_z = +0.041$ (DC = -40 V) and b) $a_z = -0.204$ (DC = +200 V). Intensity losses correspond to a) $\beta_z = 1/2$ (octopolar) and b) $\beta_z = 1/3$ (dodecapolar), $\beta_z = 1/2$ (octopolar), and $\beta_z = 2/3$ (hexapolar).

Ion Population

Ion population significantly influences higher-order field effects. Increasing the number of stored ions increases ion/ion repulsions causing displacement of ions from the center of the trap. Since higher-order fields increasingly deviate from the "ideal" quadrupolar field with increasing distance from the center of the trap, ion displacement from the center will increase the interaction of the ion with the non-"ideal" field. The $C_2H_5^+$ ion (m/z 29) again was used as a chemical probe to investigate the influence of ion population on higher-order field effects. Figure 3-8a compares the effects during storage of two ion populations created by increasing the ionization time. Here, ion population is defined as the intensity of mass-selected m/z 29 ions (expressed as ion counts) following 50 ms storage at a q_z value where higher-order field effects are not observed (i.e. $q_z=0.50$, $a_z=0$). Although not plotted in these figures, corresponding increases in the m/z 27 and 41 intensity mirror the intensity loss of m/z 29.

As noted in the previous studies, major losses in the m/z 29 signal occurred at resonance lines at $\beta_z=1/2$ (octopolar) and $\beta_z=2/3$ (hexapolar) corresponding to $q_z=0.65$ and 0.80 , respectively ($a_z=0$). Note in Figure 3-8a the dramatic enhancement of the higher-order field effects with the higher ion population. Increasing the ion population markedly increased both the magnitude of ion loss and affected mass range. The cause for the increased effects with the higher population can be attributed to increased ion-ion repulsions resulting in increased ion displacement from the center of the ion trap, thus allowing further interaction

between ions and higher-order fields. Also, the high charge density may induce a small DC potential on the electrodes (Fischer, 1959; Sheretov *et al.*, 1973; Fulford *et al.*, 1980) which reportedly can shift the entire stability diagram; this may itself be a source of higher-order fields.

Note also, that the signal minima exhibited a shift with increasing ion population. In Figure 3-8a, the signal minima, corresponding to the octopolar resonance at $\beta_z=1/2$, occurred at $q_z=0.656$ and 0.675 for the low and high populations, respectively. An even larger (approximate 10-fold) increase in ion population exhibited a shift corresponding to $q_z=0.03$ (~ 1 Da). As shown in Figure 3-8b, a linear shift was observed with increasing ion population. This observation is very important in that the q_z values corresponding to the signal minima were used in the calculation for the β_z resonance locations. Indeed, nearly every calculation for β_z slightly deviated from the theoretically predicted value; this deviation can be attributed to the ion density in the trapping volume. This phenomenon has been used to measure the absolute number of ions stored in an ion trap (Fulford *et al.*, 1980). Other experiments also have exhibited space charge induced resonance shifts of stored ions (Yates *et al.*, 1991b).

Figure 3-9 shows the influence of increasing the ion population during ion storage of m/z 29 ($C_2H_5^+$) near the octopolar resonance line at $\beta_z=1/2$ ($q_z=0.65$, $a_z=0$). By plotting the intensity of m/z 41 ($C_3H_5^+$) as a function of $C_2H_5^+$ ion population, the extent of CID (and subsequent ion/molecule reaction to form m/z 41) can be monitored as the number of $C_2H_5^+$ ions initially trapped is increased.

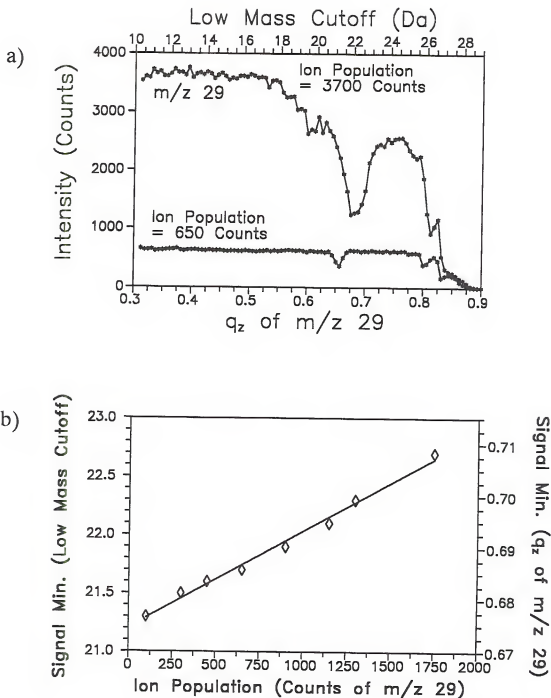


Figure 3-8: Influence of ion population on higher-order field effects in terms of a) magnitude of ion loss and b) shift in signal minimum (i.e. location of $\beta_z=1/2$ resonance in terms of low mass cutoff). The main ion loss band is due to the $\beta_z=1/2$ octopolar resonance.

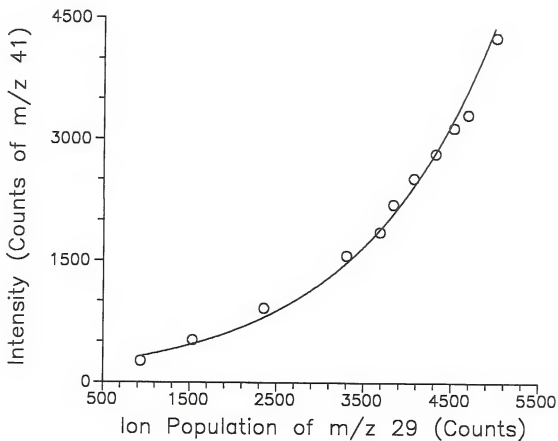


Figure 3-9: Influence of ion population of $C_2H_5^+$ (m/z 29) on the production of the $C_3H_5^+$ ion (m/z 41) originating from CID of $C_2H_5^+$ (and subsequent ion/molecule reaction) due to the octopolar resonance ($\beta_z=1/2$).

As more $C_2H_5^+$ ions are created and trapped, the extent of conversion of $C_2H_5^+$ to $C_3H_5^+$ increases. The exponential trend of Figure 3-9 demonstrates that storage of a very high population of ions markedly increases higher-order field effects. Note that to obtain the data in Figure 3-9, the q_z value for ion storage was optimized for each ion population by first obtaining data of the type shown in Figure 3-8a.

Storage Time

Storage time directly influences the ability to observe higher-order field effects; ion storage at q_z , a_z values where higher-order field effects are not observed (e.g. $q_z=0.5$, $a_z=0$) virtually has no influence on ion signal. As demonstrated in Figure 3-10a, longer storage times allow more interaction with the higher-order fields thus causing increased ion losses at the octopolar resonance ($\beta_z=1/2$) and the hexapolar resonance ($\beta_z=2/3$). Also note that longer storage times caused an earlier onset of ion ejection near the $\beta_z=1$ boundary (near $q_z=0.90$). Increasing the storage time allows more time for the ions to "leak" out of the trap.

The graph in Figure 3-10b shows the influence of storage time on three populations of mass-selected $C_2H_5^+$ ions stored near the octopolar resonance line at $\beta_z=1/2$ ($q_z=0.65$, $a_z=0$). Again, the intensity of m/z 41 was plotted as a gauge for the conversion of m/z 29 to its CID product ions. Longer storage times allowed the m/z 29 ions to absorb more power causing further CID (and subsequent ion/molecule reactions), as evidenced by the linear increase in the $C_3H_5^+$ ion intensity.

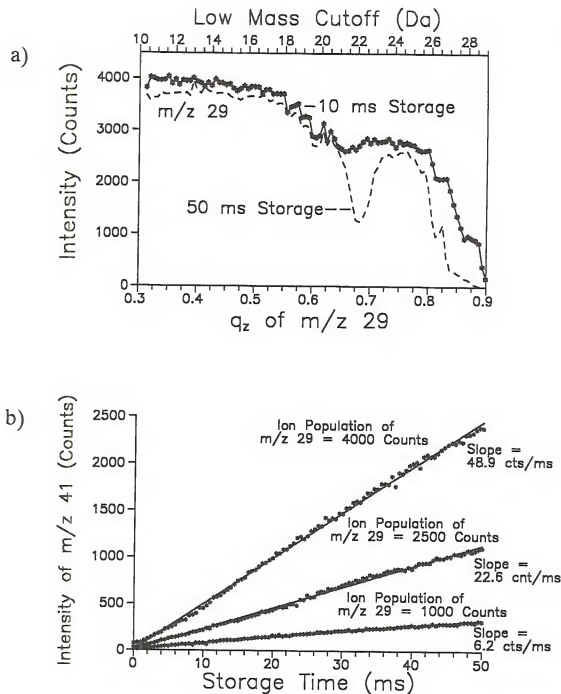


Figure 3-10: Influence of ion storage time on higher-order field effects in terms of a) magnitude of loss of the $C_2H_5^+$ ion and b) production of the CID product ion, $C_3H_5^+$ (m/z 41) while storing $C_2H_5^+$ (m/z 29) near the $\beta_2=1/2$ (octopolar) resonance ($q_z=0.65$, $a_z=0$).

Increasing the ion population by 2.5 and 4.0 fold increased the rate of production of the 41^+ ion by a factor of 3.6 and 8.0 respectively. The production of m/z 41 to a total population of 200 counts required 32 ms for the lower ion population (1000 counts of m/z 29), 9 ms for the intermediate population (2500 counts of m/z 29), and only 4 ms for the higher ion population (4000 counts of m/z 29). This trend was expected to continue; therefore, experiments utilizing very high ion populations (i.e. EI and CI of a complex mixture) will suffer from higher-order field effects even at very short storage times (<5 ms).

Mass-to-Charge Ratio (m/z)

To investigate the influence of m/z value on the higher-order field effects, a series of *n*-alkylbenzenes were used for comparison (alkyl = ethyl, butyl, heptyl, octyl). This series of compounds was employed in order to minimize the variability in the chemical structure of the ion. Each *n*-alkylbenzene molecular ion (M^+) undergoes a similar fragmentation mechanism upon resonance excitation CID (i.e. the major CID product ions are $C_6H_5CH_2^+$, m/z 91, and the lower energy fragment $C_6H_5CH_3^+$, m/z 92). The values for the M^+ ions investigated were m/z 106 for *n*-ethylbenzene, m/z 134 for *n*-butylbenzene, m/z 176 for *n*-heptylbenzene, and m/z 190 for *n*-octylbenzene.

Comparisons of higher-order field effects as a function of m/z of the *n*-alkylbenzenes suggest that the effects are virtually independent of m/z . In other words, ions of all m/z values appear to be affected equally, provided an equal

number of ions are stored for an equal time at q_z values corresponding to non-linear resonances. Under identical conditions (number of ions, storage time, q_z and a_z value), ions of differing m/z exhibit nearly identical intensity losses. As shown in Figure 3-11a, the affected mass range (i.e. the width of the loss band at 10% loss), when plotted in terms of low mass cutoff (ΔDa), exhibits a linear dependence on m/z . The very relationship between q_z and low mass cutoff (LMCO) predicts linearity with the intersection at the origin. When the RF range is expressed in terms of Δq_z , as shown in Figure 3-11b, a slight negative trend is observed (as opposed to the theoretically predicted slope of 0). Again, the nearly zero slope is due to the inverse relationship of q_z to m/z ; equal Δq_z values for two m/z ions will generate different affected mass ranges in terms of ΔDa (LMCO) or ΔRF voltage.

The slightly negative slope observed when plotting the affected mass range in terms of q_z can be explained if the "ideal" case is considered. Ideally, the ions under investigation would exhibit varying m/z which require identical amounts of power to induce fragmentation. In the "ideal" case, identical ion population and storage times should generate identical results when stored at the same q_z , a_z conditions. The results would exhibit no dependence when plotted in terms of Δq_z value. Since the series of ions used in the above study are somewhat different and require an increasing fluence for resonance excitation CID (Basic, 1992), the slightly negative trend observed in Figure 3-11b should be expected. It is important to note that ions of significantly varying structure, however, are expected to be influenced very differently by the higher-order fields.

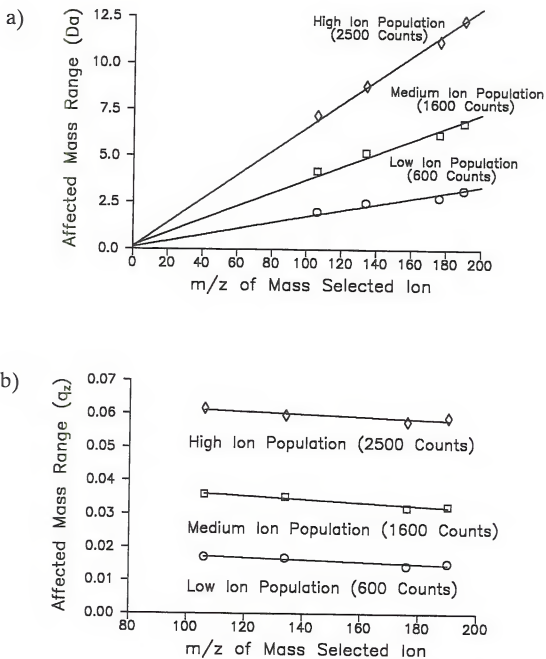


Figure 3-11: Influence of the m/z of the mass-selected ion on the octopolar field effect at $\beta_z = 1/2$ expressed as affected mass range in terms of a) low mass cutoff (Da) and b) stability parameter q_z .

Specifically, the expected relationship should follow in a manner similar to that observed upon resonance excitation CID of that species. In other words, higher-order field effects behave similarly to a low voltage, very gentle resonant excitation. The degree to which an ion will be influenced by higher-order field effects will parallel the power necessary for resonant ejection of the ionic species.

Field Penetration

The influence of field penetration due to the voltages from the electron multiplier/dynode system was investigated on both the ITMS™ and the ITS-40™ benchtop instrument. Although both systems employ a $\pm 180\text{V}$ gate lens for introduction of electrons, the substantially higher voltages from the multiplier/dynode system were expected to exhibit more of an effect. Field penetration from the multiplier/dynode system is expected to contribute higher-order odd fields (i.e. hexapolar) due to the asymmetry (i.e. penetration from exit endcap only). The additional source of the hexapolar fields is expected to cause an increased loss in ion signal near $q_z=0.80$ (hexapolar resonance line at $\beta_z=2/3$).

The ITMS™ has both the high voltage dynode and the multiplier positioned approximately one-half inch behind the exit endcap; the dynode/multiplier assembly operates with a grounded shield located between the endcap and the dynode to minimize any field penetration. The studies presented here were similar to the probe ion studies presented above in that the C_2H_5^+ ion was stored at various RF levels along the $a_z=0$ line and the ion intensity monitored. This experiment was repeated

under application of various voltages to the dynode/multiplier assembly. Following normalization of the data (due to changes in the detected ion count), identical plots of intensity versus q_z value were obtained whether low voltages (multiplier = -1100 V, dynode = 0) or high voltages (multiplier = -2000 V, dynode = -5000 V) were used. No evidence of increased ion loss near $q_z=0.80$ was observed for the higher voltage case. Apparently the grounded shield prevents substantial field penetration; thus, the contribution of field penetration to the hexapolar resonance on the ITMS™ is negligible.

Studies on the ITS-40™ benchtop instrument were performed in order to identify field penetration-induced higher-order field effects caused by the position of the multiplier. On the ITS-40™, the multiplier is positioned immediately behind the endcap (substantially closer than the ITMS™) and no dynode or grounded shield is present. Therefore, this instrumental design offers the greatest opportunity for field penetration from the multiplier. Experiments similar to those described for the ITMS™ field penetration studies were performed with the ITS-40™ by varying the multiplier voltage from -1100 V to -2000 V. Once the ion intensity for each experiment was normalized (due to changes in the detected ion count), identical plots were obtained for each multiplier voltage setting; however, ion losses due to the hexapolar resonance were markedly greater than observed with the ITMS™. The results from the low multiplier voltage (-1100 V) experiment are shown in Figure 3-12. In all studies with the ITMS™, the ion loss due to the resonance at $\beta_z=1/2$ was always greater than that at $\beta_z=2/3$.

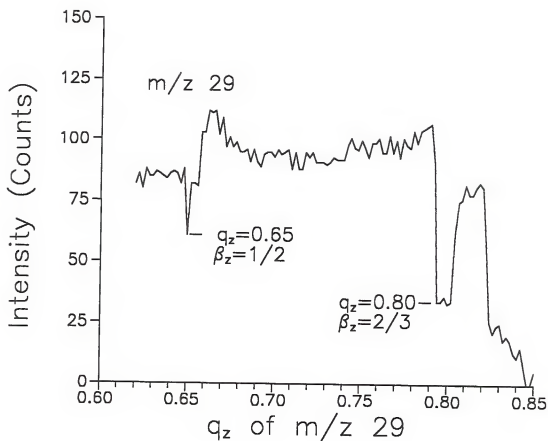


Figure 3-12: Intensity of mass-selected C_2H_5^+ ions (m/z 29) versus q_z for 70 ms storage ($a_z=0$). Data acquired with the Finnigan MAT benchtop ITS-40™ instrument. Intensity losses correspond to $\beta_z=1/2$ (octopolar) and $\beta_z=2/3$ (hexapolar).

The results discussed above suggest some degree of asymmetric distortion. This suggests that field penetration (or some type of asymmetric distortion) exists with the ITS-40™ ion trap assembly. Although measurements of the ion trap assembly showed that the endcaps of the ITS-40™ were displaced ($z_0=0.793$ cm) further than the ITMS™ ($z_0=0.783$ cm), this was a symmetrical deviation and should not contribute to the hexapolar resonance. This implies that field penetration contributes significantly to the hexapolar resonance on the ITS-40™. To reduce this effect, shielding of the multiplier, as for the ITMS™, would be beneficial but is difficult due to the vacuum system design. It should be noted that the ion trap assembly on the ITS-40™ may possess some degree of asymmetric endcap spacing which may not have been detected during the measurements of z_0 (Timothy P. Griffin, private communication). Nevertheless, due to some type of asymmetry, the ITS-40™ ion trap exhibits more effects from higher-order odd fields than the ITMS™ ion trap assembly.

Endcap Electrode Spacing

The assembly of the ion trap directly influences the existence of higher-order field effects. Symmetric deviations from the theoretical geometry (with respect to the $z=0$ plane) generate higher-order even fields; asymmetric deviations generate higher-order odd fields (see discussion in Chapter 2). The influence of assembly was investigated by comparing three differently assembled ion trap analyzers; 1) the "stretched" geometry (i.e. $z_0=0.785$ cm), 2) the "theoretical" geometry (i.e. $z_0=1/\sqrt{2}$

or 0.7071 cm), and 3) the "asymmetric" geometry in which one $z_0=0.785$ cm (exit endcap) and the other $z_0=0.7071$ cm (entrance endcap). According to theory (see Chapter 2), the "theoretical" geometry suffers from higher-order even fields due to electrode truncation and higher-order odd fields due to differences in each endcap (e.g. holes). The "stretched" geometry suffers from the same sources of higher-order fields as the "theoretical" geometry, but also includes the additional source of higher-order even fields due to the symmetric displacement of each endcap. This additional source of higher-order fields, however, reportedly contributes constructively (i.e. same sign as the quadrupolar trapping field) as opposed to destructively (i.e. opposite sign as the quadrupolar trapping field) due to the electrode truncation (Franzen, 1993). The "asymmetric" geometry suffers from the same sources of higher-order fields as the "theoretical" geometry, but also includes the additional source of higher-order odd fields due to the asymmetric displacement of the endcaps. It should be emphasized that the existence of higher-order fields, whether constructive or destructive, will influence ion motion and cause altered trajectories which may result in ejection and/or CID.

The RF level corresponding to a 10 ms storage period in each ion trap assembly was incremented along the $a_z=0$ line for the $C_2H_5^+$ probe ion. The ion population was approximately equal in each case, although exact populations were difficult to determine due to changes in the storage and detection efficiencies for each assembly. Figure 3-13a through c presents the results from this study. The results for the "stretch" and "theoretical" geometry are very similar, which is not too

surprising since both suffer from similar higher-order field effects. Apparently, the deleterious effects from electrode truncation cannot be totally overcome by the intentional addition of higher-order even fields of the same sign. The results from the "asymmetric" geometry exhibit a marked increase in ion loss near the hexapolar resonance line at $q_z=0.80$ ($\beta_z=2/3$). As predicted, asymmetric deviations from the "theoretical" geometry significantly influenced stored ions; hexapolar effects near $\beta_z=2/3$ exhibited a three-fold increase in ion loss. This supports the results obtained for the field penetration studies performed on the ITS-40™ in which asymmetry was implicated in the increased ion losses near $\beta_z=2/3$.

As diagrammed in Figure 3-2, along the $a_z=0$ line, the hexapolar resonance at $\beta_z=2/3$ is in close proximity of the octopolar resonance at $\beta_z+\beta_t=1$. In order to verify that the dramatic loss of ion signal observed near $\beta_z=2/3$ for the "asymmetric" ion trap was indeed due to the hexapolar field and not from contribution of the octopolar field, the experiment was repeated with the application of a negative DC voltage. Since the resonance lines deviate from one another at $a_z \neq 0$ (\pm DC), repeating the experiment along the $a_z=+0.047$ (-10 V DC) line would distinguish between the two. Recall that the $-a_z$ values ($+DC$ voltage) enhances higher-order field effects and broadens the loss bands, thus making it more difficult to distinguish between the hexapolar and octopolar resonance lines. Note that high ion populations and long storage times would also broaden the loss bands. With these parameters in mind, the experiment results obtained along the $a_z=+0.047$ line are shown in Figure 3-14a through c.

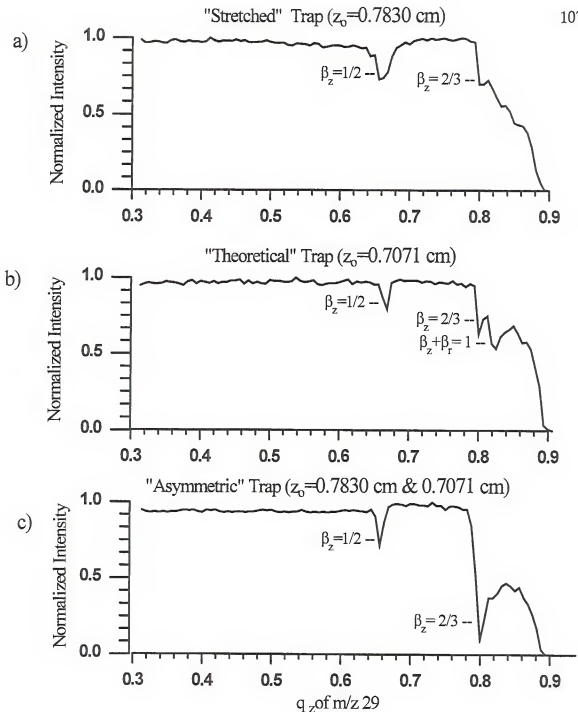


Figure 3-13: Intensity of mass-selected $C_2H_5^+$ ions (m/z 29) versus q_z for 10 ms storage ($a_z=0$) within a) a "stretched" geometry ($z_0=0.783$ cm), b) a "theoretical" geometry ($z_0=0.7071$ cm), and c) an "asymmetric" geometry ($z_0=0.783$ cm and 0.7071 cm). Intensity losses correspond to $\beta_z=1/2$ (octopolar), $\beta_z=2/3$ (hexapolar), and $\beta_z+\beta_r=1$ (octopolar).

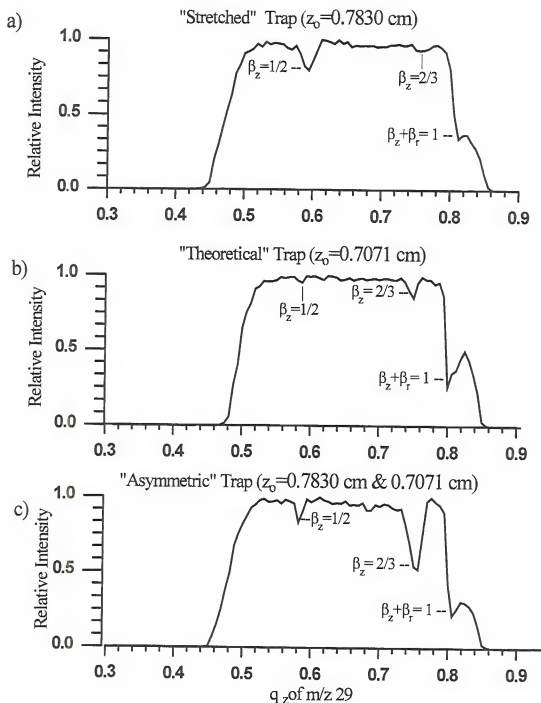


Figure 3-14: Intensity of mass-selected $C_2H_5^+$ ions (m/z 29) versus q_z for 10 ms storage ($a_z=0.047$, $DC=-10$ V) within an ion trap of a) a "stretched" geometry ($z_0=0.783$ cm), b) a "theoretical" geometry ($z_0=0.7071$ cm), and c) an "asymmetric" geometry ($z_0=0.783$ cm and 0.7071 cm). Intensity losses correspond to $\beta_z=1/2$ (octopolar), $\beta_z=2/3$ (hexapolar), and $\beta_z+\beta_r=1$ (octopolar).

Although all of the higher-order field effects are diminished due to the applied -DC voltage, the hexapolar effects are clearly separated from the octopolar effects. Figure 3-13c conclusively demonstrates that the "asymmetric" geometry contributes dramatically to higher-order odd fields which can be observed as ion losses near $\beta_z=2/3$.

Conclusions

The $C_2H_5^+$ ion, generated by ion/molecule reactions with methane, was used successfully as a chemical probe to identify higher-order field effects. Upon absorbing power from higher-field resonances, $C_2H_5^+$ (m/z 29) underwent CID by neutral loss of H_2 to yield $C_2H_3^+$ (m/z 27) which reacted further with neutral methane to form $C_3H_5^+$ (m/z 41). Detection of either the loss of signal for m/z 29 or the increase in signal for m/z 27 or 41 allowed the identification of higher field resonances. While storing the probe ion along the $a_z=0$ line (0V DC), losses of $C_2H_5^+$ signal were observed at $q_z=0.65$, $q_z=0.80$, and $q_z=0.83$ which corresponded to higher field resonances due to $\beta_z=1/2$ (octopolar), $\beta_z=2/3$ (hexapolar), and $\beta_z+\beta_r=1$ (octopolar).

Higher-order field effects were investigated in this chapter by characterizing the influence of instrumental parameters. The parameters discussed in this chapter were 1) storage conditions (q_z , a_z values), 2) ion population, 3) storage time, 4) m/z of the ion, 5) field penetration, and 6) endcap electrode spacing. The parameters exhibiting the most influence on the magnitude of ion loss due to higher field

resonances were due to the storage conditions, ion population, storage time, and endcap electrode spacing.

Results presented in this chapter showed that storing the ions in the lower portion of the stability diagram (below the $a_z=0$ line; $a_z<0$, +DC voltage) markedly enhanced ion losses (either due to ejection or CID). With increasingly positive applied DC voltage, a linear loss of m/z 29 was observed until approximately 90% was lost. The affected mass range also was observed to increase linearly with increasingly positive DC. The increased effects with increasingly positive applied DC is believed to be due to the increased amplitude of z -motion. While storing n -butylbenzene in the lower portion of the stability diagram ($a_z = -0.204$, DC = +200 V), evidence was observed for the above mentioned resonances as well as for the dodecapolar resonance due to $\beta_z = 1/3$. This is the first reported observation of the influence from the dodecapolar field.

Ion population was shown to dramatically influence higher-order field effects. Increasing the ion population increased the magnitude of ion loss exponentially; the affected mass range also increased markedly. Increasingly long storage times also were observed to linearly increase ion losses while storing the probe ion near the octopolar resonance line ($\beta_z = 1/2$). Longer storage times allowed the ion to absorb more power from the higher-order field thus increasing the magnitude of ion loss.

Electrode spacing was shown to dramatically influence the higher-order field effects. An asymmetric endcap spacing (with respect to the $z=0$ plane) produced enhanced ion losses near the hexapolar resonance at $\beta_z = 2/3$. The "theoretical"

spacing ($z_0=0.7071$ cm) and the "stretched" spacing ($z_0=0.783$ cm), both of which are symmetrical, showed very similar results to one another.

CHAPTER 4 HIGHER-ORDER FIELD EFFECTS ON CHEMICAL IONIZATION

Introduction

This chapter will present the implications of higher-order field effects on chemical ionization (CI). Higher-order field effects on the CI reagent ion, $C_2H_5^+$ from methane, will be discussed in detail through a three-dimensional and a topographic plot of its stability region. Ion losses observed throughout the experimental stability region due to higher-order resonances will be identified and discussed. Higher-order field induced CID and subsequent ion/molecule reactions of the resulting product ions for $C_2H_5^+$ ions stored at various points in the stability diagram also will be presented. The influence of higher-order fields with regards to ion ejection and CID of several other CI reagent ions will be presented. The chapter will close with a detailed study of the influence of higher-order fields on both the quantitation and spectral quality obtained in the mass-selected CI mode.

Chemical Ionization with the Quadrupole Ion Trap

Chemical ionization (CI) on more common mass spectrometers (e.g. quadrupole mass filters) typically requires a high pressure (1 torr) CI source. This is due to the very short reaction times (e.g. 10 μ s) between the CI reagent ions and

the neutral analyte species prior to entering the mass analyzer. The CI mode on the quadrupole ion trap, however, is conducted within the trapping volume where reaction times between the CI reagent ions and neutral analyte species is user-controlled and typically approaches 50 ms to 100 ms. Since the quadrupole ion trap operates tandem-in-time, the trapping volume serves as both the CI source and the mass analyzer. Since the reaction times are 3 to 4 orders of magnitude longer than in conventional sources, the required CI reagent gas pressure is substantially lower within the quadrupole ion trap (e.g. approximately 1×10^{-5} torr for methane).

In general, CI on the quadrupole ion trap is performed by first generating CI reagent ions by internal electron ionization (EI) followed by ion/molecule reactions between the newly created ions and the neutral analyte species. One drawback to the tandem-in-time nature of the quadrupole ion trap for CI is that the neutral analyte is present during the formation of the CI reagent ions by the EI process (Brodbelt *et al.*, 1987). Consequently, EI-like ions are produced from the analyte; therefore upon acquisition of the CI spectrum, both EI- and CI-like ions are present. This complicates the CI mass spectrum thus causing a discrepancy between spectra acquired on a quadrupole mass filter and those acquired on a quadrupole ion trap. One method of overcoming this drawback is to operate the instrument in such a way that during ion formation by EI only low mass ions (i.e. CI reagent ions) are stored while high mass ions (i.e. EI-like analyte ions) are ejected. This can be accomplished by applying a small DC voltage (e.g. +5 V) on the ring thus creating and storing ions near the $\beta_z=0$ stability edge (see Figure 1-4 of Chapter 1). Another method for

selectively storing only low mass ions is to apply a broad band signal (i.e. white noise, Kelley *et al.*, 1993) to resonantly eject all ions above a specified frequency (or m/z). Indeed, both of these methods have been successful at improving the CI spectral quality obtained with the quadrupole ion trap.

One advantage of the tandem-in-time feature of the quadrupole ion trap is that CI can be performed in an MS/MS type mode. During the first stage of MS, reagent ions of a single m/z are selected; all other ions are removed from the trap. The second stage of MS is mass analysis following the reaction of the CI reagent ions with neutral analyte species. This CI process is referred to as mass-selective CI (Berberich *et al.*, 1989). Non-mass-selective CI allows the reaction of neutral analyte species with all reagent ions present following the EI event. Mass-selective CI requires that the specific CI reagent ion of interest be mass-isolated prior to reaction with the neutral analyte. This method allows more control of the CI process, especially in terms of energy deposition during analyte ion formation. Due to the mass-selection of the CI reagent ion, all EI-produced analyte ions also are eliminated from the ion trap.

The scan function shown in Figure 4-1 is a general mass-selected CI scan; the scan function specifically used for $C_2H_5^+$ is tabulated in Table 4-1. Omitting the mass-isolation process generates the non-mass-selective CI mode. During the ionization event several reagent ions are created for a given CI reagent gas. For example, as discussed in Chapter 3, EI of methane produces a number of primary reagent ions.

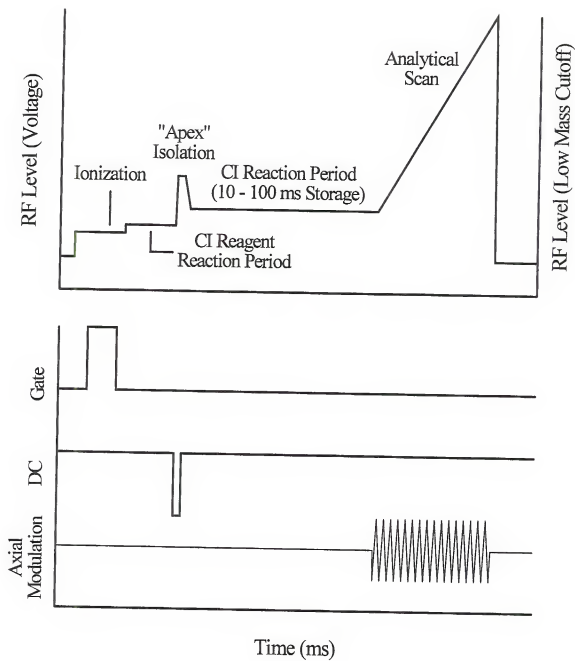


Figure 4-1: Scan function (signal timing sequence) employed for mass-selective chemical ionization. The "apex" isolation was used to select the reagent ion prior to reaction with analyte neutrals.

Table 4-1: Mass-Selected CI Scan Function

#	Table Comment	Start Mass (amu)	End Mass (amu)	Table Time (uS)	DC Volts	a_z value	Axial Mod.
1	Trigger	0	0	300	0	0	
2	Pre-Ionization	10	10	300	0	0	
3	Ionization	10	10	1000	0	0	
4	Reagent Reaction	13	13	5000	0	0	
5	RF Ramp to $q_z=0.78$	13	24.9	1000	0	0	
6	Apex Isolate	24.9	24.9	1000	-25	0.15	
9	RF Ramp to CI Reaction Level	24.9	15.0	1000			
10	CI Reaction	15.0	15.0	50000			
15	EM Warm Up	15.0	15.0	2000	0	0	530 kHz 6V _{pp}
16	Data Acq.	15.0	650	50000	0	0	530 kHz 6V _{pp}
17	RF Shut Down	0	0	2000	0	0	

In order to accumulate the specific reagent ion of interest, a variable reagent formation period follows the ionization event and precedes the ion isolation process. The time allowed for this formation period varies for the specific reagent ion of interest. Following the CI reagent ion formation period, the specific ion of interest is mass-selected by RF/DC isolation; "apex" isolation (Weber-Grabau *et al.*, 1987; Todd *et al.*, 1987) is shown in Figure 4-1. Next, the CI reaction period occurs between the CI reagent ions and the neutral analyte species; the resulting ions are detected by the mass-selective instability scan (Stafford *et al.*, 1983ab).

Although mass-selective CI allows more control over the CI process, some drawbacks remain. Due to the tandem-in-time nature, CI reactions occur continuously throughout the scan function. During the formation and accumulation of CI reagent ions, CI-produced analyte ions are formed also. Upon isolation of the specific CI reagent ion of interest, all other ions, including these analyte ions, are ejected from the trap. Thus, sensitivity may be reduced. Another issue is that high amounts of analyte neutrals can react with the majority of CI reagent ions prior to the isolation step. This will reduce the total number of CI reagent ions available during the CI reaction period. Typically, this occurs only with very high analyte concentrations.

Until the CI reagent ion population has been totally depleted, a first approach to increase the sensitivity for the CI-produced analyte ions is to increase the population of the CI reagent ions and/or increase the CI reaction time. Increasing the CI reagent ion population increases the number of ions available for reaction

with the neutral analyte. Increasing the reaction time allows more time for the reactions to take place thus utilizing more of the CI reagent ions present.

For a given CI reagent ion species, an optimum RF level exists for the ionization event, the CI reagent ion formation period, and the CI reaction period. The only limitations are that the RF levels for each process must be at a q_z value within the stable range of q_z values for the CI reagent ion (i.e. $0.10 < q_z < 0.85$ at $a_z = 0$). For the most efficient and sensitive CI process, the RF levels employed throughout the scan function need to be optimized. The RF levels for the ionization event and the CI reagent formation period are dependent only on the CI reagent ion of interest. In general, optimum ion creation during the ionization event occurs near $q_z = 0.3$. Similarly, optimum secondary ion formation occurs at $q_z = 0.3$. If the CI reagent ion of interest is a secondary ion formed from an ion of lower m/z (as in the case of methane reagent ions, see Chapter 3), then the optimum RF level for each ion's formation is different. For example, if the CI reagent ion of interest is m/z 41, the $C_3H_5^+$ ion from methane, the primary ions are m/z 14, CH_2^+ , and m/z 27, $C_2H_3^+$. The optimum RF level for primary ion formation corresponds to a low mass cutoff of 9 Da ($q_z = 0.3$ for m/z 27); optimum RF level for CI reagent ion accumulation corresponds to 14 Da ($q_z = 0.3$ for m/z 41).

The optimum RF level for the CI reaction period, however, is dependent on both the CI reagent ion and the analyte ions produced. During the CI reaction period, not only are the CI reagent ions required to possess stable q_z values, but upon formation, the q_z of all analyte ions needs to be within the stable range (i.e.

$0.1 < q_z < 0.85$ at $a_z = 0$). For instance, the highest RF level allowable for the CI reagent ion $C_2H_5^+$, m/z 29, corresponds to a low mass cut off of 27 Da ($q_z = 0.85$ for m/z 29). At this low mass cutoff, an analyte ion of m/z 300 would therefore be created and stored at a $q_z = 0.08$. Although the analyte ion will be detected, the reduced storage efficiency at this q_z value will decrease the CI sensitivity for this quantitation ion.

This chapter will address the issues regarding appropriate RF levels during the CI mode of operation with the quadrupole ion trap. Specifically, the influence of higher-order field effects on CI reagent ions, CI sensitivity, and CI spectral quality will be demonstrated and discussed.

Experimental

All experiments were performed on a Finnigan MAT (San Jose, CA, USA) ion trap mass spectrometer (ITMS™) maintained at 100° C. Careful measurements of the ion trap assembly exhibited a z_0 distance of 0.785 cm. Helium (Liquid Air, Walnut Creek, CA) was used as the buffer gas. Isobutane (Alphagaz, LaPorte, TX), HPLC grade methanol and acetonitrile (Fisher Scientific, Fair Lawn, NJ), and methane (Matheson Gas Products, Morrow, GA) were introduced into the ITMS™ via a fine metering valve (Negretti, Southampton, England). The n-butylbenzene and (Eastman Kodak, Rochester, NY) and the isopropylether (Chem Service, West Chester, PA) were introduced into the ITMS™ via a Granville-Phillips (Boulder, CO) series 203 variable leak valve mounted directly on a 1/2" O.D. stainless steel probe.

Carbaryl and methomyl (Pesticide Chemical Repository, Research Triangle Park, NC) were introduced via a solids probe heated to 100°C.

Pressures in the ITMS™ were indicated by a Bayard-Alpert ionization gauge (Granville-Phillips, Boulder, CO) mounted on the vacuum chamber and are reported with no correction factors. Typical indicated pressures for all experiments were 1.1×10^{-4} torr for helium, 1.0×10^{-5} torr for methane and 2.0×10^{-6} torr for the n-alkylbenzenes.

The instrument software, ICMS© (developed by Nathan A. Yates, University of Florida), was used for all experiments on the ITMS™. The software allows data acquisition while varying the RF amplitude either by incrementing the RF digital-to-analog converter (DAC) step or by incrementing the low mass cutoff (LMCO). For these experiments, a FORTH procedure was used to increment the RF amplitude by a user-defined Δ DAC value, typically 2 DACs. The relevant lines of code required to increment the RF by two DAC units are shown below:

```

]] <Times> [[
    TAKE-ONE-SCAN          \ begin loop
    8 -> SAP-TBL#           \ acquire 1 scan
    2 BIT#->SAP-TBL-ADDR    \ designate table #3 (i.e. storage)
    PEEKWL DUP DV-MB SWAP   \ byte #2 = Start-RF-DAC
    LINE24 8 U.R. 8 U.R.    \ read byte and convert to mass bucket
    2 BIT#->SAP-TBL-ADDR    \ show dac val and mass bucket
    PEEKWL 2 +              \ designate byte address
    2 BIT#->SAP-TBL-ADDR    \ increment 2 dacs
    POKEWL                  \ designate byte address
                              \ place new dac value in address
]] Loop [[
    \ end loop

```

Scan functions used for these experiments were similar to that displayed in Figure 4-1 and tabulated in Table 4-1. Briefly, a 1 ms ionization time was employed

at $q_z=0.3$ for the CI reagent ion followed by a variable ion/molecule reaction period (typically 10 ms). The ion of interest was mass-selected by RF/DC "apex" isolation at $q_z=0.78$, $a_z=0.15$ (Weber-Grabau *et al.*, 1987; Todd *et al.*, 1987). The RF amplitude was then ramped to the desired q_z value for ion storage for up to a maximum of 100 ms.

All calculations were performed according to the corrected equations for the "stretched" ion trap design (Johnson *et al.*, 1992). ITMS™ data reduction was performed using the BASIC programs, CHROLIST and SPECLIST (written by Randall E. Pedder and Nathan A. Yates, University of Florida), which retrieves original ITMS™ data files, averages selected mass intensities, and writes the data into a tabular ASCII format. All data manipulation was performed with the commercial spreadsheet program QUATTRO (Borland International, Inc., Scotts Valley, CA).

The 3-dimensional and the topographic plots were generated normalizing each file and appending all files into a main spreadsheet in QUATTRO. The spreadsheet was then read into the program SURFER (Golden Software, Inc., Golden, CO) where the data was transferred into a 50x50 grid. The data was then smoothed by the spline smoothing algorithm provided by SURFER which created a new 223 X 223 grid. The a_z values were calculated using calibrated DC voltages and the equations for the "stretched" trap geometry (Johnson *et al.*, 1992). The q_z values were calculated by first determining the low mass cutoff through multiplying the corresponding DAC value by the experimentally determined slope of the calibration

curve for low m/z ions (e.g. 6.314 DACS/amu). The low mass cutoff was then used in the equation below to calculate the q_z value:

$$q_z = \frac{\text{LowMassCutoff} * 0.906}{m/z} \quad (4-1)$$

All β_u values and ion frequency determinations were calculated by the BASIC program AQFORM (written by Donald M. Eades and Matthew Booth, University of Florida). This program used the continued fraction method (McLachlan, 1947) for β_u calculations (see Equation 1-13 of Chapter 1).

The RF drive frequency was 1.1 MHz and a $6V_{p-p}$ axial modulation (Weber-Grabau *et al.*, 1988; Tucker *et al.*, 1988) signal was employed at 530 kHz (resonant ejection at $q_z=0.906$) during the mass-selective instability scan (Stafford *et al.*, 1983ab). The electron multiplier (EM) voltage was set to yield 10^5 gain and no dynode voltage was used. A grounded shield was present in front of the dynode/EM assembly of the ITMS™.

The Experimental Stability Region for $C_7H_7^+$

An ion stored in the quadrupole ion trap will exhibit stable ion trajectories if the applied RF and DC voltage combination is within the stability boundaries defined by the Mathieu stability diagram shown in Figure 1-1 of Chapter 1. This two-dimensional stability diagram is plotted in terms of q_z (\propto RF voltage) along the x-axis and a_z (\propto DC voltage) along the y-axis. An "ideal" Mathieu stability diagram would exhibit constant storage efficiency throughout the entire stability region.

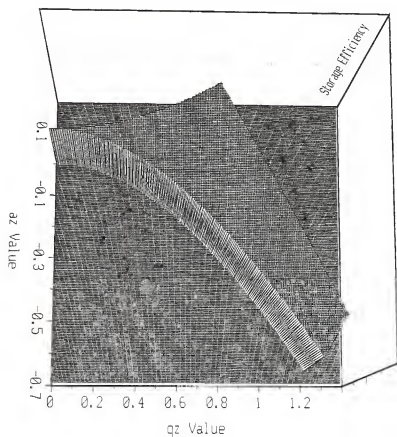


Figure 4-2: "Ideal" Mathieu stability diagram. Storage efficiency is plotted on the z-axis, the a_z stability parameter on the y-axis, and the q_z stability parameter on the x-axis.

The boundaries separating the stable and unstable portions of the "ideal" stability region would be very sharp. An example of this "ideal" stability region is shown in Figure 4-2 in which a_z is plotted on the y-axis, q_z on the x-axis, and storage efficiency on the z-axis. Ideally, an ion stored very close to any stability edge for any length of time will remain stable; only when placed outside of the well-defined stability region will the ion be lost. Likewise, storage anywhere throughout the "ideal" stability region will result in constant storage efficiency; thus, the ion population does not increase or decrease for any amount of storage time.

Realistically, however, the "ideal" stability region does not exist. Storage close to the stability edges (i.e. $q_z < 0.1$ or $q_z > 0.85$, $a_z = 0$) results in some degree of ion loss; increasing the storage time near these edges increases the severity of the loss. The result is that the stability edges are not well defined, but rather are very ambiguous. Furthermore, the experimentally observed stable q_z range (i.e. $0.1 < q_z < 0.85$ at $a_z = 0$) is dependent on ion population; increasing the ion population increases the severity of ion loss and decreases the stable q_z range. Within the experimentally observed stable q_z range, however, the storage efficiency has been thought to be relatively constant.

Obtaining information regarding the "real" experimental stability region for a given m/z ion offers two advantages. First, a more general view of the "real" experimental stability diagram offers a better understanding of the consequences of changing the storage conditions (i.e. q_z , a_z values). Secondly, understanding the storage efficiency and the fate of CI reagent ions throughout the stability region

provides insight into the fundamental aspects of the CI mode on the quadrupole ion trap.

To investigate the "real" experimental stability region for the CI reagent ion, C_2H_5^+ ($m/z 29$) of methane, storage efficiency throughout the Mathieu stability was measured. With only methane introduced into the quadrupole ion trap, the C_2H_5^+ ion was "apex" isolated by the using the scan function described in Figure 4-1. The mass-selected ion was then stored for 100 ms at various RF/DC combinations throughout the stability region. While applying a constant DC voltage (i.e. along an iso- a_z line), the q_z value of the 100 ms storage period was varied by incrementing the RF voltage as described in the Experimental section. This procedure was repeated for 28 different values of the applied DC voltage at 2.5 V increments; the range of DC voltages was -10 V to $+60$ V which corresponds to values of a_z from -0.05 to 0.30 .

The results are shown in Figure 4-3 in which a_z is plotted on the y-axis, q_z on the x-axis, and ion intensity on the z-axis. This three dimensional (3-d) map shows that the experimental stability region for C_2H_5^+ is far from "ideal". Although there appears to be constant storage efficiency in the region depicted by the plateau area (i.e. $q_z < 0.61$ and $a_z > -0.05$), significant ion losses are observed throughout the stability region. Here, storage efficiency is simply related to the detected ion intensity. Ion losses in the 3-d map are observed along iso- β lines corresponding to $\beta_z = 1/3$ (dodecapolar), $\beta_z = 1/2$ (octopolar), $\beta_z = 2/3$ (hexapolar), and $\beta_r = 1/2$ (octopolar).

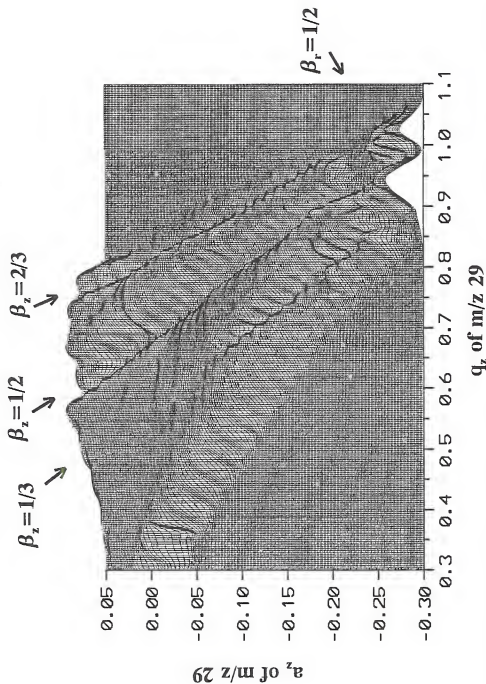


Figure 4-3:

Three-dimensional plot of the experimentally determined stability region for the mass-selected $C_2H_5^+$ ion (m/z 29). Ion intensity following 100 ms storage is plotted on the z -axis, the a_z stability parameter on the y -axis, and the q_z stability parameter on the x -axis. Signal minima fall along the iso- β_z lines corresponding to $\beta_z = 1/3$ (dodecapolar), $\beta_z = 1/2$ (octopolar), $\beta_z = 2/3$ (hexapolar), and $\beta_r = 1/2$ (octopolar).

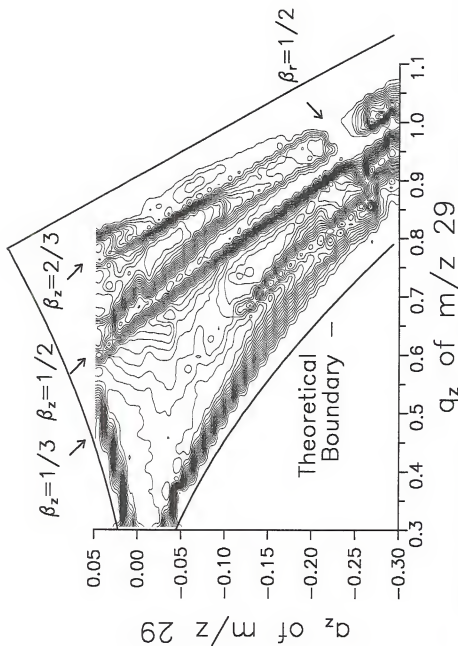


Figure 4-4: Topographical plot of the experimentally determined stability region for the mass-selected $C_2H_5^+$ reagent ion $C_2H_5^+$ ($m/z = 29$). Ion intensity, following 100 ms storage, is plotted on the z-axis, the q_z stability parameter on the y-axis, and the q_z stability parameter on the x-axis. Signal minima fall along the iso- β_z lines corresponding to $\beta_z = 1/3$ (dodecapolar), $\beta_z = 1/2$ (octopolar), $\beta_z = 2/3$ (hexapolar), and $\beta_z = 1/2$ (octopolar).

These compare very well to the theoretically predicted resonance lines shown in Figure 2-6 of Chapter 2. As described in Chapter 3, a corresponding increase in the ion signal for $C_2H_3^+$ (m/z 27) and $C_3H_5^+$ (m/z 41) mirror the observed losses of m/z 29 ion intensity. This is due to the $C_2H_3^+$ ion absorbing power from the higher field resonances and undergoing CID producing $C_2H_5^+$ which further reacts with neutral methane to form $C_3H_5^+$. Note also that as described by the characterization studies discussed in Chapter 3 (see Figures 3-5 through 3-7), the higher-order field effects become more significant in the lower portion of the stability diagram (i.e. with application of +DC voltage).

The appearance of the "ripples" in the 3-d surface is due to the gridding and smoothing programs of SURFER and is not inherent to the "real" stability diagram. The "ripples" indicate the smoothing of the data between the discrete experiments (i.e. along individual a_z lines).

Figure 4-4 is the same data of Figure 4-3 shown in terms of a topographic plot. Note that the data were acquired only from $a_z = +0.05$ to -0.30 and that the solid line is the theoretically predicted stability boundary of a m/z 29 ion. A wider range of a_z values could not be mapped due to increased losses of ion signal observed in the lower portion of the stability diagram. In order to store the ions in the lower region, the scan function was required to undergo a "stairstep" type process. This consisted of alternating between RF and DC ramps in order to work down to the lower right edge of the stability diagram. Upon doing so, the stored ions cross several times over the higher-order field resonance lines, resulting in

increased losses of ion signal. Note that from Figure 1-1 of Chapter 1, the widest range of a_z values along an iso- q_z line lies just below the apex along $q_z=0.78$. This vertical line intersects the $\beta_z=0$ boundary near $a_z=-0.3$, therefore representing the highest a_z value attainable without requiring the "stairstep" scan function. The topographic plot shown in Figure 4-4 also makes the ion losses near the $\beta_z=1$ stability edge more apparent. The early onset of ejection near this boundary (i.e. $q_z=0.85$, $a_z=0$) arises from the long storage times (100 ms) employed in the scan function. Evident in the topographic plot, but less apparent in the 3-d plot, are ion losses along the iso- β line corresponding to $\beta_r=1/2$ (octopolar). This is only the second evidence ever reported for r-type resonance effects; the first report being by Dawson and Whetten (1969b). Although difficult to observe in both of the plots, the data suggest small contributions from the $\beta_z+2\beta_r=1$ (dodecapolar) and $\beta_z+\beta_r=1$ (octopolar) sum resonance lines. Results from ion injection from an external off-axis ion source also indicate some influence from these sum resonance lines (Randall E. Pedder, private communication). Note that the appearance of "rings" or "dimples" in the topographic plot (especially along the $\beta_z=1/3$ line) are due to the gridding and smoothing procedure of SURFER. These anomalies represent the smoothing of the data between the discrete experiments which make up the surface.

As discussed in Chapter 3, higher-order field effects become more significant in the lower portion of the stability diagram due to increased axial amplitude of the ion motion. Only in the lower portion of the experimentally determined stability region for $C_2H_5^+$ was the influence of the dodecapolar resonance at $\beta_z=1/3$ observed.

Along the $a_z=0$ line, however, this resonance is not observed in the above graphs or any graphs shown in Chapter 3. Recall that the dodecapolar resonance at $\beta_z=1/3$ was observed in Figure 3-7b of Chapter 3 while storing the molecular ion of *n*-butylbenzene in the lower portion of the stability diagram. Nevertheless, evidence of dodecapolar resonances effects previously have not been observed for ions which have not been displaced from the center of the ion trap. Evidence for dodecapolar effects at $\beta_z=1/3$ have been observed during ion injection experiments (Pedder *et al.*, 1989; Williams *et al.*, 1991b).

While storing the m/z 29 ions in the lower portion of the stability diagram ($a_z < -0.2$) further ion/molecule reactions were observed. As discussed above, $C_2H_5^+$ ions (m/z 29) undergo CID and ion/molecule reactions when stored near higher resonance lines. Upon storage near the dodecapolar resonance line at $\beta_z=1/3$, however, $C_3H_5^+$ ions further reacted by undergoing CID to form $C_3H_3^+$ ions, which subsequently reacted with neutral methane to form $C_4H_5^+$ ions. The mechanism, which is shown below (Harrison, 1992), was confirmed by resonance excitation CID of $C_3H_5^+$ ions at other q_z values where higher resonances are not predicted.



The source of power required to generate the CID product ion at m/z 39 from $C_3H_5^+$ originates from the $\beta_z=0$ stability edge for m/z 41. As shown in Figure 4-5, the instrumental conditions required to store mass-selected m/z 29 near the $\beta_z=1/3$ line in the lower portion of the stability diagram (i.e. $-a_z$ values) place the m/z 41 ion near its own $\beta_z=0$ stability edge. The long storage time used in these experiments (i.e. 100 ms) allows the m/z 41 ions to absorb power and undergo ejection and CID, as described by the so-called "boundary-induced dissociation" effect (Paradisi *et al.*, 1992). The stability diagram in Figure 4-5, plotted in terms of RF and DC voltage, shows that the $\beta_z=1/3$ line for m/z 29 actually crosses the $\beta_z=0$ boundary for m/z 41, at which point, no ion signal for m/z 41 is observed.

It should be noted that the experimentally determined β_z values which correspond to the higher-order field effects show a slight discrepancy from the theoretically predicted values for the resonance lines. The experimentally observed higher-field resonances fall slightly to the right of the theoretical iso- β_z lines. Several factors may contribute to the observed discrepancy. The most important factor is believed to be the ion population stored in the ion trap during the experiments. As discussed in the characterization studies in Chapter 3, observed signal minima shift to higher q_z values with increasingly higher ion population. The reason for this is believed to be ion frequency shifts due to the effects of space charge or higher-order fields. Space charge induced shifts of ion resonance and stability boundaries have been addressed by other authors (Fischer, 1959; Fulford *et al.*, 1980; Sheretov *et al.*, 1973).

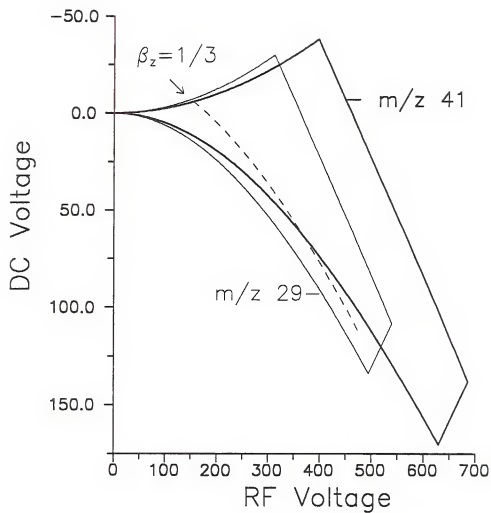


Figure 4-5: Mathieu stability diagrams for $C_2H_5^+$ (m/z 29) and $C_3H_5^+$ (m/z 41) plotted in RF/DC space. Note that the $\beta_z=1/3$ for m/z 29 crosses the $\beta_z=0$ boundary for m/z 41.

The above authors treated the space charge effects as the application of a DC potential on the electrodes which shifts the stability edges and causes the ions to be stored at a_z values that deviate from the theoretical predictions. Theoretical calculations (Wang, 1992) predict shifts in the ion secular frequency and in the stability boundary due to contributions of higher-order fields. Although no obvious influence on ion calibration was observed, these effects may contribute to errors in calculations of q_z values and, consequently, β_z values. Another factor contributing to errors in these calculations is the uncertainty in the exact q_z of ejection, the value of which is used in Equation 4-1. The equation assumes that all ions are ejected at $q_z=0.906$ due to the axial modulation employed at 530 kHz. For low m/z ions, however, less than $6V_{p-p}$ axial modulation can result in ion ejection; consequently, the $6V_{p-p}$ resonant ejection employed here will yield an earlier-than-predicted ejection point and hence a lower q_z value for resonant ejection during mass analysis. Indeed, when the axial modulation voltage is decreased, the m/z 29 ion appears later in the mass spectrum (i.e. at higher m/z values). The use of 0.906 in equation 4-1 rather than the correct (lower) value will yield incorrect (falsely high) calculations for q_z and β_z . Replacing 0.906 with the correct q_z value would improve the agreement between the calculated and theoretical β_z values. This exact q_z of ejection, however, is very difficult to determine. Other factors, such as uncertainty in the applied DC voltage and subsequent calculation of the a_z values, are believed to be minimal since the DC voltages were calibrated with a digital multimeter and the a_z values were calculated using the equations for the "stretched" geometry (Johnson *et al.*, 1992).

Effects on CI Reagent Ions

The influence of higher-order field effects on various CI reagent ions were investigated for the mass-selective CI mode. The effects of higher-order fields on the $C_2H_5^+$ reagent ion were well characterized in Chapter 3; therefore, this reagent ion will not be discussed in detail here. The other CI reagent ions discussed in this section arise from the reagent gases methane, methanol, acetonitrile, and isobutane. Specifically, reagent ions of interest include: the $(M+H)^+$ ion, CH_5^+ , and the $C_3H_5^+$ ion from methane, the $(M+H)^+$ ion, $CH_3OH_2^+$ of methanol, the $(M+H)^+$ ion, CH_3CNH^+ of acetonitrile, and the $(M-H)^+$ ion, $C_4H_9^+$, of isobutane. All of these reagent ions showed evidence for the influence of higher-order field effects.

Collision-Induced Dissociation

When performing mass-selected CI, the assumption is that reagent ions of only one m/z value are reacting with the neutral analyte. All spectral interpretation is based on that one assumption. If the CI reagent ion undergoes CID to form other reagent ions which also can react with the neutral analyte, the appearance of the resulting spectra may be altered. Therefore, identifying CID products originating from higher-order field effects on reagent ions is of practical importance.

The $(M+H)^+$ ion of methane, CH_5^+ (m/z 17), is a primary ion formed during EI of neutral methane in the ion trap (see Chapter 3) and can be used for CI. The influence of higher-order fields was investigated by conducting experiments similar to those described earlier; the m/z 17 ion was isolated and stored for 50 ms at

various q_z values along the $a_z=0$ line. The results are shown in Figure 4-6a. Since CH_5^+ is a relatively low m/z ion, only a narrow range of RF levels can be investigated. An ion signal minimum is observed near $q_z = 0.64$ and 0.78 along with a corresponding increase in the ion signal for m/z 29. While stored near $\beta_z=1/2$ octopolar resonance, the CH_5^+ ion absorbs power and undergoes CID to form CH_3^+ which further reacts with neutral methane to form C_2H_5^+ by the following mechanism (Harrison, 1992):



Indeed, resonance excitation of CH_5^+ ions at other stable q_z values showed an increase in m/z 29, thus lending support to the mechanism.

The C_3H_5^+ reagent ion, m/z 41, is formed by a series of secondary reactions. The primary ion, CH_2^+ , formed by EI, reacts with neutral methane, to form C_2H_3^+ which further reacts with neutral methane to form C_3H_5^+ (see Chapter 3). Consequently, ion formation times required for this reagent ion far exceed that of the CH_5^+ reagent ion. The influence of higher-order fields is demonstrated in Figure 4-6b. While storing the reagent ion for 50 ms at various q_z values along the $a_z=0$ line, the ion intensity exhibited a minimum near $q_z=0.65$ along with a corresponding increase in m/z 39 and 53.

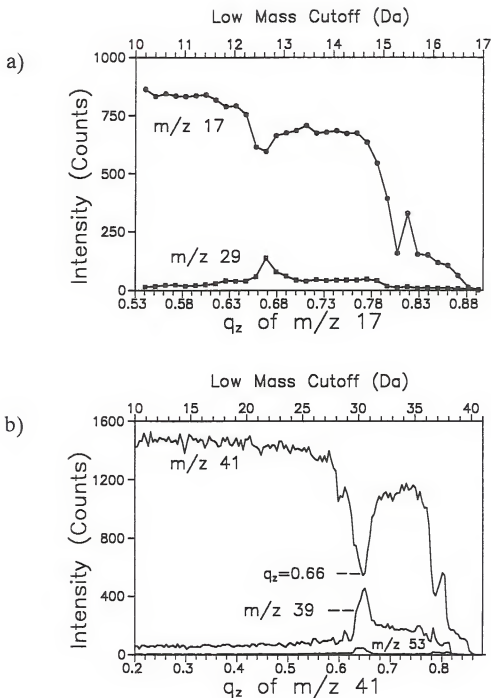


Figure 4-6: Intensities, following 50 ms storage, of a) mass-selected CH_5^+ (m/z 17) and CID product ion C_2H_5^+ (m/z 29) and b) mass-selected C_3H_5^+ (m/z 41) and CID product ions C_2H_3^+ (m/z 39) and C_4H_5^+ (m/z 53) versus q_z of the mass-selected ion.

The reagent ion absorbs power from the higher-order resonance and undergoes CID and subsequent product ion/molecule reactions via the same mechanism observed above (Harrison, 1992):



The proposed mechanism was confirmed by resonance excitation CID of C_3H_3^+ ions at other stable q_z values.

Ion Ejection

Chemical ionization can be accomplished using a variety of reagent ions including those from methanol, acetonitrile, and isobutane. The primary ions formed upon EI of methanol, CH_3OH^+ , CH_2OH^+ , CH_2O^+ , CHO^+ , react rapidly with neutral methanol to form CH_3OH_2^+ , the main reagent ion. Upon EI of acetonitrile, the primary ion, CH_3CNH^+ ($m/z\ 41$), quickly reacts with neutral acetonitrile to form the main reactant ion, the protonated nitrile (CH_3CNH^+). The primary ions formed upon EI of isobutane are C_4H_9^+ , the t-butyl ion, and C_3H_3^+ which reacts with neutral isobutane by hydride abstraction to form the main reagent ion, C_4H_9^+ (Harrison, 1992).

Protonated methanol, CH_3OH_2^+ ($m/z\ 33$), protonated acetonitrile, CH_3CNH^+ ($m/z\ 42$), and the $(\text{M}-\text{H})^+$ ion of isobutane, $(\text{CH}_3)_3\text{C}^+$ ($m/z\ 57$) are relatively stable

ions and exhibited only ion ejection while stored near $q_z=0.65$ ($\beta_z=1/2$) and 0.80 ($\beta_z=2/3$). These results are shown graphically in Figure 4-7a in which the RF level is plotted in terms of the low mass cutoff. Each reagent ion shows two signal minima which correspond to the $\beta_z=1/2$ octopolar resonance and the $\beta_z=2/3$ hexapolar resonance. As the low mass cutoff approaches the m/z value of the reagent ion, the ion intensity drops to zero due to ion ejection at the $\beta_z=1$ boundary (i.e. $q_z=0.906$). This figure also shows that higher m/z reagent ions exhibit a wider range of stable RF levels (in terms of ΔDa). The $(M-H)^+$ ion of isobutane, m/z 57, shows a constant ion signal from a low mass cutoff of 10 Da ($q_z=0.16$) to 35 Da ($q_z=0.56$); the $(M+H)^+$ ion of methanol, m/z 33, exhibits constant ion signal between a low mass cutoff of 10 Da ($q_z=0.27$) to 21 Da ($q_z=0.58$). Figure 4-7b shows the same data when plotted in terms of q_z of the mass-selected reagent ion. All the reagent ions show the same range of stability (in terms of q_z values) and approximately the same degree of ion loss near $q_z=0.65$ and 0.80. The observed minor differences in the location of the resonance (i.e. ion intensity minima) and the amount of ion loss is most likely attributable to the difference in ion population of each reagent ion.

Although the $(M-H)^+$ ion of isobutane exhibits primarily ejection near the higher resonance lines, evidence of CID exists under conditions of high ion populations and long storage times (both of which magnify higher-order field effects).

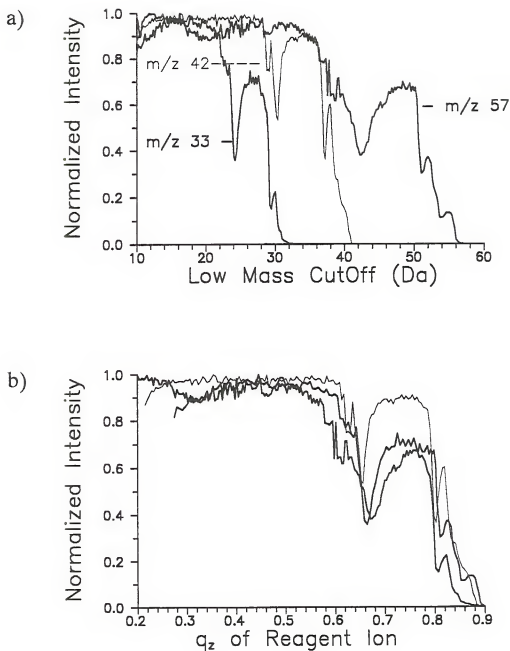


Figure 4-7: Intensities of mass-selected CH_3OH_2^+ (m/z 33, protonated methanol), CH_3CNH^+ (m/z 41, protonated acetonitrile), and C_4H_9^+ (m/z 57, hydride abstracted ion of isobutane) following 50 ms storage plotted in terms of a) low mass cutoff (Da) and b) q_z of the reagent ion.

The observed fragment ion, m/z 41, is presumably the neutral loss of methane to yield $C_3H_5^+$. Indeed, resonance excitation CID of the m/z 57 ion of isobutane generates the product ion at m/z 41.

Effects on CI Quantitation

Loss of CI reagent ions by ejection due to higher field resonances will lower the reagent ion population available for the CI process. This ion loss will decrease the sensitivity of the technique. For quantitation of a high m/z analyte ion, a high m/z CI reagent ion allows a higher value for the low mass cutoff, placing the analyte ion at a higher q_z value where it will be stored more efficiently. Due to the higher-order field effects on CI reagent ions (i.e. CID and ejection), quantitation in the mass-selected CI mode is affected by higher-order field induced losses. Reagent ion losses due to ejection ultimately result in reduced sensitivity of the CI mode of operation. Reagent ion losses due to CID not only reduce the sensitivity but also can result in altered spectra due to the formation of other CI reagent ions and, thus different analyte ions. These issues become critical when determining the limit of detection (LOD) and linear dynamic range (LDR) in the CI mode. As discussed in the introduction, the optimum RF level for CI of the analyte is dependent on both the CI reagent ion and the analyte ions produced. Both the analyte and the CI reagent ions need to be stored within the stable q_z range defined by $0.1 < q_z < 0.85$ (at $a_z=0$).

This issue is shown graphically in Figure 4-8 in which the ion intensity for the CI reagent ion, $C_2H_5^+$ is plotted together with the ion intensity from a model analyte ion, an EI produced ion (m/z 414) from the calibration compound perfluorotributylamine (PFTBA). Both ions were individually mass-selected and stored for 10 ms. Although the CI reagent ion exhibits constant signal (i.e. constant storage efficiency) below a low mass cutoff corresponding to 20 Da ($q_z=0.62$ for m/z 29; $q_z=0.04$ for m/z 414), the relatively high m/z analyte ion does not exhibit constant storage efficiency until a low mass cutoff of approximately 26 Da ($q_z=0.81$ for m/z 29; $q_z=0.06$ for m/z 414). If the m/z 414 analyte ions were created via CI with $C_2H_5^+$, the RF level for optimum production would necessarily correspond to a low mass cutoff of 26 Da. This RF level, however, corresponds to the vicinity of the hexapolar resonance line for the $C_2H_5^+$ ion, thus causing CI reagent ion losses. If CI were performed at an RF level free from higher-order resonances (i.e. $q_z < 0.60$, low mass cutoff < 20 Da) an approximate 80% loss of analyte ion signal would result. Furthermore, a first hand approach at increasing the sensitivity of CI is to increase the CI reagent ion population, and/or increase the CI reaction period. As discussed in Chapter 3, both of these parameters magnify the higher-order field effects. Increasing either of these two parameters "broadens" and "deepens" the CI reagent ion loss band. The result, therefore, would be a competing process between the CI reactions to produce analyte ions and CI reagent ion losses.

The practicality of this issue was investigated with regards to the application of mass-selected CI for the detection of compounds of environmental concern.

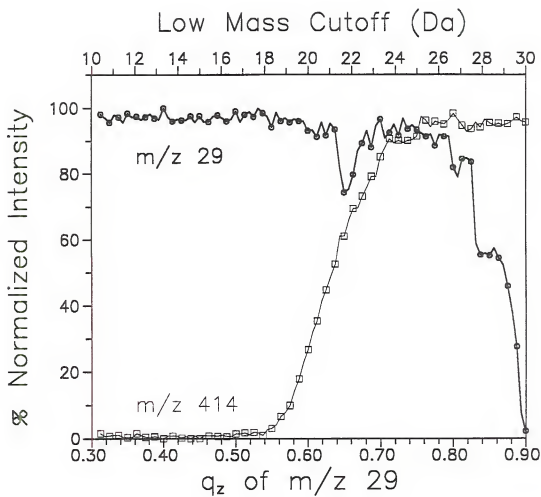
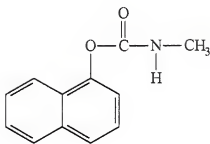


Figure 4-8: Normalized intensities of mass-selected m/z 29 and mass-selected m/z 414 versus RF level (in terms of low mass cutoff and q_z of m/z 29) following 10 storage ($a_z=0$).

The compounds of interest carbaryl, a carbamate pesticide, and methomyl, a sulfur-based pesticide, are shown in Figure 4-9. Shown in Figure 4-10 are the corresponding CI mass spectra acquired via the reaction with mass-selected $C_2H_5^+$ at an RF level free of higher-order field effects (i.e. $q_z=0.5$, $a_z=0$).

To investigate the optimum RF level for quantitation of the two compounds of interest, the $C_2H_5^+$ ion from methane and the CH_3CNH^+ ion from acetonitrile served as the CI reagent ions. These two reagent ions were chosen due to the different consequences exhibited upon storage near the octopolar resonance line at $\beta_z=1/2$ (i.e. the $C_2H_5^+$ ion readily undergoes CID while the CH_3CNH^+ ion undergoes ejection only). With the introduction of a constant amount of analyte into the quadrupole ion trap, the RF level during the CI reaction was varied. Shown in Figure 4-11a and 11b are the results obtained for the CI reaction, as a function of the q_z of the reagent ion, between carbaryl and the $C_2H_5^+$ and CH_3CNH^+ reagent ions, respectively. The base peak in the CI spectrum, m/z 145, is the obvious candidate for the quantitation ion for this compound. As demonstrated in Figure 4-11, however, acquisition of the CI spectrum near $q_z=0.64$ for the CI reagent ion results in nearly 50% loss of analyte signal for both reagent ions employed. A less dramatic effect is observed with the CH_3CNH^+ CI reagent ion due to the fact that CH_3CNH^+ does not undergo CID easily and its loss due to ejection requires more power than that required for the $C_2H_5^+$ ion. Consequently the CH_3CNH^+ CI reagent ion is less susceptible to higher-order field effects; thus its loss band is markedly less than that observed for the $C_2H_5^+$ CI reagent ion.

a)

**Carbaryl (MW=201)**

b)

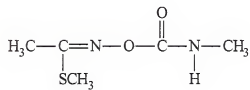
**Methomyl (MW=162)**

Figure 4-9: Chemical structures of the pesticides a) carbaryl and b) methomyl.

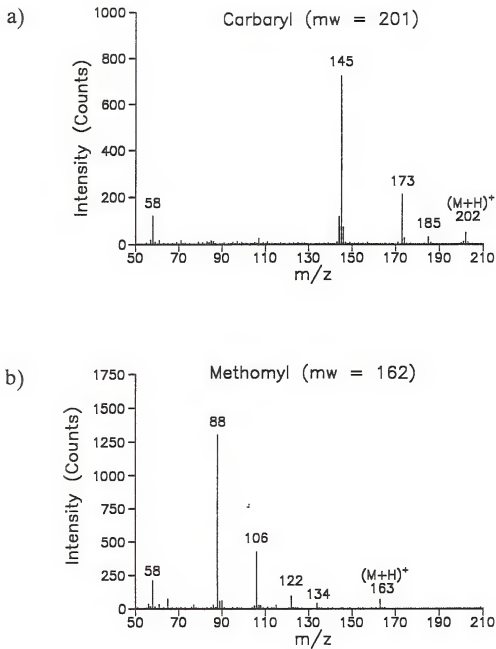


Figure 4-10: Mass-selected CI spectra of a) carbaryl and b) methomyl. Spectra acquired with $C_2H_5^+$ (m/z 29) as the CI reagent ion at a q_z value corresponding to 0.50 for m/z 29.

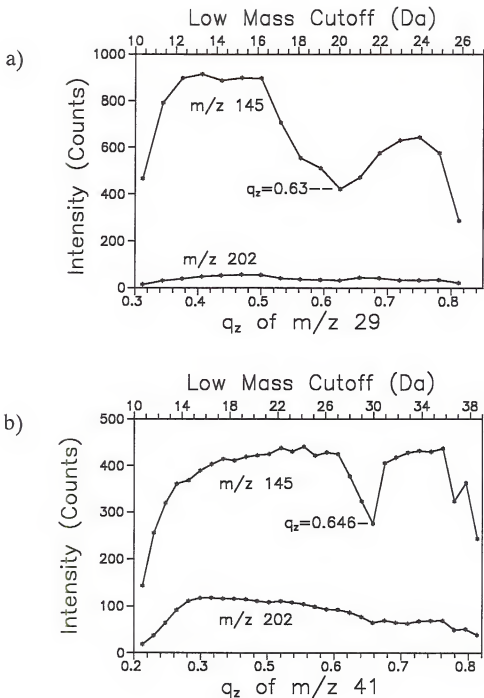


Figure 4-11: Intensities of the base peak (m/z 145) and the protonated molecular ion of carbaryl (m/z 202) versus the RF level (q_z of the CI reagent ion and low mass cutoff) employed for the CI reaction between neutral carbaryl and a) $C_2H_5^+$ (m/z 29, from methane) and b) CH_3CNH^+ (m/z 41, protonated acetonitrile).

Similar experiments were performed with the sulfur-based pesticide, methomyl. Based upon the CI mass spectrum shown in Figure 4-10, the m/z 88 fragment ion would be the most likely candidate for quantitation due to its abundance. Results from the RF level study are shown in Figures 4-12a and 12b for the mass-selected $C_2H_5^+$ and CH_3CNH^+ CI, respectively. For each CI reagent ion, approximately 40 % of the quantitation ion is lost near the $\beta_z=1/2$ octopolar resonance line at $q_z=0.64$. All CI produced ions show reduced intensity near the resonance line. As observed similarly with carbaryl, the $C_2H_5^+$ reagent ion exhibits broader effects due to the ease of CID.

Shown in Table 4-2 are a number of CI reagent ions together with RF levels (in terms of low mass cutoff) where higher-order field effects become significant due to the influence of the main octopolar resonance, $\beta_z=1/2$, and the main hexapolar resonance, $\beta_z=2/3$. The tabulated RF levels represent the regions that should be avoided when performing CI with the specific reagent ion. As demonstrated in the previous two examples, any RF level beyond that corresponding to the octopolar resonance (i.e. $q_z=0.65$) results in an attenuated signal; therefore, if possible, all CI should be performed at q_z values for the reagent ions less than $q_z=0.65$.

Effects on CI Spectral Quality

Higher-order field effects on CI reagent ions can alter the resulting CI spectra. Due to CID of the CI reagent ions, the analyte fragment ion intensities may vary.

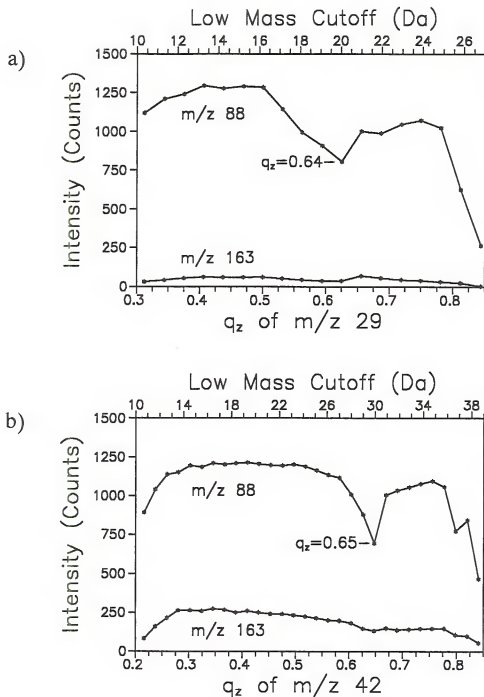


Figure 4-12: Intensities of the base peak (m/z 88) and the protonated molecular ion of methomyl (m/z 163) versus the RF level (q_z of the CI reagent ion and low mass cutoff) employed for the CI reaction between neutral methomyl and a) $C_2H_5^+$ (m/z 29, from methane) and b) CH_3CNH^+ (m/z 41, protonated acetonitrile).

Table 4-2: RF Levels Corresponding to $\beta_z = 1/2$ and $2/3$ (along $a_z = 0$) for Various CI Reagent Ions.

CI Reagent Gas	CI Reagent Ion	m/z	$\beta_z = 1/2$ ($q_z = 0.645$) Low Mass Cutoff (Da)	$\beta_z = 2/3$ ($q_z = 0.790$) Low Mass Cutoff (Da)
Methane	CH_5^+	17	12.1	14.8
Water	H_3O^+	19	13.5	16.5
Methane	C_2H_5^+	29	20.6	25.2
Methanol	CH_3OH_2^+	33	23.4	28.7
Methane	C_3H_5^+	41	29.1	35.7
Acetonitrile	CH_3CNH^+	42	29.8	36.5
Isobutane	$(\text{CH}_3)_3\text{C}^+$	57	40.5	49.6

Obtaining reproducible CI mass spectra is critical in mass spectrometry; therefore, the dependence on the RF level with the appearance of the spectra needs to be understood. Additionally, higher-order field effects are of particular concern in the acquisition of CI spectra due to the inherent aspects of the technique (i.e. long storage times and high ion populations). Both of these factors magnify the effects which ultimately are manifested as lower sensitivity (as discussed above) and altered CI spectra. The mass-selected CI spectral quality can be altered by the presence of several CI reagent ion species due to CID of the mass-selected CI species (and subsequent ion/molecule reactions). For example, mass-selected CI using $C_2H_5^+$ of methane at an RF level corresponding to a higher field resonance can result in ionization of the analyte by not only $C_2H_5^+$ (m/z 29), but also by $C_2H_3^+$ (m/z 27), and $C_3H_5^+$ (m/z 41).

The influence of each CI reagent ion on a particular analyte neutral is dependent on both the proton affinity (PA) and hydride ion affinity (HIA) of the CI reagent ion and the neutral analyte. Table 4-3 lists the PA and HIA values for several of the CI reagent ions discussed in this chapter. The CI species possessing high PA values are less likely to transfer a proton to a neutral analyte (i.e. to form the $(M+H)^+$ ion of the analyte); species with a lower HIA are more likely to remove a proton from a neutral analyte (i.e. to form the $(M-H)^+$ ion of the analyte). The conversion of $C_2H_5^+$, which favors proton transfer, to $C_3H_5^+$, which favors hydride abstraction (Berberich *et al.*, 1989), can alter the resulting CI mass spectrum due to the inherent affinities of each species.

Table 4-3: Proton and Hydride Ion Affinities of Selected CI Reagent Ions

CI Reagent Gas	CI Reagent Ion (BH) ⁺	Proton Affinity ^a of (B)		Hydride Ion Affinity ^a of (BH) ⁺	
		kcal/mol ^b	eV	kcal/mol ^b	eV
Methane	CH ₅ ⁺	131.6	5.71	269	11.7
Methane	C ₂ H ₅ ⁺	162.6	7.05	271	11.8
Water	H ₃ O ⁺	166.5	7.22	234	10.2
Methanol	CH ₃ OH ₂ ⁺	181.9	7.89	219	9.5
Methane	C ₃ H ₅ ⁺	181.9	7.89	254	11.0
Isobutane	(CH ₃) ₃ C ⁺	195.9	8.49	233	10.1

a) Harrison, 1992

b) Conversion from kcal/mol to eV is 23.0609(kcal/mol)/eV.

An example of altered CI spectra due to higher-order field effects is illustrated in Figure 4-13, where mass-selected reagent ions of methane were reacted with neutral n-butylbenzene. Mass-selected CI employing $C_2H_5^+$ at an RF level corresponding to a stable region for the reagent ion (e.g. $q_z=0.50$, $a_z=0$; Figure 4-13a) yielded the $(M+H)^+$ ion of n-butylbenzene (m/z 135) due to proton transfer from $C_2H_5^+$, as well as a number of characteristic fragment ions at m/z 107, 91, 79, 71, and 57.. Mass-selected $C_2H_5^+$ CI at an RF level corresponding to the octopolar resonance for m/z 29 at $\beta_z=1/2$ (e.g. $q_z=0.66$, $a_z=0$; Figure 4-13b) resulted in an increase in the relative ion intensities of several ions, most notably the hydride abstracted ion, $(M-H)^+$, and its associated fragment ions (m/z 105 and 119) as well as the $(M+13)^+$ adduct ion at m/z 147. These spectra can be compared to the CI mass spectrum acquired by pure hydride abstraction (shown in Figure 4-13c), where n-butylbenzene was reacted with mass-selected $C_3H_5^+$ (m/z 41) at a stable region for the CI reagent ion (e.g. $q_z=0.50$, $a_z=0$). The hydride ion abstraction mass spectrum exhibits a high abundance of the $(M-H)^+$ ion and its unique fragment ions, m/z 105 and 119, as well as the $(M+13)^+$ ion (presumably arising from the neutral loss of C_2H_4 from the $M+C_3H_5^+$ adduct ion). Inspection of Figure 4-13b revealed that under the conditions of this spectrum nearly equal contributions from the proton transfer and hydride abstraction CI mechanisms comprise the resulting CI mass spectrum.

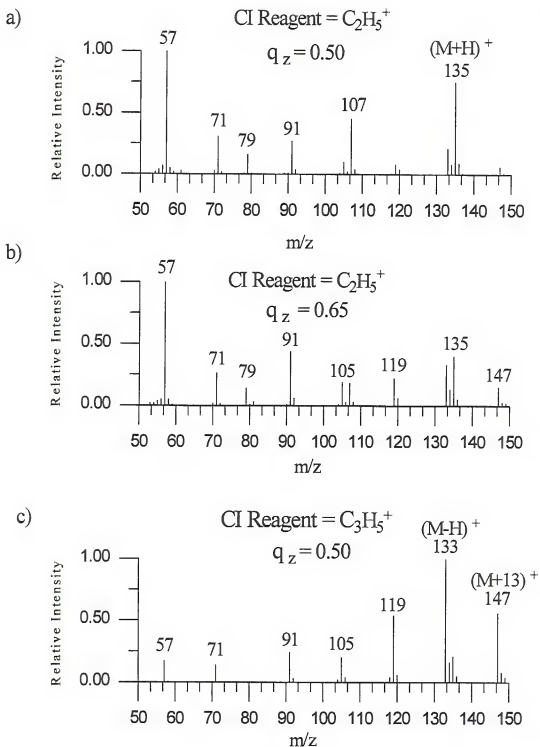


Figure 4-13: Mass-selected CI spectra of n-butylbenzene acquired with a) C_2H_5^+ (m/z 29) at a q_z value of 0.50 for m/z 29, b) C_2H_5^+ (m/z 29) at a q_z value of 0.65 for m/z 29, and c) C_3H_5^+ (m/z 41) at a q_z value of 0.50 for m/z 41.

It should be noted that not all compounds will experience such a significant change in CI mechanism based on the identity of the CI reagent ion, and therefore may not exhibit altered CI spectra. Certain classes of compounds, however, are very susceptible to the hydride abstraction mechanism of CI. With the appropriate CI reagent ions, compounds such as aliphatic hydrocarbons, ethers, and polyamines will exhibit hydride abstracted ions in the CI spectrum. An example of this is shown in Figure 4-14 where isopropylether was subjected to mass-selected CI with $C_2H_5^+$ of methane. The top spectrum, Figure 4-14a, is the result of performing the CI reaction at an RF level corresponding to $q_z=0.50$ for the reagent ion; the bottom spectrum, Figure 4-14b, corresponds to an RF level of $q_z=0.65$ for the reagent ion. Similarly to the n-butylbenzene case, the spectrum of isopropylether acquired near $q_z=0.65$ exhibits an increased amount of the $(M-H)^+$ hydride abstracted molecular ion, m/z 101. Note also, the increase in the associated fragment ions at m/z 83, $(M-H-H_2O)^+$, and m/z 59, $(M-H-C_3H_6)^+$. Again, this is due to the increased abundance of the $C_3H_5^+$ reagent ion which originates from higher-order field resonance induced CID (and subsequent ion/molecule reactions) of the mass-selected $C_2H_5^+$ ion. The m/z 41 ion favors hydride abstraction and alters the resulting CI spectrum when acquired near $q_z=0.65$.

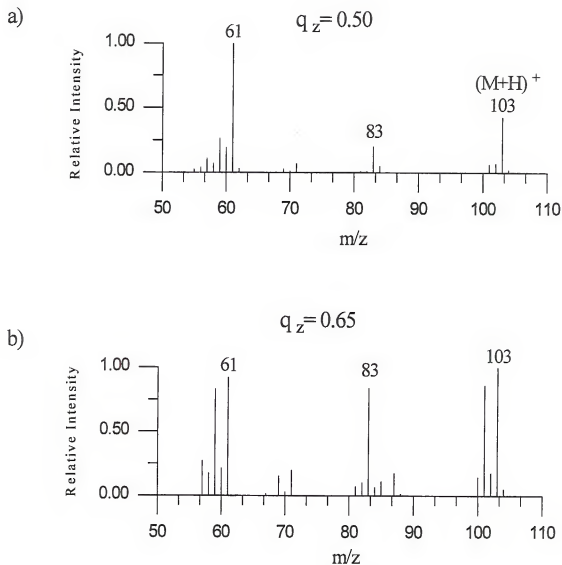


Figure 4-14: Mass-selected CI spectra of isopropylether acquired with a) $C_2H_5^+$ (m/z 29) at a q_z value of 0.50 for m/z 29 and b) $C_2H_5^+$ (m/z 29) at a q_z value of 0.65 for m/z 29.

Conclusions

This chapter has presented a detailed investigation into higher-order field effects on the mass-selected chemical ionization (CI) mode on the quadrupole ion trap. In general, ion trap users need to be conscious of RF levels during the entire CI process in order to avoid regions of the stability diagram near β_z values corresponding to higher-order field resonances. The most stable region (free from higher-order non-linear resonances) can be found in the upper left portion (e.g. $q_z < 0.61$, $a_z > -0.05$) of the stability diagram; higher-order field effects become more significant in the lower portion of the stability diagram ($a_z < 0$).

The effects are of concern for ions whose m/z is less than 1.5 times that of the low mass cutoff, since this dictates q_z values greater than 0.61. Due to the relatively low m/z ions employed in CI, higher-order field effects are observed during this mode of operation. Users of quadrupole ion traps, therefore, must be aware of q_z values for the CI reagent ions during acquisition of CI spectra. This is true for both mass-selected and non-mass-selected CI. For analytes of high molecular weight (i.e. > 400 Da), CI is typically performed at high q_z values of the reagent ion in order to store the resulting CI product ion at a q_z value which offers efficient storage (i.e. $q_z > 0.1$). Particular concern must be made to avoid resonances near $q_z = 0.645$ and 0.790 (along $a_z = 0$) of the CI reagent ion in order to achieve maximum ion signal for the desired analyte ions. In general, and until the reagent ion population is depleted, increasing the CI reaction time will increase analyte ion intensity; if storage is performed near a higher resonance, however, a competing process will exist between

CI reactions to produce analyte ions and CI reagent ion losses. As demonstrated in Chapter 3, increasing the ion population or increasing the storage time will magnify the effects.

Effects on CI Reagent Ions

Higher-order resonances were found to influence all CI reagent ions investigated. The CI reagent ions of methane (i.e. CH_5^+ , C_2H_5^+ , and C_3H_5^+) were observed to readily undergo CID to form other reagent ions which rapidly react with neutral methane to form other, higher m/z reagent ions. While storing CH_5^+ near higher-order field resonances, the ion underwent CID via the neutral loss of H_2 producing CH_3^+ which reacted with neutral methane to yield C_2H_5^+ . Under similar mechanisms, the C_2H_5^+ produced reagent ions at m/z 27 and 41; the C_3H_5^+ reagent ion produced ions at m/z 39 and 53. The main CI reagent ions from methanol (CH_3OH_2^+), acetonitrile (CH_3CNH^+), and isobutane ($(\text{CH}_3)_3\text{C}^+$) underwent ejection only. Under very high ion populations and storage times, however, the $(\text{M}-\text{H})^+$ ion of isobutane did exhibit CID to form C_3H_5^+ , m/z 41.

Effects on CI Quantitation

Due to ejection and CID of CI reagent ions, sensitivity is reduced when acquiring CI spectra at RF levels corresponding to the main octopolar resonance ($\beta_z=1/2$) or the main hexapolar resonance ($\beta_z=2/3$). Obtaining LOD and LDR information while employing mass-selected CI on the quadrupole ion trap, therefore

needed to be acquired at $q_z < 0.60$ for the CI reagent ion. Data presented in this chapter showed that quantitation with the $C_2H_5^+$ reagent ion can result in up to 50% loss of analyte signal if acquired near higher-order field resonances; quantitation with CH_3CNH^+ reagent ion showed approximately 30% loss of signal.

Effects on CI Spectral Quality

Due to CID and ejection of CI reagent ions near higher-order resonances, the resulting CI spectra can be altered. Dissociation of the mass-selected reagent ion to form other species which can react with the neutral analyte can alter the spectra. The $C_3H_5^+$ ion is produced from CID of $C_2H_5^+$ via the $C_2H_3^+$ intermediate. All three ions can react with analyte neutral molecules. For the compounds discussed in this chapter, the dominating CI processes observed with the $C_2H_5^+$ ion was proton transfer; the dominating CI processes observed with the $C_3H_5^+$ ion was hydride abstraction and adduct formation. Consequently, the resulting CI mass spectrum will be comprised of contributions from all the above processes. Under non-mass selected CI conditions (as in the more common quadrupole mass spectrometers), these processes occur routinely. However, the advantage of mass-selected CI with the quadrupole ion trap allows more control of the CI process. To correctly control the energy deposition process and to correctly interpret the resulting data, the RF level during the CI reaction needs to be free of higher-order field effects (i.e. $a_z < 0.6$ for the CI reagent ion).

CHAPTER 5 HIGHER-ORDER FIELD EFFECTS ON ION MOTION

Introduction

This chapter will present preliminary results from a qualitative investigation of higher-order field effects on ion motion. Due to the nonideal quadrupole ion trap employed in commercial instruments, the ion motion in the z-direction is not completely decoupled from that in the r-direction. Therefore, due to higher-order fields, resonance excitation at an axial frequency can result in power absorption in the radial direction (and vice versa). The goals for this work were three-fold: 1) to characterize quadrupolar resonance excitation, 2) to employ both dipolar and quadrupolar resonance excitation over a broad frequency range to identify frequency components of ion motion, and 3) to detect the influence of higher-order field effects on ion motion.

While holding the resonance excitation amplitude and duration constant, the excitation frequency is incremented over a wide range and the ion intensity is monitored. At specific frequencies, the ions absorb power from the excitation field and undergo losses due to either ejection or dissociation. The ion intensity minima can be correlated to ion frequencies of motion. By acquiring ion intensities over a

broad excitation frequency range, a power absorption spectrum is generated and frequency components can be identified.

This chapter will begin with an overview of resonance excitation on the quadrupole ion trap. Results from previously published simulations which are pertinent to these studies will be discussed. Previously reported experimental results for the evidence of coupled motion also will be discussed in detail. Next, the experimental considerations for performing the current experiments will be presented. A number of power absorption spectra acquired at various points in the Mathieu stability diagram will be presented in this chapter. Specifically, the regions investigated were 1) near the $\beta_z=0$ boundary, 2) along the $a_z=0$ line, and 3) near the apex ($q_z=0.78$, $a_z=0.15$). Each absorption band in the power absorption spectrum will be correlated to frequency components of ion motion.

Ion Motion Under Resonance Excitation

Ion motion in the quadrupole ion trap can be described, for the "ideal" case of a single isolated ion, by independent Mathieu equations. The frequency of ion oscillations in each direction (z- and r-direction) can be characterized by a series of frequencies, $\omega_{n,u}$, represented by the following equation (March and Hughes, 1989):

$$\omega_{n,u} = \left(\frac{\beta_u}{2} + n \right) \Omega \quad (5-1)$$

where n is an integer between $-\infty$ and $+\infty$, $0 < \beta_u < 1$, Ω is the frequency of the applied RF storage field, and u is either r or z . Recall that the main frequency

(secular), designated by $n=0$, is related to the frequency of the RF storage field by $\omega_u = \beta_u \Omega / 2$. Substituting ω_u and rewriting the equation in order to express the frequency components in terms of positive numbers gives the following equations:

$$\omega_{n,u} = (n + \omega_u) \Omega \quad n = 0, 1, 2, 3 \dots \quad (5-2)$$

$$\omega_{n,u} = -(n + \omega_u) \Omega \quad n = -1, -2, -3 \dots \quad (5-3)$$

where ω_u is the secular frequency.

The ion trajectories appear as Lissajous curves composed of the two main frequencies, ω_x and ω_r . A higher frequency micro-motion, due largely to $n = \pm 1$, appears superimposed on top of the secular frequencies; these frequencies correspond to $\Omega - \omega_u$ and $\Omega + \omega_u$ (March and Hughes, 1989). Except for very low q_u of storage ($q_u < 0.01$, Vedel *et al.*, 1990), the micro-motion contributes significantly to the total ion motion and, therefore, cannot totally be neglected. The contribution of higher frequency components to the total ion motion increases rapidly for very high q_u values. For example, while storing ions at $q_x = 0.20$, $a_z = 0$, contributions to the total ion motion are theoretically predicted (Pedder, 1992) to be 87% ω_u ($n=0$), 9% $\Omega - \omega_u$ ($n=-1$), and 4% $\Omega + \omega_u$ ($n=+1$); storage near $q_x = 0.85$, $a_z = 0$ results in 53% ω_u , 37% $\Omega - \omega_u$, and 6% $\Omega + \omega_u$ (4% contribution due to $n > \pm 1$). In general, with increasing values of n (i.e. $n > \pm 1$) contribution to the total ion motion decreases. Therefore, unless very precise calculations are required, contributions due to $2\Omega \pm \omega_u$, $3\Omega \pm \omega_u$, and higher frequencies can be neglected.

Stored ions can be resonantly excited by applying an AC signal at a frequency corresponding to any component of ion motion; the greater the contribution of the specific frequency to the total motion, the greater the ability of the ion to absorb power from the applied field. Upon absorbing power, the ion increases its trajectory and thus increases its kinetic energy. This technique was first used by the early pioneers of quadrupole ion traps in order to detect ions (Paul *et al.*, 1958; Fischer, 1959). The resonance excitation signal can be applied in one of three modes: monopolar, dipolar, or quadrupolar. Monopolar excitation is accomplished by applying the AC signal to only one endcap; the other endcap is grounded. Dipolar excitation is accomplished by applying the AC signal to both endcaps, 180° out-of-phase to each other; applying the signal in-phase results in the quadrupolar excitation mode. Application of quadrupolar excitation signal results in a symmetric field similar to the RF trapping field. This mode of excitation does not favor either the radial or the axial frequencies of motion; therefore, ions can be excited at any frequency component of motion in the r- or z-direction. Application of a dipolar excitation signal is asymmetrical and is predicted to favor axial motion over radial motion (March *et al.*, 1989); monopolar excitation signals, which also are asymmetric are expected to favor axial motion.

From the earliest pioneering work of resonance excitation with quadrupole ion traps (Fischer, 1959), a major assumption for ions cooled to the center was that excitation at ω_r would cause increased ion motion only radially, and at the limit, ions would be lost due to striking the ring electrode or ejection through a hole in the ring.

Likewise excitation at ω_z would cause increased motion axially and, at the limit, ions would be lost due to striking the endcap or ejection through holes in the endcap. With the nonideal quadrupole ion trap, however, ion motion in the r- and z-direction are coupled; therefore, increased motion in one direction can influence the motion in the other direction (Wang, 1992).

Due to the supplemental excitation field, the trapping conditions are somewhat altered. The forces experienced by the ions under resonance excitation are due to both the quadrupolar trapping field and the excitation field. The resulting ion trajectories no longer follow the traditional Mathieu equations; thus, the exact theoretical frequencies of motion are altered (March *et al.*, 1993). The exact solution to the equations of ion motion under resonance excitation are extremely difficult to solve; therefore, simulations of resonance excitation typically involve approximation methods.

Previously Reported Simulation Results

Although well characterized experimentally, very little information exists regarding theoretical predictions of ion motion under resonance excitation. The theoretical approach to deriving the equations of motion for each resonance excitation mode has been presented (March *et al.*, 1989); the solution to the equations for dipolar and monopolar modes, however, have yet to be reported. Although monopolar excitation has been employed experimentally for ion ejection (Armitage *et al.*, 1979), this mode is less common and thus is not well characterized.

Dipolar excitation is the most commonly employed resonance mode. Indeed, nearly every commercial instrument employs dipolar resonance excitation; thus this mode of excitation has been well characterized experimentally. Quadrupolar excitation, which traditionally has been less common than dipolar excitation, recently has been reported for experimental application (Vedel, 1991; Vedel *et al.*, 1990, 1991) and theoretical simulations (March *et al.*, 1989, 1990, 1991, 1993). The exact solution to the equations of motion under quadrupolar excitation recently have been presented (March *et al.*, 1993).

To simulate ion motion, Pedder *et al.* (1988, 1992) developed the program, HyperIon, which calculates ion trajectories by numerical integration of the Mathieu equations of motion. The equations of motion were modified by incorporating a parallel plate capacitor model for simulation of dipolar resonance excitation. The program was used successfully for simulating electron trajectories and calculating ion kinetic energy. Simulations of ion motion under resonance excitation compared well to the experimental results for the effectiveness of dipolar resonance excitation at harmonic frequencies of ion motion (Pedder *et al.*, 1992). Due to the equations employed for this program, only the theoretical frequencies were predicted (i.e. ω_v , $\Omega \pm \omega_v$, $2\Omega \pm \omega_v$). Since the HyperIon program does not account for a nonideal quadrupole ion trap or for a nonideal dipolar field, conditions for ion motion under "real" perturbed conditions can not be explored with this program. The parallel plate capacitor model for a dipolar field is an "ideal" case. Experimentally, the application of an AC signal to the endcaps (180° out-of-phase) only approximates a dipolar field.

Due to the electrode surface geometry (the hyperbolic surface, the truncation, and the holes), an "ideal" dipolar field cannot be constructed (Reiser *et al.*, 1992). Furthermore, as discussed in Chapter 2, the presence of higher-order fields result in a perturbed quadrupolar trapping field which alters the ion motion. The result is that the three differential equations describing ion motion in each direction become coupled and, therefore, are very difficult to solve exactly. This is the justification for employing numerical methods and simple models for the applied dipolar field.

The simulation program ITSIM, developed by Reiser *et al.* (1992), employs a Taylor expansion for numerical solution to the Mathieu equations. To simulate dipolar resonance excitation, a "forced" Mathieu equation was developed which includes terms that account for the force on the ion due to a dipole field (Williams *et al.*, 1991b). This program assumes an "ideal" dipolar field and no perturbations in the quadrupolar trapping field; therefore, as discussed above, the simulations are not truly representative of the environment of the trapped ion. This program produces the theoretical frequencies as predicted by the Mathieu equations of motion for an unperturbed ion (i.e. ω_w , $\Omega \pm \omega_w$, $2\Omega \pm \omega_w$...). The addition of higher-order field terms (Williams *et al.*, 1991b) to the "forced" Mathieu equations, however, reportedly predicts other frequencies of motion due to the influence of a hexapolar field.

In a series of papers, March *et al.* (1989, 1990, 1991, 1993) reported results from simulations of quadrupolar excitation. The equations of motion resulting from the application of in-phase signals to the endcaps (quadrupolar) can be solved

exactly; therefore, exact simulations of ion motion under quadrupolar excitation can be performed on a computer. The simulations discussed in these reports, however, did not consider distortions in the quadrupolar trapping field due to higher-order fields. By solving the equations of motion under quadrupolar excitation (i.e. perturbed conditions), frequency components due to $2\omega_z$ were predicted. Furthermore, the simulations predicted that the strongest resonance condition (i.e. most absorption of power) would result at twice the ion's axial secular motion (i.e. $2\omega_z$). This can be understood by considering the relationship between axial motion and the excitation mode. An ion will pass an endcap electrode twice during one axial oscillation. For optimum power absorption, each endcap needs to be charged with the correct polarity when the ion is near. Since the quadrupolar excitation is applied in-phase to each endcap, in order for each endcap to be charged correctly when the ion is near, the excitation frequency must be applied at twice the ion's axial frequency. Similarly, since dipolar excitation is applied 180° out-of-phase, each endcap can be charged at the same frequency of the ion's axial secular frequency.

With their simulations, March *et al.* (1989) reported that quadrupolar excitation at ω_z exhibited pronounced absorption while storing ions at $q_z=0.1$ ($a_z=0$) and only minimal absorption at high q_z values ($q_z>0.5$). Strong absorption was reported also near $q_z=0.79$ ($\beta_z=2/3$). No rationalization was offered in the report for this observation; the results, however, will be explained in the discussion section below. Similar trends were reported for excitation at ω_r , although less overall absorption was observed. Ion simulations of quadrupolar excitation at frequencies

corresponding to $\Omega - \omega_z$ and $\Omega + \omega_z$ resulted in detectable absorption with the former exhibited more absorption than the latter. At all q_z values investigated (along the $a_z=0$ line), quadrupolar excitation at $2\omega_z$ resulted in the strongest absorption; excitation at $2\omega_r$ exhibited somewhat less absorption than $2\omega_z$.

With the use of the field interpolation model (FIM), March *et al.* (1991) reported results from ion simulations of monopolar, dipolar, and quadrupolar excitation. This simulation model determines the component field forces on an ion at specific r - and z -coordinates. Based on the previous field forces, the ion is relocated, the field forces at the new location are evaluated, and, again, the ion is relocated. The simulated ion trajectory is determined by this point-by-point process. The results from the FIM simulation showed that for excitation at ω_z ($a_z=0$), the ion absorbs the most power under dipolar excitation, less by monopolar excitation, and the least via quadrupolar excitation. With increasing q_z ($a_z=0$), absorption due to quadrupolar excitation decreases. Upon excitation at $2\omega_z$, the quadrupolar mode displayed the most absorption (as predicted by theory); no absorption was observed via the dipolar or monopolar mode. Upon excitation at ω_r , absorption was observed in all three modes; however, with increasing q_r , all absorptions reduced rapidly. In general, simulations of the monopolar mode mirrored those of the dipolar mode, although with reduced efficiency.

Several reports of ion simulations have been offered by Franzen (1991, 1993, 1994). These reports simplify ion motion to only the z -direction; thus, motion in the r -direction is not observed. Nevertheless, the simulations were successfully employed

in the investigation of the higher-order field contributions to the quadrupolar trapping field. A mathematical analysis of the calculated ion trajectories was performed via fast Fourier transform (FFT). The results of the FFT for ions stored at $q_z=0.68$, $a_z=0$ ($\beta_z=0.54$) in an "ideal" quadrupolar ion trap produced, as predicted from Mathieu theory, frequencies of ion motion due to ω_z , $\Omega \pm \omega_z$, and $2\Omega \pm \omega_z$ (March and Hughes, 1989). The same analysis with the incorporation of a 20% hexapolar field revealed a new frequency of motion corresponding to the trapping frequency, Ω , and a number of frequency components comprised of multiples of ω_z and higher harmonics. The new frequencies which contributed the most (out of all of the new frequency components) were due to $2\omega_z$, $\Omega - 2\omega_z$, $3\omega_z$, and $\Omega - 3\omega_z$. Frequency analysis with the incorporation of 20% octopolar produced mainly contributions from $3\omega_z$, $\Omega - 3\omega_z$ and other odd multiples. The contributions of all of the newly produced frequency components were markedly less than the contributions due to the main frequencies of motion from ω_z and $\Omega \pm \omega_z$.

Previously Reported Experimental Results

Since simulations cannot truly represent the environment of the stored ions, experimental investigations can be employed to identify frequency components of ion motion in a nonideal quadrupole ion trap. A recently published report (Vedel *et al.*, 1990) described the experimental investigation of ion motion via dipolar and quadrupolar excitation. A non-commercial quadrupole ion trap was employed for these studies; the electrodes were constructed out of steel mesh and conformed to

the theoretical geometry and spacing for a pure quadrupolar field (i.e. $r_0=1$ cm, $z_0=0.7071$ cm). Ions of N_2^+ were stored at $q_z=0.50$, $a_z=0$ during resonance excitation of either the dipolar or quadrupolar mode. While holding the excitation amplitude and duration constant, the excitation frequency was varied, thus producing a "motion" spectrum (Vedel *et al.*, 1990). Under dipolar excitation, the main absorption band was due to ω_z as expected from theory; the next most significant band, however, was due to $2\omega_r+\omega_z$. No explanation was offered as to the origin or magnitude of this absorption band. Other bands easily observed were due to $\omega_z/2$ (minor), ω_r , $2\omega_r$, $\omega_r+\omega_z$, $2\omega_r-\omega_z$, and $2\omega_z$. The magnitude of the ω_r and $2\omega_r$ bands were similar, although both were substantially lower than the main band at ω_z . Nevertheless, this was the first report of observing radial absorption under dipolar excitation. The experimental observation of excitation at ω_r and $2\omega_r+\omega_z$ agrees with the theoretical simulations using the FIM method (March *et al.*, 1991).

Quadrupolar excitation of ions stored at $q_z=0.50$, $a_z=0$ revealed very broad absorption bands of approximate equal magnitude for $2\omega_r$ and $2\omega_z$ (Vedel *et al.*, 1990). Indeed, strong absorptions at twice the secular frequency are predicted by theory. The ratio of the magnitude of the absorptions agreed with those predicted by simulations using the FIM method (March *et al.*, 1991). The experimental results also showed evidence for excitation at ω_z and $\omega_z+\omega_r$, although somewhat reduced compared to the $2\omega_r$ and $2\omega_z$ bands. Detectable absorptions were observed at $\omega_z-\omega_r$, $2\omega_r-\omega_z$, ω_r , $2\omega_z+\omega_r$, and $3\omega_z-\omega_r$.

Under quadrupolar excitation, absorptions due to $2\omega_z$ and $2\omega_x$ are theoretically predicted for the quadrupolar mode (March *et al.*, 1993). These absorptions have been referred to as "parametric resonances" (Vedel *et al.*, 1990). The absorptions resulting from combinations of ω_z and ω_x are due to the higher-order field effects of the nonideal quadrupole ion trap (recall that the quadrupole ion trap employed in the above report was constructed, in-house, out of steel mesh). Sources of higher-order fields, therefore, are expected to significantly contribute due to the difficulty in conforming to exact electrode geometry and spacing (see Chapter 2). The observation of many of the coupled terms (i.e. combinations of ω_z and ω_x) may be attributed to this nonideal ion trap.

Experimental

Instrumentation and Chemicals

Experiments were performed on a Finnigan MAT (San Jose, CA, USA) ion trap mass spectrometer (ITMS™) maintained at 100° C. Helium (Liquid Air, Walnut Creek, CA) was used as the buffer gas. Methane (Matheson Gas Products, Morrow, GA) and argon (Alphagaz, Walnut Creek, CA) were introduced into the ITMS™ via a fine metering valve (Negretti, Southampton, England). Pressures on the ITMS™ were those indicated by a Bayard-Alpert ionization gauge (Granville-Phillips, Boulder, CO) mounted on the vacuum chamber and are reported with no correction factors.

Table 5-1: Scan function for probing ion frequencies while storing m/z 40 ions near the $\beta_z=0$ boundary

#	Table Comment	Start Mass (amu)	End Mass (amu)	Time (μ S)	DC Volts	Resonance Excitation
1	Trigger	0	0	100	0	
2	Pre-Ionization	10	10	100	0	
3	Ionization	10	10	1000	0	
4	Cool Table	10	10	500	0	
5	Ramp to $q_z=0.78$	10	34.3	1000	0	
6	Apex Isolate	34.3	34.3	500	-40 ($a_z=0.15$)	
7	Cool Table	34.3	34.3	1000	0	
8	DC Ramp to a_z	34.3	34.3	500	+55 ($a_z=-0.186$)	
9	RF Ramp to q_z	34.3	30.9	500	+55 ($a_z=-0.186$)	
10	Cool at q_z - a_z Point	30.9	30.9	5000	+55 ($a_z=-0.186$)	
11	Resonance Excitation	30.9	30.9	10000	+55 ($a_z=-0.186$)	100 kHz (3000 mV)
12	Remove Res. Exc.	30.9	30.9	2000	+55 ($a_z=-0.186$)	
13	Return to $q_z=0.78$	30.9	34.3	500	+55 ($a_z=-0.186$)	
14	Return to $a_z=0$	34.3	34.3	500	0	
15	EM Warm Up	34.3	10	2000	0	
16	Data Acquisition	10	100	20000	0	530 kHz (6000 mV)
17	RF Shut Down	0	0	2000	0	

The instrument software, ICMS® (developed by Nathan A. Yates, University of Florida) was used for all experiments on the ITMS™. The software allows the application of the resonance excitation for frequencies between 0 kHz and 1.6 MHz. A typical scan function used for these experiments is tabulated in Table 5-1. This specific scan function was used for resonance excitation near the $\beta_z=0$ boundary. Briefly, a 1 ms ionization time was employed at $q_z=0.3$ followed by a variable ion/molecule reaction period. The ion of interest was mass-selected by RF/DC "apex" isolation at $q_z=0.78$, $a_z=0.15$ (Weber-Grabau *et al.*, 1987; Todd *et al.*, 1987). The RF amplitude was then ramped to the desired q_z value where resonance excitation was applied for a variable period of time. Next, the resonance excitation signal was removed and the storage conditions were initialized for the beginning of the analytical scan.

All calculations were performed according to the corrected equations for the "stretched" ion trap design (Johnson *et al.*, 1992). ITMS™ data reduction was performed using the BASIC program, CHROLIST (written by Randall E. Pedder and Nathan A. Yates, University of Florida), which retrieves original ITMS™ data files, averages selected mass intensities, and writes the data into a tabular ASCII format. All data manipulation were performed with the commercial spreadsheet program QUATTRO (Borland International, Inc., Scotts Valley, CA). All β_u values and ion frequency determinations were calculated by the BASIC program AQFORM (written by Donald M. Eades and Matthew Booth, University of Florida) which uses

the continued fraction method (McLachlan, 1947) for β_u calculations (see Equation 2-13 of Chapter 2).

The RF trapping frequency, Ω , was 1.1 MHz. A $6V_{pp}$ axial modulation signal (Weber-Grabau *et al.*, 1988; Tucker *et al.*, 1988) was employed at 530 kHz (resonance ejection at $q_z=0.906$) during the mass-selective instability scan (Stafford *et al.*, 1983ab). The electron multiplier (EM) voltage was set to yield 10^5 gain and no dynode voltage was used. A grounded shield was present in front of the dynode/EM assembly of the ITMS™.

Experimental Considerations

Dipolar resonance excitation, the standard mode offered on the Finnigan MAT ITMS™, is accomplished by applying a supplementary AC signal to each endcap. The requested signal exits the electronics box of the ITMS™ and enters a balun circuit where the signal is split such that the two resulting signals applied to the endcaps are 180° out-of-phase. The balun circuit also serves as a protection device from the high RF voltages which may be induced onto the endcaps and, thus, may be fed back into the electronics box. By employing a "matching signal" protection, any stray signals common to both endcaps are filtered out through the balun circuit. The experimental setup used in these studies for quadrupolar excitation employed a simple BNC "tee" from one of the output signals from the balun circuit. Since the balun circuit employs a "matching signal" protection mechanism, and only one signal is employed, no protection from high RF voltages

is offered with this setup. Consequently, the RF should not be scanned to high m/z values, thus keeping the applied RF voltage low. For the low m/z ions employed in these studies (i.e. m/z 29 and 40), the RF was not ramped above 50 Da. The RF signal measured on the endcaps was on the order of one volt.

When conducting resonance excitation at very high frequencies, measurements with an oscilloscope should be obtained in order to verify the amplitude and frequency of the applied excitation signal. For the ITMS™ frequency synthesizer, the amplitude of the signal is attenuated at frequencies greater than 900 kHz. Upon requesting $6V_{p-p}$, the resulting amplitude was observed to be $4.5V_{p-p}$ at 1.0 MHz, $3.2V_{p-p}$ at 1.3 MHz, and $2.6V_{p-p}$ at 1.6 MHz. Furthermore, the waveform is degraded at frequencies greater than 1.6 MHz (i.e. other frequency components are present). Regardless of the source of the excitation signal, these measurements need to be checked.

When performing resonance excitation over a broad frequency range, several precautions must be taken in order to obtain valid data. Particular attention must be paid to the specific scan function employed. Crucial to the success of these experiments is the assurance that changes in the RF, DC, and resonance excitation signals are completely separated in time so that no two signals are varying simultaneously. Due to computer overhead time and rise and fall times of each signal, changes do not occur instantaneously; therefore, time must be allowed for all signals to equilibrate in order for the trapping conditions to be stable. Data taken from a digital storage oscilloscope suggest that the computer overhead time for each

scan table of a scan function is 300 μs (based on requesting 0 ms in the software). Required times for some specific signals include 200 μs for the application of +60 V DC to reach full amplitude, 400 μs for the excitation voltage to reach 300 mV, and 500 μs for ramping the RF amplitude by 230 $V_{0,p}$ (20 Da). One reason for the delays is due to the sequence in which the computer executes the signals as requested in the scan function. For the ICMS© software, the sequence is 1) trigger, 2) DC voltage, 3) resonance excitation frequency and amplitude, and 4) RF level. It should be noted that the standard ITMS™ software may exhibit a different order.

Several consequences can result from two signals varying simultaneously. Since an ion's frequencies of motion are dependent on the storage conditions, changes in the trapping field will ultimately vary the ion's frequencies. Probing ion frequencies during varying storage conditions will result in anomalous absorptions which can be mistaken as components of motion. Due to the execution sequence of the ICMS© software used to control the quadrupole ion trap, each signal is applied sequentially in time. Since resonance excitation is initiated prior to reaching the final RF level, care must be taken to ensure that the desired storage conditions are met prior to the excitation process. Similarly, resonance excitation must be terminated prior to changes in the RF or DC voltages. Due to the sequence order, changes in the DC voltage occur before changes in the resonance excitation signal; therefore, the excitation signal must be terminated prior to altering the applied DC voltage. Furthermore, depending on the magnitude of the RF ramp, reaching the desired RF level may require up to 2 ms; therefore, a delay time must accompany changes in the

storage conditions so that all signals are equilibrated. Note that in the scan function listed in Table 5-1, all of these precautions were taken. Once the storage conditions were met (scan table 9), a 5 ms delay time was employed to allow the ions to cool to the center of the trap (scan table 10). The excitation process was initiated (scan table 11) and terminated (scan table 12) prior to any changes in the storage conditions.

The time required for the signals to equilibrate will depend on the magnitude of the changes in the storage conditions. This can be observed experimentally by probing the ions via resonance excitation. While holding the excitation amplitude and duration constant, the excitation frequency is varied and the ion signal is collected. The minimum of this curve represents the maximum absorption and thus the optimum excitation frequency which is a close approximation of the secular frequency of ion motion. This curve has been referred to as a frequency optimization curve (Johnson *et al.*, 1990b). By probing the ions at various times following the changes in storage conditions associated with "apex" isolation, insight can be obtained regarding the times required for the signals to equilibrate. Shown in Figure 5-1a is a comparison of dipolar resonance frequency optimization curves obtained at two delay times following the isolation of M^+ (m/z 40) of argon. Resonance excitation immediately following the isolation step produces a signal minimum near 357 kHz (dashed line); excitation 10 ms following the isolation step produces a minimum near 358 kHz (solid line).

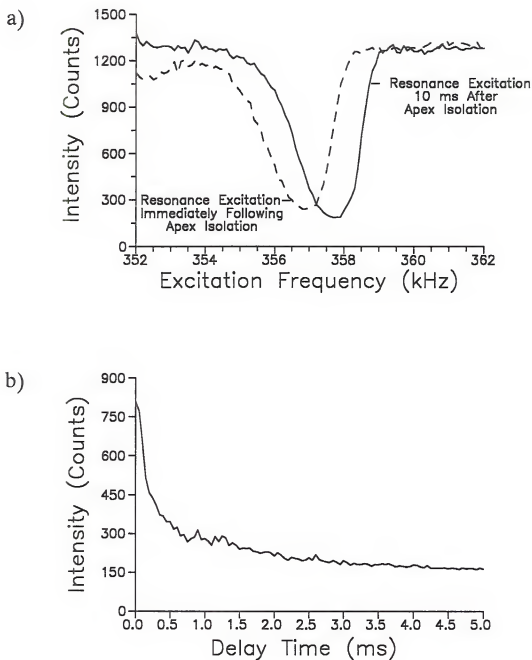


Figure 5-1: Dipolar resonance excitation of M^+ of argon (m/z 40). Intensity is plotted versus a) resonance excitation frequency (kHz) and b) delay time prior to resonance excitation at 357.8 kHz.

This shift in frequency results from the change in storage conditions with the removal of the -DC voltage (from the "apex" isolation) and the time required for the ions to cool to the center of the ion trap and re-equilibrate to the new storage conditions. Figure 5-1b is a plot of ion signal versus the delay time between isolation and resonance excitation at 357.8 kHz (the minimum of the solid curve in Figure 5-1a). Note that the ion signal represents those ions which have not been resonantly ejected. As the delay time increases, the storage potentials have sufficient time to equilibrate and the optimum excitation frequency more closely matches the excitation signal, thus resulting in an increased degree of ejection. As demonstrated in this plot, approximately 5 ms is required for the ion to reach the equilibrated frequency; therefore, following the any changes in the storage conditions, time must be allowed for the potentials to reach the desired amplitudes before initiating resonance excitation. This delay time was employed in scan table 10 of the scan function listed in Table 5-1.

The minimum of the frequency optimization curve is a close approximation of the ion's secular frequency. The exact secular frequency, however, is difficult to determine due to shifts in the observed frequency. As demonstrated in Figure 5-1a and 1b, the minimum can shift with delay time following changes in the storage conditions. The minimum also can shift due to the amplitude of the applied excitation signal. Shown in Figure 5-2a is the dipolar resonance frequency optimization curves for an ion stored near the apex (i.e. $q_z=0.78$, $a_z=0.118$).

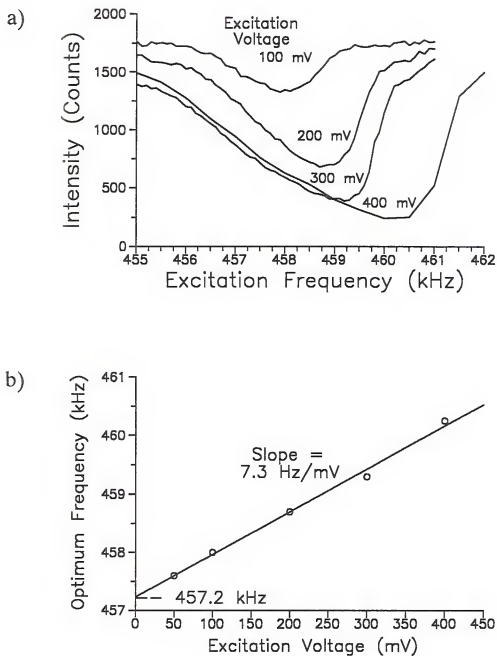


Figure 5-2: Dipolar resonance excitation of M^+ of argon (m/z 40); a) intensity versus resonance excitation frequency (kHz) at various excitation voltages and b) optimum excitation frequency versus resonance excitation voltage.

With an increase in the excitation amplitude, the observed minimum shifts to higher values. The optimum resonance frequency for 100 mV excitation is 458 kHz; the optimum for 400 mV excitation is 460 kHz, a 2 kHz shift. Shown in Figure 5-2b is the optimum frequency versus the applied excitation voltage. The linear trend suggests that the y-intercept (i.e. extrapolation to 0 mV) may be the best indication of the true ion frequency. It should be noted that increasing the excitation duration under constant excitation voltage does not cause a shift in the optimum frequency.

Other factors also contribute to inaccuracies in the ion frequency assignment. The pressure of the helium buffer gas also contributes to deviations between the experimentally determined and true ion frequency. Based on the physics of a damped harmonic oscillator, the frequency will shift to lower values with increasing buffer gas pressure (Resnick and Halliday, 1966). Another factor which contributes to inaccurate frequency assignments is space charge. Due to ion-ion interactions, increasing ion populations (and thus increasing space charge) causes the ion frequency to shift to lower values (Yates, 1991b).

The theoretically predicted ion frequency rarely corresponds exactly to that observed experimentally. This discrepancy is due not only to the above stated reasons but also to uncertainty of the exact RF voltage applied to the ring electrode of the ion trap. Although the RF can be monitored on the circuit boards, the exact voltage reaching the ring electrode is very difficult to determine. Consequently, the observed ion frequencies are only approximations of the true ion frequencies. If only qualitative information is desired (i.e. identification of the absorption band), the

approximations are sufficient; however, identifying and understanding the sources causing discrepancies between the theoretically and experimentally determined frequency components are important. If a more accurate determination of the frequency components are desired, all of the above mentioned concerns must be addressed.

Probing Ion Frequencies Near the $\beta_z=0$ Boundary

To investigate ion frequency components near the $\beta_z=0$ boundary, the scan function described in Table 5-1 was employed. The ions selected for these experiments were the M^+ ion (m/z 40) of argon, and the $C_2H_5^+$ ion (m/z 29) of methane CI. The Ar^+ ion is useful for its inability to undergo dissociation while absorbing power from the excitation signal; hence, resonance ejection accounts for the only ion loss. The $C_2H_5^+$ ion was selected as it readily absorbs power and dissociates to form a number of product ions; therefore, it offers a more sensitive probe. The specific storage conditions used ($q_z=0.70$, $a_z=-0.186$) place the ion on the Mathieu stability diagram in the vicinity of that employed for the first step of "2-step" isolation (see Figure 1-4 of Chapter 1). For m/z 40, a low mass cutoff (LMCO) of 30.9 Da corresponds to $q_z=0.70$ and +55 V DC corresponds to $a_z=-0.186$; for m/z 29, a LMCO of 22.4 Da ($q_z=0.70$) and +40 V DC ($a_z=-0.186$) is required to store the ion in the same q_z , a_z location. At this specific storage condition, the theoretically predicted secular frequencies are 135 kHz and 223 kHz for ω_z and ω_r , respectively.

Dipolar Excitation

A power absorption spectrum can be obtained by performing a similar experiment as that described for the frequency optimization curves. At constant resonance excitation amplitude and duration, the excitation frequency is incremented and the ion signal is recorded. Shown in Figure 5-3a is the absorption spectrum obtained while employing a sufficiently low excitation amplitude and duration (i.e. 250 mV for 1 ms) in order to avoid 100% ejection at the main frequency (i.e. to keep the absorption band on scale). Observed in this spectrum is the main axial secular frequency ($\omega_z = 126$ kHz) and a small absorption due to the higher frequency of motion at $\Omega - \omega_z$ (recall that $\Omega = 1100$ kHz). If the excitation amplitude and duration is increased, weaker frequency components can be observed. Shown in Figure 5-3b is the absorption spectrum corresponding to the same storage conditions but obtained with a much higher excitation field (6000 mV for 10 ms). This spectrum shows the pronounced absorption at ω_z (off scale) as well as significant absorption due to $\Omega - \omega_z$ and $\Omega + \omega_z$ (also off scale), all of which are predicted by the equations of motion for an ion stored in a quadrupole ion trap. The presence of the new absorption bands at $3\omega_z$, $\Omega - 3\omega_z$, and $\Omega + 3\omega_z$, however, are not predicted by the theoretical Mathieu equations of motion. To verify that the absorptions were indeed due to components of $3\omega_z$, additional absorption spectra were acquired at various a_z points along the $q_z = 0.70$ line (i.e. at other applied DC voltages). When the observed intensity minima for each absorption are plotted versus the experimental ω_z , the slope of the line yields its relationship with the ω_z frequency.

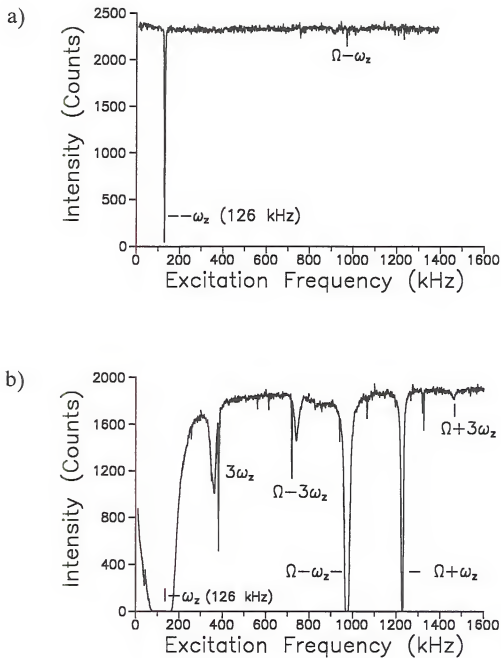


Figure 5-3: Dipolar resonance excitation of M^+ of argon (m/z 40) while stored near the $\beta_z=0$ boundary ($q_z=0.70$, $a_z=-0.186$). Intensity of m/z 40 following resonance excitation is plotted versus resonance excitation frequency of a) 250 mV for 1.0 ms and b) 6000 mV for 10 ms.

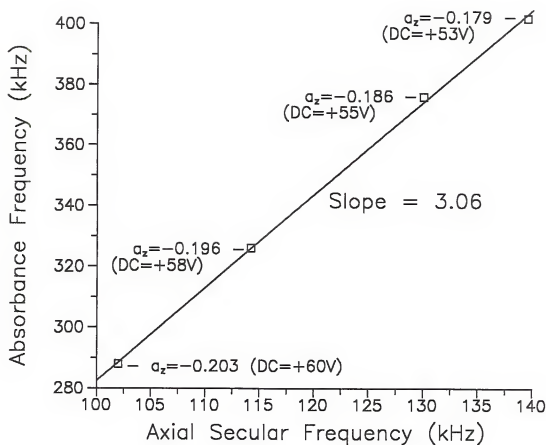


Figure 5-4: Absorption frequency observed with dipolar resonance excitation versus theoretical axial frequency of ions stored at various a_z values ($-0.203 < a_z < -0.179$) at $q_z = 0.70$ (near the $\beta_z = 0$ boundary).

Such a plot for the $3\omega_z$ absorption band (Figure 5-4) shows a linear trend with slope = 3.06 (theoretical slope = 3.0; i.e. the frequency is 3 times ω_z), thus confirming the identity.

The absorptions due to combinations of $3\omega_z$ are more significant with increasingly negative values of a_z (i.e. $a_z \leq -0.186$; $q_z = 0.70$); the absorptions are less apparent when stored further away from the $\beta_z = 0$ boundary (i.e. $a_z \geq -0.186$). This trend is similar to that observed with higher-order field effects characterized in Chapter 3; the effects are more significant in the lower portion of the stability diagram (i.e. increased effects with increasing applied +DC voltage). The absorptions due to combinations of $3\omega_z$ are believed to be evidence for the influence of higher-order fields on the ion motion. Although this may be a result of the dodecapolar field resonance along the $\beta_z = 1/3$ line (Yang Wang, private communication), contributions from the hexapolar and octopolar fields also may induce these frequencies. Since the main contributions from all higher-order fields originate from the lowest orders, the frequencies at combinations of $3\omega_z$ may result from hexapolar and octopolar fields. Indeed, frequency analysis of ion simulations predict (Franzen, 1994) frequency components due to combinations of $3\omega_z$ when hexapolar and octopolar fields contribute to the quadrupolar storage field. Since octopolar fields have been calculated to contribute the most to the quadrupole ion trap used in these studies (Franzen, 1993), the induced frequencies at $3\omega_z$ may very well be a direct result of this higher-order field.

The sharp spikes on the higher frequency side of the $3\omega_z$ band and lower frequency side of the $\Omega-3\omega_z$ band are presumably due to the collective behavior of the ion cloud. This behavior has been reported previously (Vedel *et al.*, 1990) for excitation at $2\omega_z$. Collective behavior is observed often with quadrupolar excitation since the main absorption bands occur at twice the secular frequency (i.e. $2\omega_u$). This issue will be discussed further throughout this chapter.

Quadrupolar Excitation

The m/z 40 ions of argon were stored near the $\beta_z=0$ boundary of the Mathieu stability diagram at the same storage conditions as used above (i.e. $q_z=0.70$, $a_z=-0.186$). The frequency components of ion motion were investigated via quadrupolar resonance excitation in an experiment similar to that described above for the dipolar excitation. The resulting power absorption spectrum obtained from quadrupolar excitation is shown in Figure 5-5a. Each frequency assignment displayed in the spectrum was verified by acquiring spectra at various a_z values along the $q_z=0.70$ line and constructing calibration curves similar to that shown in Figure 5-4. This spectrum exhibits a number of bands, with the greatest absorption occurring at $2\omega_z$. Recall that under quadrupolar excitation, the frequency corresponding to $2\omega_z$ is predicted to be the main absorption band; thus, the corresponding bands at $\Omega\pm2\omega_z$ also are observed. The ω_z absorption also is observed in this case; the ω_r frequency (expected at approximately 220 kHz) may be hidden in the large absorption due to $2\omega_z$. It is important to note that the absorptions due to combinations of $2\omega_z$ do not

directly represent frequencies of motion; instead, these frequencies only represent those that result in absorption of power. In other words, the absorption at $2\omega_z$ is due to the ion's motion at ω_z ; likewise, the absorptions occurring at frequencies corresponding to $\Omega \pm 2\omega_z$ are due to the ion's micromotion at $\Omega \pm \omega_z$. The observed absorption bands at ω_z and $\Omega - \omega_z$ could be evidence of the subharmonic motion due to $\omega_z/2$ (and thus appearing at a frequency twice that of $\omega_z/2$). This absorption may also arise from the main secular motion at ω_z . Since this frequency comprises most of the motion in the axial direction, the ion could absorb power from the excitation field, albeit not as efficiently. These results are consistent with simulations of quadrupolar excitation (March *et al.*, 1989) where absorption at ω_z was observed.

The observation of the absorption band for $2\omega_r$ is evidence for the non-discriminating nature of the quadrupolar excitation technique. Absorption at this frequency is due probably to the secular frequency in the radial direction (ω_r). Indeed, ion simulations of quadrupolar excitation (March *et al.*, 1989) exhibit absorption of power at $2\omega_r$. Evidence for the radial frequencies of motion is not observed for the dipolar excitation mode, thus, making these two techniques complimentary.

The region of the stability diagram near the $\beta_z=0$ boundary was investigated further with the $C_2H_5^+$ ion. A similar quadrupolar excitation experiment to that described above was conducted with $C_2H_5^+$ stored at $q_z=0.70$, $a_z=-0.186$. The resulting power absorption spectrum is shown in Figure 5-5b.

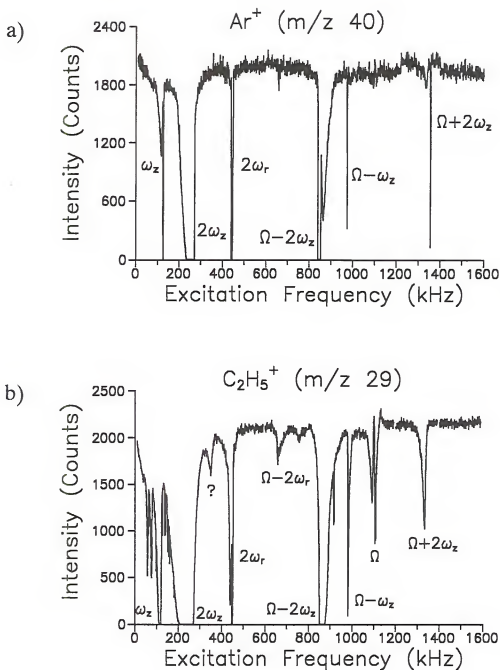


Figure 5-5: Quadrupolar resonance excitation while stored near the $\beta_z=0$ boundary ($q_z=0.70$, $a_z=-0.186$). Following resonance excitation of 6000 mV for 10 ms, the intensities of a) M^+ of argon (m/z 40) and b) C_2H_5^+ (m/z 29) are plotted versus resonance excitation frequency.

The absorption bands for $C_2H_5^+$ compare favorably to those observed for M^+ of argon. This spectrum, however, exhibits a number of additional absorptions, most notably the significant absorption corresponding to the RF trapping frequency (Ω). This absorption band, appearing as a split band centered exactly around 1100 kHz, can be attributed to higher-order field effects on motion (Franzen, 1994). Due to contributions of a hexapole field, the high frequency component, Ω , is induced on the stored ion. The absorption near 650 kHz can be attributed to $\Omega - 2\omega_r$ (a slight indication of this absorption is observed in Figure 5-5a). The new absorptions observed at 350 kHz and 750 kHz (likely related as their sum equals 1100 kHz) are unknown at this time; although unconfirmed at this time, these bands may be indications of the coupled frequencies due to $\omega_z + \omega_r$ and $\Omega - (\omega_z + \omega_r)$. The observation of the new absorption bands with the $C_2H_5^+$ ion is attributed to its ease of dissociation, thus resulting in a more sensitive probe.

Probing Ion Frequencies Along the $a_z=0$ Line

The ion frequencies of motion were investigated along the $a_z=0$ line. Operation of the quadrupole ion trap in the absence of applied DC voltages (RF only) is the more commonly employed mode. The application of DC typically is employed only during mass-isolation techniques. Due to the commonly employed RF-only mode of operation, frequencies of ion motion in this mode traditionally have been investigated in more detail than in the RF/DC mode. According to theory (March and Hughes, 1989), only ω_a and $\Omega \pm \omega_a$ significantly contribute to ion motion

with the relative contributions of the $\Omega \pm \omega_u$ frequencies to the total ion motion increasing with increasing q_z . More correctly, the higher frequency components contribute more to the total ion motion when stored at high β_u values (i.e. high ω_u). Theoretical calculations (Pedder, 1992) predict the ω_u frequency component to comprise greater than 87% of the total ion motion for $q_z < 0.20$ ($a_z = 0$); the $\Omega - \omega_u$ comprises the majority of the remaining contribution. For $q_z > 0.75$ ($a_z = 0$), the ω_u frequency components contribute less than 60% to the total ion motion; again, the $\Omega - \omega_u$ comprises the majority of the remaining contribution. Interestingly, at very high values of q_z (i.e. $q_z > 0.85$), contributions from $\Omega + \omega_u$ decrease, while contributions from $2\Omega - \omega_u$ increase to the point of being equal in magnitude to $\Omega + \omega_u$ (due to their frequencies being equal).

Dipolar Excitation

The frequency components of motion for an ion stored at $q_z = 0.30$, $a_z = 0$ were investigated for the $C_2H_5^+$ ion. At this storage condition the theoretical secular frequencies are 118 kHz and 59 kHz for ω_z and ω_r , respectively. In a manner similar to that described in the above section, the excitation frequency was incremented while the excitation amplitude and duration were held constant. Shown in Figure 5-6 is the resulting power absorption spectrum obtained by applying a $6V_{p-p}$ dipolar excitation for 10 ms. The absorption band at ω_z (off scale) is very broad as expected due to the high excitation amplitude.

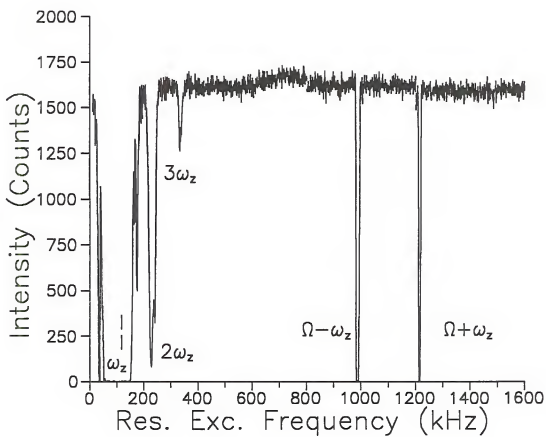


Figure 5-6: Dipolar resonance excitation (6000 mV for 10 ms) of C_2H_5^+ (m/z 29) while stored at $q_z=0.30$, $a_z=0$. Intensity versus resonance excitation frequency.

The absorption of power at frequencies due to $\Omega - \omega_z$ and $\Omega + \omega_z$ are observed with the former absorbing more power, as predicted by theory. Theoretical calculations predict (Pedder, 1992) the $\Omega - \omega_z$ component to contribute 12.7% to the total ion motion while stored near $q_z = 0.30$, $a_z = 0$; the $\Omega + \omega_z$ component is predicted to contribute 5.0%. The degree of contribution observed experimentally can be approximated by integrating the area of each absorption curve. The results from calculations of the absorptions in Figure 5-6 yield 71.7% due to ω_z , 7.3% due to $\Omega - \omega_z$, and 5.1% due to $\Omega + \omega_z$. Contributions from $2\omega_z$ and $3\omega_z$ were calculated to be 13.7% and 2.2%, respectively; no theoretical predictions were available to compare these results.

The absorptions observed at the lower frequencies (i.e. $\omega_z/2$, $2\omega_z$, and $3\omega_z$) were investigated further with the argon M^+ ions. Shown in Figures 5-7a and 7b are the power absorption spectra ($6V_{p-p}$ dipolar excitation for 10ms) obtained while storing m/z 40 at $q_z = 0.30$ and 0.25, respectively. Again, absorptions due to $\omega_z/2$, ω_z , and $2\omega_z$ are observed in each case. Although not shown, absorption due to $3\omega_z$ also were observed. Note the existence of a minor absorption due to $\omega_z + \omega_r$; an enhanced absorption for this band is observed at $q_z = 0.25$. The general trend observed along the $a_z = 0$ line was that stronger absorptions occurred at lower q_z values; absorptions due to $\omega_z/2$, $2\omega_z$, and $3\omega_z$ were undetectable beyond $q_z > 0.40$. Component frequencies corresponding to $\omega_z/2$, $2\omega_z$, and $3\omega_z$ can be attributed to higher field-induced effects on ion motion. Indeed, these frequencies are predicted under "forced" Mathieu equations accounting for hexapolar contributions (Williams *et al.*, 1991b).

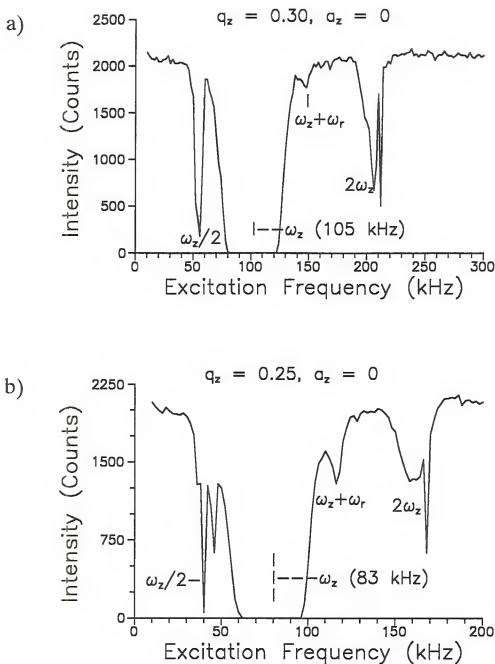


Figure 5-7: Dipolar resonance excitation of M^+ of argon while stored along the $a_z=0$ line. Following resonance excitation of 6000 mV for 10 ms, the intensities of m/z 40 are plotted versus resonance excitation frequency for ion storage at a) $q_z=0.30$ and b) $q_z=0.25$.

Evidence for coupled motion also was observed to follow the same trend as that observed for absorptions at $\omega_z/2$, $2\omega_z$, and $3\omega_z$. At very low q_z values (i.e. $q_z < 0.35$), absorption due to $\omega_z + \omega_r$ was observed; beyond $q_z = 0.35$, absorption was undetectable. The existence of coupled motion is due to the nonideal quadrupole ion trap. Due to higher-order field effects, ion motion in each direction is not entirely decoupled; therefore, these frequency components are observed experimentally.

The absorptions due to the lower frequencies (other than ω_z) may originate from several sources. A small contribution of $\omega_z/2$ and $2\omega_z$ may be present in the ion motion. The absorptions also can be produced due to harmonics of the applied dipole field (Williams *et al.*, 1991b) or higher-order fields may be introduced by the nonideal dipole field used in these studies. Incorporation of hexapolar nonlinear terms into the "forced" Mathieu equations of motion produced resonance conditions at $\omega_z/2$, ω_z , $2\omega_z$, and $3\omega_z$ (Williams *et al.*, 1991b). Indeed, while storing N_2^+ ions near $q_z = 0.50$, $a_z = 0$, Vedel *et al.* (1990) reported observing $\omega_z/2$ and $2\omega_z$ as well as several coupled terms (i.e. combinations of ω_z and ω_r). Due to the qualitative approach of the investigations presented here, exact contributions of each frequency component were not determined.

Evidence exists indicating that the observed absorption at $2\omega_z$ is not due solely to the harmonics of the excitation field. Note that the sharp spike at a slightly higher frequency than the $2\omega_z$ absorption band is presumably due to the collective behavior of the ion cloud. This phenomenon previously has been observed

experimentally for resonance excitation at $2\omega_z$ (Vedel *et al.*, 1990) and during resonance detection (Jungmann *et al.*, 1987). When the excitation duration is sufficiently long enough, each ion "locks" onto the signal resulting in a collective oscillation instead of independent oscillations of each ion. This resonance was found to be dependent on ion population (Vedel *et al.*, 1990). To investigate the behavior observed in the results presented here, the $2\omega_z$ absorption band was acquired for various ion populations. Shown in Figure 5-8 is a comparison of two ion populations stored at $q_z=0.30$, $a_z=0$ while undergoing dipolar resonance excitation near $2\omega_z$. A 2-fold increase in the ion population produced the collective behavior while the lower population did not. This evidence suggests that the $2\omega_z$ is a true component of the ion motion. These results agree also with previous experimental results (Vedel *et al.*, 1990) and simulations of ion motion under the influence of higher-order fields (Franzen, 1994).

Quadrupolar Excitation

While storing $C_2H_5^+$ ions at $q_z=0.3$, $a_z=0$, quadrupolar excitation was applied at frequencies varying from 10 kHz to 1.6 MHz. In a manner similar to that described in the above section, a power absorption curve was acquired. The results from this experiment are shown in Figure 5-9a; an expanded view of the lower frequency portion is shown in Figure 5-9b. The main absorption bands observed are due to $2\omega_r$, $2\omega_z$, $\Omega-2\omega_r$, and $\Omega-2\omega_z$. Interestingly, the absorption bands for $2\omega_r$ and $2\omega_z$ are nearly equal in magnitude.

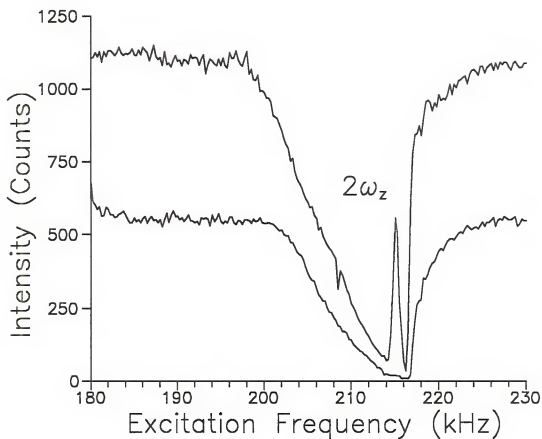


Figure 5-8: Dipolar resonance excitation of Ar^+ (m/z 40) near the $2\omega_z$ resonance. Intensity of two ion populations are plotted versus the resonance excitation frequency. The higher population is approximately twice that of the lower.

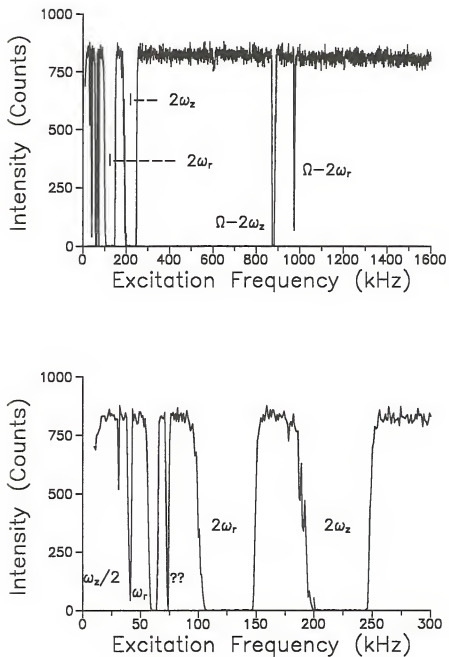


Figure 5-9: Quadrupolar resonance excitation (6000 mV for 10 ms) of $C_2H_5^+$ (m/z 29) while stored at $q_z=0.30$, $a_z=0$. Intensity versus resonance excitation frequency over a) the entire frequency range and b) the low frequency range only.

Recall in Figure 5-5, that the absorptions due to $2\omega_z$ were markedly less at $q_z=0.70$, $a_z=-0.186$ than those observed here. The theoretical secular frequencies for storage at $q_z=0.30$ ($a_z=0$) are 118 kHz and 59 kHz for ω_z and ω_r , respectively; storage near the β_z boundary (i.e. $q_z=0.70$, $a_z=-0.186$) produces theoretical frequencies at 135 kHz and 223 kHz for ω_z and ω_r , respectively. While the ω_z frequencies are similar (as well as the magnitude of absorption), the lower ω_r frequency at $q_z=0.30$ shows markedly stronger absorptions. The lower frequency may allow more interaction with the supplemental quadrupolar field resulting in more absorption of power and, thus, increased ion ejection. Indeed, ion simulations under quadrupolar excitation show decreasing absorption with increasing q_z (and therefore, increasing ω_z) (March *et al.*, 1991).

The low frequency absorption observed near 60 kHz (the broadest of the low frequency absorption bands) could originate from $\omega_z/2$, ω_r , or $\omega_z-\omega_r$ (or a combination of any of them), all of which exhibit frequencies in the vicinity of 60 kHz. Due to the uncertainties in the exact frequencies of ion motion (as discussed in the Experimental section), these absorptions are difficult to assign to a specific frequency. The minor absorptions at 40 kHz and 70 kHz may be due to harmonics of the quadrupolar signal. A small degree of a second harmonic would excite the ions near the 125 kHz band, thus resulting in an absorption. This hypothesis has not been confirmed.

An interesting observation with the quadrupolar excitation of $C_2H_5^+$ near $q_z=0.3$ is the shape of the absorption bands as shown in Figures 5-10a and 10b.

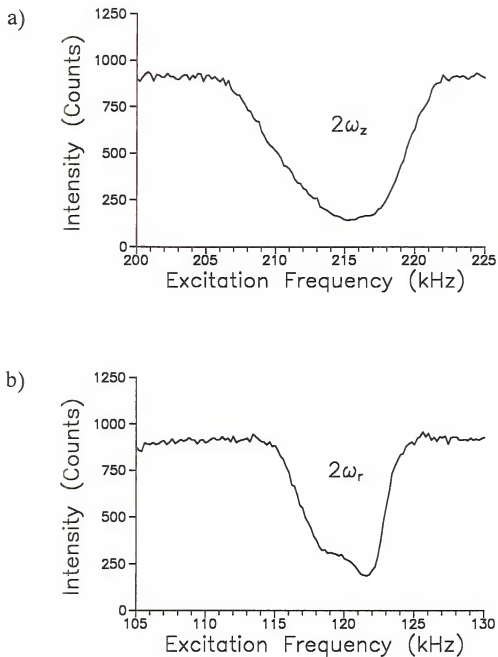


Figure 5-10: Quadrupolar resonance excitation (700 mv for 5 ms) of $C_2H_5^+$ (m/z 29) while stored at $q_z=0.30$, $a_z=0$. Intensity versus resonance excitation frequency near a) the $2\omega_z$ absorption band and b) the $2\omega_r$ absorption band.

Figure 10 shows the absorption bands for $2\omega_z$ and $2\omega_x$, respectively, acquired with the excitation amplitude and duration sufficiently reduced in order to keep the main absorption bands on scale. The $2\omega_z$ band exhibits a relatively symmetric absorption curve while the $2\omega_x$ absorption band exhibits asymmetry. This may be an indication of the nonideal quadrupolar excitation field. Note that under dipole resonance excitation, the absorption at $2\omega_z$ showed asymmetry (see Figure 5-8) while excitation at ω_z exhibited symmetric bands (see Figure 5-1a).

Quadrupolar excitation along the $a_z=0$ line was explored further with the $C_2H_5^+$ ion. At various q_z values along the $a_z=0$ line, quadrupolar excitation was applied and power absorption spectra were recorded. Shown in Figure 5-11a through 11d are absorption spectra acquired at $q_z=0.60, 0.70, 0.81$, and 0.87 , respectively. Note the very broad absorption bands observed at $q_z=0.81$. This is due to an overlap of the corresponding absorption bands labelled next to each broad band (e.g. the band near 775 kHz is due to the combined absorptions at $2\omega_z$ and $\Omega-2\omega_x$). The overlapping absorptions bands are well separated at other q_z values. As diagrammed in Figure 5-12, the occurrence of overlapping frequency components of ion motion can be observed more easily if the theoretical frequencies are plotted versus the q_z value. At $q_z=0.81$, $a_z=0$ ($\beta_z=2/3$), a strong absorption occurs near 775 kHz due to the overlap of $2\omega_z$ and $\Omega-2\omega_x$; likewise, a strong absorption occurs near 367 kHz due to the overlap of $2\omega_x$ and $\Omega-2\omega_z$. Similarly, while storing near $q_z=0.645$ ($\beta_z=1/2$), a strong absorption is expected near 550 kHz where $2\omega_z$ and $\Omega-2\omega_x$ meet.

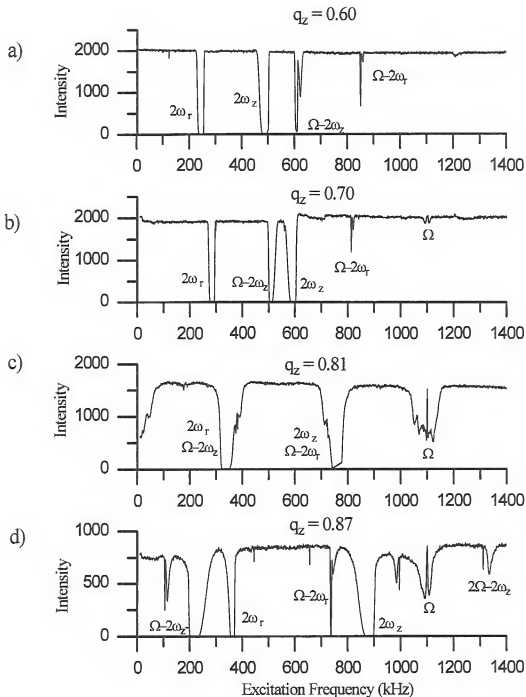


Figure 5-11: Quadrupolar resonance excitation (6000 mv for 10 ms) of $C_2H_5^+$ (m/z 29) while stored along the $a_z=0$ line. The intensities of m/z 29 are plotted versus resonance excitation frequency for ion storage at a) $q_z=0.60$, b) $q_z=0.70$, c) $q_z=0.81$, and d) $q_z=0.87$.

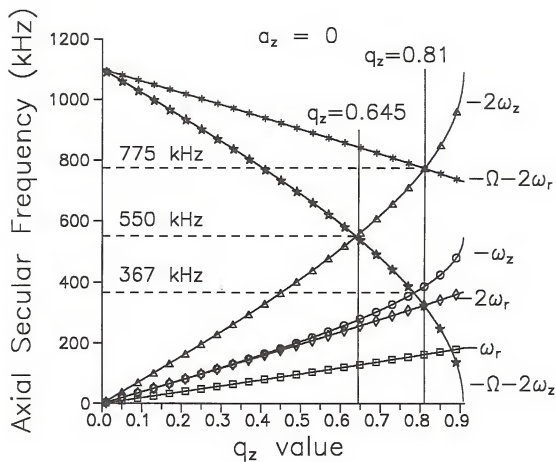


Figure 5-12: Theoretical frequencies plotted versus the q_z stability parameter. The frequencies plotted correspond to the main absorption bands experimentally observed during quadrupolar excitation.

Other interesting features are present in Figure 5-11. An increase in the magnitude of the absorption bands are observed with an increase in q_z values. Upon comparison of the absorption spectra at $q_z=0.60$, 0.70 , and 0.87 (omitting the spectrum at $q_z=0.81$ due to the overlapping bands), absorption bands significantly increase for Ω , $2\omega_z$, $\Omega-2\omega_z$, and $\Omega-2\omega_z$; however, the degree of asymmetry appears to increase as well. Note that the absorption at Ω is a frequency component of motion induced by contributions of a hexapolar field. The existence of two new absorption bands at 110 kHz and 990 kHz for storage at $q_z=0.87$ remains unexplained at this time. Although these bands are believed to be associated with each other (due to their sum equaling Ω), the frequency assignment is uncertain.

The absorption band at 1350 kHz in the spectrum acquired at $q_z=0.87$ can be attributed to $2\Omega-2\omega_z$. This is the first report of the experimental observation of this frequency component. This band has been verified by comparing the shift in the band placement at other q_z values in the vicinity (i.e. the band appears at 1390 kHz and 1475 kHz for spectra acquired at $q_z=0.84$ and 0.81 , respectively). The absorption band shifts to higher frequency with decreasing q_z as expected for the $2\Omega-2\omega_z$ frequency component.

Probing Ion Frequencies Near the Apex

Components of ion motion were investigated while storing ions near the apex of the stability diagram. Typically, this portion of the stability diagram is used for isolation of ions of either a narrow range or a single m/z . The absolute apex,

$q_z=0.78$, $a_z=0.15$, is where the $\beta_z=1$ boundary meets the $\beta_r=0$ boundary; therefore, the ion motion in this region is predicted to exhibit a very high axial secular frequency and a very low radial secular frequency. The storage condition used for these experiments was directly below the apex at $q_z=0.78$, $a_z=0.118$; for the M^+ ion of argon, $q_z=0.78$ corresponds to a LMCO of 34.3 Da and $a_z=0.118$ corresponds to -35 V DC. The theoretically predicted secular frequencies are 468 kHz and 71 kHz for ω_z and ω_r , respectively.

Dipolar Excitation

While storing Ar^+ ions near the apex of the stability diagram ($q_z=0.78$, $a_z=0.118$), dipolar resonance excitation was applied. Shown in Figure 5-13a is the absorption spectrum acquired with the excitation amplitude and duration sufficiently reduced (i.e. 300 mV_{p-p} for 1 ms) in order to keep the main absorption bands on scale. Nearly equal absorption is observed for the ω_z and $\Omega-\omega_z$ frequencies. Although the q_z value is not extremely high, the β_z value is close to unity ($\beta_z=0.88$); therefore, the higher frequency components (i.e. $\Omega\pm\omega_u$) will contribute significantly to the total ion motion. At this β_z value, contributions to the total ion motion are predicted (Pedder, 1992) to be approximately 51% due to ω_z , 40% due to $\Omega-\omega_z$, 6% due to $\Omega+\omega_z$, and 3.0 % due to $2\Omega-\omega_z$. The contributions of the absorptions shown in Figure 5-13a were calculated to be 54.5% and 45.5% for ω_z and $\Omega-\omega_z$, respectively.

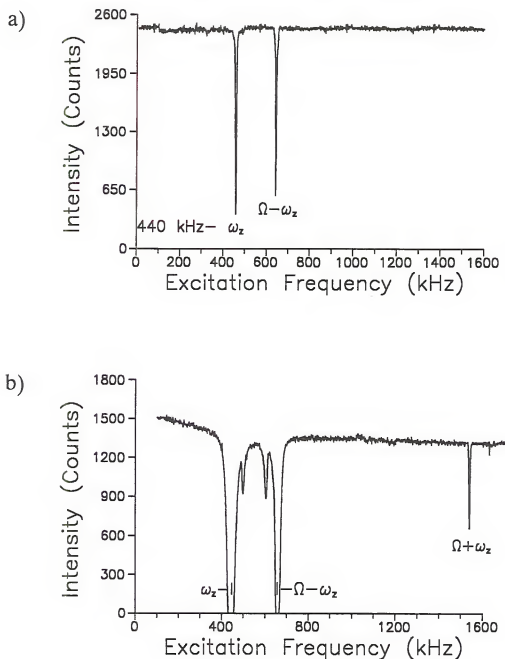


Figure 5-13: Dipolar resonance excitation of M^+ of argon (m/z 40) while stored near the apex of the stability diagram ($q_z=0.78$, $a_z=0.118$). Intensity of m/z 40 following resonance excitation is plotted versus resonance excitation frequency of a) 300 mV for 1.0 ms and b) 3000 mV for 5 ms.

Although no absorption is observed in Figure 5-13a for $\Omega + \omega_z$ near 1540 kHz or $2\Omega - \omega_z$ near 1730 kHz, the excitation signal is attenuated at these very high frequencies; therefore, discrimination against these frequency components of motion occurs.

Shown in Figure 5-13b is the absorption spectrum acquired with an increased excitation signal. In this spectrum, evidence for the $\Omega + \omega_z$ frequency component is observed; however, as stated above, the absorption is somewhat reduced due to attenuation of the excitation signal at this frequency. Also, due to the existence of several frequency components in the excitation signal beyond 1600 kHz, the absorption expected near 1730 kHz for $2\Omega - \omega_z$ was not investigated. The identities of the absorptions observed just to the right of ω_z and to the left of $\Omega - \omega_z$ are uncertain at this time. Although apparently related due to their sum equaling Ω , the bands have not been identified. Acquisition of absorption spectra at various a_z values along the $q_z = 0.78$ line in order to monitor the shift in absorption bands did not offer any conclusive evidence for assignment of these bands.

Quadrupolar Excitation

While storing Ar^+ ions near the apex of the stability diagram, (i.e. $q_z = 0.78$, $a_z = 0.118$), quadrupolar excitation was performed. The resulting power absorption spectrum, acquired with $6V_{pp}$ for 5 ms, is shown in Figure 5-14. Several absorption bands are observed with this mode of excitation; the parametric resonances due to twice the ion frequency dominate the spectrum. The main absorption band is due

to $2\omega_z$; the bands corresponding to $2\omega_z$ and $\Omega - 2\omega_z$ also exhibit strong absorptions, although both are significantly reduced compared to $2\omega_z$. These results are consistent with the observation made earlier in the chapter in which lower ω_z frequencies exhibited larger absorption bands. The reduction in the magnitude of the absorption band for $2\omega_z$ (as compared to that observed along the $a_z=0$ line) can be explained by the high β_z of storage. As stated earlier, at this storage condition (i.e. $q_z=0.78$, $a_z=0.118$), the total ion motion in the z-direction is comprised of 51% due to ω_z and 40% due to $\Omega - \omega_z$. Therefore, due to less contributions from the secular frequency, absorptions due to $2\omega_z$ will be reduced.

The spectrum shown in Figure 5-14 is expanded in Figures 5-15a and 15b for the lower frequencies (i.e. <300 kHz) and higher frequencies (>800 kHz), respectively. Note the significant absorption due to the trapping frequency at Ω . This is the first evidence of this absorption band when employing the M^+ ion of argon. Again, this absorption is due to the frequency component, Ω , induced on the ion due to contributions from a hexapolar field (Franzen, 1994). As observed before, this peak is split at exactly 1100 kHz. Also observed in this spectrum is evidence of the $2\Omega - 2\omega_z$ absorption band which corresponds to the $2\Omega - \omega_z$ frequency component of ion motion. Due to the high β_z of storage (high axial secular frequency), the higher frequency components significantly contribute to the total ion motion; therefore, absorption of power due to the $2\Omega - \omega_z$ frequency component is observed.

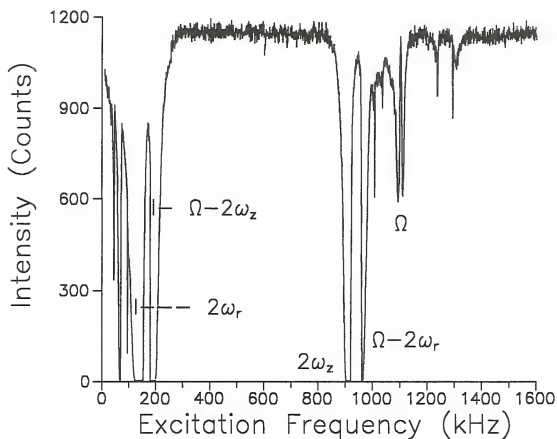


Figure 5-14: Quadrupolar resonance excitation (6000 mv for 5ms) of Ar^+ (m/z 40) while stored near the apex of the stability diagram ($q_z=0.78$, $a_z=0.118$). Intensity is plotted versus resonance excitation frequency.

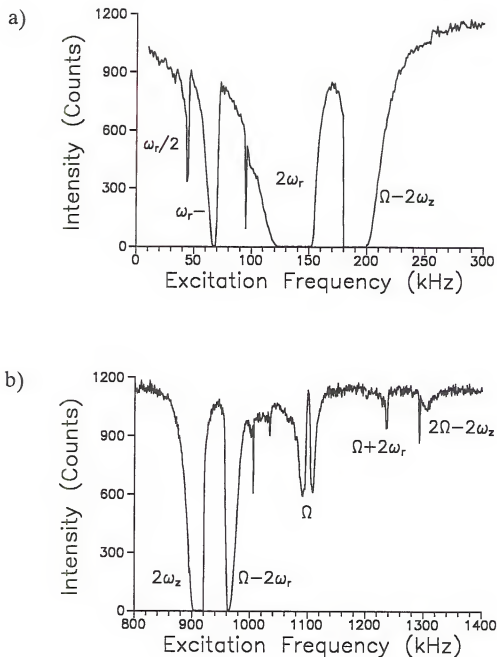


Figure 5-15: Quadrupolar resonance excitation (6000 mv for 5ms) of Ar^+ (m/z 40) while stored near the apex of the stability diagram ($q_z=0.78$, $a_z=0.118$). Expansion of Figure 5-14; intensity versus resonance excitation frequency over a) the low frequency range and b) the high frequency range.

Conclusions

Qualitative investigations of higher-order field effects on ion motion have been presented. The frequency components of ion motion were determined via dipolar and quadrupolar resonance excitation. Either the M^+ ion of argon (m/z 40), or the $C_2H_5^+$ ion of methane CI (m/z 29), was mass-selected and stored at various points throughout the Mathieu stability diagram. At each location, the ion intensity was recorded as the excitation frequency was varied under constant excitation amplitude and duration, thus generating power absorption spectra. Each absorption band corresponds either directly or indirectly to a frequency of ion motion; the magnitude of absorption is dependent on the contribution of that frequency component to the total ion motion.

In general, the dipolar resonance excitation mode produced major absorption bands corresponding to ion frequencies at ω_z and $\Omega \pm \omega_z$. The magnitude of absorption corresponding to the ω_z band decreased with increasing β_z of storage; the $\Omega \pm \omega_z$ absorption band increased with increasing β_z of storage. All of these findings were consistent with those predicted by ion simulations (Reiser, 1992; Pedder, 1992; Franzen, 1994).

In general, the quadrupolar resonance excitation mode produced major absorption bands at $2\omega_z$, $2\omega_r$, $\Omega \pm 2\omega_z$, and $\Omega \pm 2\omega_r$. These bands correspond to the frequency components of ion motion due to ω_z , ω_r , $\Omega \pm \omega_z$, and $\Omega \pm \omega_r$. The most significant absorption, due to $2\omega_z$, decreased with increasing β_z of storage; the $\Omega - 2\omega_z$ absorption band increased with increasing β_z of storage. The magnitude of

absorption due to $2\omega_r$ also decreased with increasing β_r of storage. These observations agree with those predicted by simulations (March *et al.*, 1991).

As evidenced by the numerous absorptions observed under both modes, ions can be resonantly excited at frequencies other than their secular frequencies. Ion ejection and/or dissociation, therefore, can be accomplished at any absorption frequency. Besides the theoretically predicted frequencies of motion at ω_u and $\Omega \pm \omega_u$, excitation can occur at a number of higher field-induced frequency components of motion. Specifically, evidence was presented for the frequency components corresponding to $3\omega_z$, $\Omega - 3\omega_z$, and $\Omega + 3\omega_z$ for ions stored near the $\beta_z = 0$ boundary. Power absorption corresponding to these frequency components increased with decreasing β_z (i.e. increasingly negative a_z values at $q_z = 0.70$). These frequencies may be the result of the influence of the dodecapolar resonance at $\beta_z = 1/3$ (Yang Wang, private communication); however, a more probable cause is the existence of an octopolar field since this contributes the most (of the higher-order fields) to the quadrupolar trapping field (Franzen, 1993).

Frequency components corresponding to $\omega_z/2$, $2\omega_z$, $3\omega_z$, and $\omega_z + \omega_r$ were identified for ions stored at low β_z values ($\beta_z < 0.2$) along the $a_z = 0$ line (i.e. 0V DC, or RF only mode). Increasingly lower β_z of storage (and thus lower q_z values) resulted in more pronounced absorptions at these frequencies. Components corresponding to these frequencies may be the result of higher field-induced effects on ion motion. Indeed, these frequencies are predicted under "forced" Mathieu equations which account for hexapolar contributions (Williams *et al.*, 1991b). The

existence of coupled motion (i.e. $\omega_z + \omega_r$) is due to the nonideal quadrupole ion trap (Wang, 1992). Due to higher-order field effects, ion motion in each direction is not entirely decoupled; therefore, these frequency components can be observed experimentally.

Evidence was presented for the higher field-induced frequency component corresponding to the trapping frequency, Ω . As with all of the higher frequency components, the magnitude of the absorption due to the Ω frequency increased with increasing β_z of storage. The frequency component at Ω was attributed to contributions of a hexapolar field to the quadrupolar trapping field (Franzen, 1994).

The results presented here show that ions can be resonantly excited at a number of different frequencies. Not only can excitation be accomplished at the theoretically predicted frequencies at ω_u and $\Omega \pm \omega_u$, but also at higher field-induced frequency components of motion. A thorough understanding of the motion of ions in a nonideal quadrupole ion trap is important for such experiments as MS/MS, high resolution, high mass analysis, efficient detection, and ion injection.

CHAPTER 6 CONCLUSIONS AND FUTURE WORK

Conclusions

This dissertation has presented a series of studies which investigate higher-order field effects on stored ions in a quadrupole ion trap. Due to the fact that an "ideal" quadrupole ion trap is both impossible and impractical to construct, a perturbed storage field exists. This results in the superposition of higher-order fields (i.e. hexapolar and octopolar) on the quadrupolar trapping field. Any deviation from the "ideal" electrode surface geometry, spacing, or assembly will introduce higher-order fields. If a deviation is asymmetric with respect to the $z=0$ plane (i.e. halfway point between the endcap electrodes), higher-order odd fields are introduced; sources of this type include differing size or number of holes in each endcap and differing endcap spacing. Deviations symmetric to the $z=0$ plane result in higher-order even fields; the main sources are electrode truncation and equal displacement of the endcaps from the ring electrode.

The existence of higher-order fields creates resonance conditions in which stored ions can absorb power. The ion can then undergo trajectories that differ from those predicted for a pure quadrupolar field. The specific resonance conditions for each higher-order field can be represented by iso- β_n lines on a Mathieu stability

diagram. Storage conditions corresponding to higher field resonances allow ions to absorb power which can result in dissociation or, at the limit, ion ejection.

The potentials of a trapping field superimposed with higher-order fields deviate from the purely quadrupolar field potentials only in the outer regions of the ion trap; furthermore, higher-order field potentials increasingly deviate from quadrupolar fields with increasing distance towards the electrodes; therefore, ions displaced from the center of the trap will be influenced to a greater extent than ions stored in the center. Ion displacement can be caused by resonance excitation, ion injection, ion formation in the outer regions, and absence of buffer gas. Therefore, any experiment utilizing these techniques will be more susceptible to higher-order field effects.

Influence of Instrumental Parameters

The magnitude of the effects from higher-order field contributions were found to be influenced significantly by parameters such as storage conditions (q_z , a_z values), ion population, storage time, and endcap electrode spacing. Each parameter was observed to dramatically influence the degree of ion loss (either by dissociation or ejection) when stored near a higher field resonance.

Ion storage in the lower portion of the stability diagram (below the $a_z=0$ line; $a_z<0$, +DC voltage) near higher field resonances markedly enhanced ion losses (either due to ejection or CID) when compared to storage near the same resonance along the $a_z=0$ line. With increasingly positive applied DC voltage, both the

magnitude of ion loss and the affected mass range was observed to increase linearly. The increased effects with increasingly applied +DC was attributed to the increased amplitude of z-motion.

Ion population was shown to dramatically influence higher-order field effects. While storing ions near the octopolar resonance, $\beta_z=1/2$, increasingly higher ion populations increased the magnitude of ion loss exponentially; the affected mass range increased markedly. Increasingly longer storage times near the octopolar resonance, $\beta_z=1/2$, resulted in linearly increasing ion losses. Longer storage times allow the ion to absorb more power from the higher-order field thus increasing the magnitude of ion loss.

The influence of m/z on higher-order field effects was shown to be negligible provided ions of very similar structure were considered. The relationship between ion structure and higher-order field effects is expected to follow the trend exhibited with resonance excitation CID. An ionic species that is difficult to dissociate will be influenced to a lesser degree by higher-order fields effects.

Endcap electrode displacement significantly influences the magnitude of higher-order field effects. A "symmetric" distortion (i.e. equal displacement of each endcap) was shown to have much less of an influence than the "asymmetric" distortion (i.e. differing endcap spacing). This may be due to the presence of higher-order even fields due to electrode truncation. The "asymmetric" geometry showed a markedly increased ion loss due to the hexapolar resonance near the $\beta_z=2/3$ resonance line.

Effects on Chemical Ionization

Higher-order field effects were shown to influence ions whose m/z is less than 1.5 times that of the low mass cutoff, since this dictates q_z values greater than 0.61 (for $a_z=0$). Due to the relatively low m/z ions employed in chemical ionization (CI), this mode of operation was shown to be susceptible to higher-order field effects. This is true for both mass-selected and non-mass-selected CI. Particular attention must be taken to avoid higher resonances near $q_z=0.645$ and 0.790 (along $a_z=0$) for the CI reagent ion in order to achieve maximum ion signal for the desired analyte ions. In general, and until the reagent ion population is depleted, increasing the CI reaction time will increase analyte ion intensity. If storage is performed near a higher resonance, however, a competing process will exist between CI reactions to produce analyte ions and CI reagent ion losses due to higher-order field effects.

The CI reagent ions of methane (i.e. CH_5^+ , C_2H_5^+ , and C_3H_5^+) were observed to readily undergo CID by neutral loss of H_2 to form reagent ions which rapidly react with neutral methane to form other, higher m/z reagent ions. Other CI reagent ions, such as methanol (CH_3OH_2^+), acetonitrile (CH_3CNH^+), and isobutane ($(\text{CH}_3)_3\text{C}^+$), underwent ejection only.

Due to ejection and CID of CI reagent ions, sensitivity was reduced when acquiring CI spectra at RF levels corresponding to the main octopolar resonance ($\beta_z=1/2$) or the main hexapolar resonance ($\beta_z=2/3$). Obtaining LOD and LDR information while employing mass-selected CI on the quadrupole ion trap, therefore, should be acquired at $q_z<0.60$ for the CI reagent ion. Quantitation with the C_2H_5^+

reagent ion was observed to suffer up to 50% loss of analyte signal if acquired near higher-order field resonances; quantitation with CH_3CNH^+ reagent ion showed approximately 30% loss of signal for the same analyte of interest.

Higher field resonances can cause dissociation of the mass-selected reagent ion to form other species which then can react with the neutral analyte. The resulting CI spectra can be altered when compared to acquisition far from higher resonances. The C_3H_5^+ ion, produced from CID of the mass-selected C_2H_5^+ reagent ion, can react with analyte neutral molecules. The dominating CI processes observed with the C_2H_5^+ ion are proton transfer and adduct formation; the dominating CI processes observed with the C_3H_5^+ ion are hydride abstraction and adduct formation. Consequently, acquisition of the CI spectrum near a higher field resonance will be comprised of contributions from each of the above processes. Under non-mass selected CI conditions (as in the more common quadrupole mass spectrometers), these processes occur routinely. However, the advantage of mass-selected CI with the quadrupole ion trap allows more control of the CI process and thus the energy deposition. To correctly control the energy deposition process and to correctly interpret the resulting data, the RF level during the CI reaction needs to be free of higher-order field effects (i.e. $a_z < 0.6$ for the CI reagent ion).

Effects on Ion Motion

The frequency components of ion motion were determined via dipolar and quadrupolar resonance excitation for ions stored at various points throughout the

Mathieu stability diagram. At each location, the ion intensity was recorded as the excitation frequency was varied under constant excitation amplitude and duration, thus, generating power absorption spectra. Each absorption band corresponded either directly or indirectly to a frequency of ion motion.

In general, the dipolar resonance excitation mode produced the main absorption bands corresponding to ion frequencies at ω_z and $\Omega \pm \omega_z$; the quadrupolar resonance excitation mode produced the main absorption bands at $2\omega_z$, $2\omega_r$, $\Omega \pm 2\omega_z$, and $\Omega \pm 2\omega_r$, which corresponded to components of ion motion due ω_z , ω_r , $\Omega \pm \omega_z$, and $\Omega \pm \omega_r$. Due to the non-discriminating nature of the quadrupolar mode (i.e. absorption due to motion in both the z- and r-direction), the resulting absorption spectra are much more complex than the dipolar mode. As evidenced by the numerous absorptions observed under both modes, however, ions can be resonantly excited at several frequencies other than their secular frequencies. Ion ejection and/or dissociation, therefore, can be accomplished at any absorption frequency.

Investigations of higher-order field effects on ion motion were presented for ions stored near the $\beta_z=0$ boundary. Under dipolar resonance excitation, frequency components due to $3\omega_z$, $\Omega-3\omega_z$, and $\Omega+3\omega_z$ were identified. The magnitude of the absorptions increased with decreasing a_z value (i.e. increasing +DC). These frequency components were attributed to the influence of higher-order fields on ion motion. Storage near the $\beta_z=0$ boundary places the ions near the dodecapolar resonance line at $\beta_z=1/3$. The dodecapolar field induces odd frequencies of ion motion (Yang Wang, personal communication). The frequencies also may be

induced by contributions of hexapolar and octopolar fields. Analysis of simulated ion motion in the presence of either hexapolar or octopolar fields predicts frequency components due to $3\omega_z$, $\Omega-3\omega_z$, and $\Omega+3\omega_z$ (Franzen, 1994).

Under quadrupolar resonance excitation, no evidence for combinations of the $3\omega_z$ components were observed; however, evidence was observed for the subharmonic motion corresponding to $\omega_z/2$ as well as the frequency component of motion corresponding to the RF storage frequency, Ω . The absorption at Ω is attributed to contributions of a hexapolar field to the quadrupolar trapping field (Franzen, 1994). Similarly to all of the higher frequency components, the magnitude of the absorption due to the Ω frequency increased with increasing β_z of storage.

Investigations of higher-order field effects on ion motion were presented for ions stored along the $a_z=0$ line (i.e. 0V DC, or RF only mode). Under dipolar resonance excitation, absorptions at $\omega_z/2$, $2\omega_z$, and $3\omega_z$ were observed as well as the predicted absorptions at ω_z and $\Omega\pm\omega_z$. The magnitude of the absorptions due $\omega_z/2$, $2\omega_z$, and $3\omega_z$ decreased with increasing q_z (and thus increasing β_z). Evidence for coupled motion (i.e. $\omega_z+\omega_z$) also was observed at very low q_z values. The existence of coupled motion is due to the non-"ideal" quadrupole ion trap. Due to higher-order field effects, ion motion in each direction is not entirely de-coupled; therefore, these frequency components can be observed experimentally.

Under quadrupolar resonance excitation, ion storage near $q_z=0.80$ ($\beta_z=2/3$) resulted in very broad absorptions near 367 kHz and 750 kHz. This was the result of overlapping bands due to $2\omega_z$ and $\Omega-\omega_z$ (367 kHz) and ω_z and $\Omega-2\omega_z$ (750 kHz).

At this storage condition (and at higher q_z values), broad absorption also was observed due to the trapping frequency, Ω . Again, the frequency of motion corresponding to Ω is due to hexapolar field contributions to the quadrupolar trapping field (Franzen, 1994). Evidence for the frequency component $2\Omega-2\omega_z$ also was observed.

Investigations of higher-order field effects on ion motion were presented for ions stored near the apex ($q_z=0.78$, $a_z=0.118$) of the Mathieu stability diagram. Under dipolar resonance excitation, nearly equal absorption was observed for ω_z and $\Omega-\omega_z$. An unidentified absorption occurred immediately following the ω_z absorption band and immediately preceding the $\Omega-\omega_z$ absorption band. The source of these absorptions is unknown at this time.

Under quadrupolar resonance excitation, absorption at $2\omega_z$ was the main band in the spectrum. Nearly equal magnitudes were observed for $2\omega_z$ and $\Omega-2\omega_z$. Significant absorption at Ω was observed. As observed with the spectrum acquired at high q_z values along the $a_z=0$ (i.e. $q_z=0.87$), high β_z of storage resulted in increased absorption at Ω . Similarly, the presence of $2\Omega-2\omega_z$ also was observed for quadrupolar excitation of ions stored at the apex.

Future Work

Future studies related to the fundamental aspects of higher-order fields would involve characterization with regard to ion displacement from the center of the ion trap. Since higher-order field potentials increasingly deviate with distance from the

center of the ion trap, ion displacement enhances higher resonance effects. This aspect could be investigated with respect to helium buffer gas pressure, resonance excitation, application of a DC voltage, and ion injection.

A reduction in pressure of the helium buffer gas will result in longer times required to cool the ions towards the center. This allows more time for the ions to reside in the outer regions of the trap and, thus, experience higher-order field effects. An investigation of the influence of helium pressure on the magnitude of higher-order field effects is very difficult under static conditions. Any variation in the helium pressure also alters the efficiencies of storage and detection. Changes in these conditions make it difficult to ensure the same ion population under various helium pressures. This is critical for a direct comparison since the magnitude of the higher-order field effects is dependent on ion population.

The influence of helium pressure, however, could be successfully investigated if the detection efficiency is decoupled from the storage efficiency. This can be accomplished with a pulsed-valve introduction of helium during the detection process. Preliminary investigations suggest that the helium pressure required for detection can be decoupled from that required for trapping (James L. Stephenson, private communication). This would enable variable helium pressures during ion storage, while that employed for ion detection remains constant.

Ion displacement also could be investigated by resonance excitation. Application of a sufficiently low voltage and duration will displace the ions without a large degree of ejection or dissociation. Application of resonance excitation in

conjunction with a variable helium pressure may allow more control over the degree of ion displacement.

Ion displacement could be investigated by a "pump" and "probe" type experiment. Ion storage near the boundaries causes the amplitude of motion to increase dramatically. Application of a fast DC voltage pulse to the ring electrode can place the ions near a boundary, thus, displacing the ion from the center of the trap. At various delay times following the "pump", measurements of ion loss due to ion storage near a higher field resonance would offer insight into the influence of ion displacement.

Ion injection may provide the most sensitive method for investigating the relationship between the magnitude of higher-order field effects and ion displacement. Ion injection is very susceptible to higher field resonances due to the inherent displacement from the center of the ion trap when the ions enter the trapping field. Indeed, several groups already have reported preliminary results from these effects (Williams *et al.*, 1991b; Pedder *et al.*, 1989); however, a thorough investigation has not been performed. Injection of the $C_2H_5^+$ probe ion may provide a very sensitive tool for characterization studies.

Of particular interest with the characterization of higher-order field effects with ion injection would be conclusive identification of the influence from higher field sum resonances. Preliminary investigations suggest some influence from the octopolar resonance, $\beta_z + \beta_r = 1$, and the dodecapolar resonance, $\beta_z + 2\beta_r = 1$, during ion injection. Also of interest is the relationship between higher resonance effects during

ion injection and specie of the injected ion. Preliminary investigations reveal effects from higher resonances on injected Ar^+ ions and m/z 69 ions from the calibration compound perfluorotributylamine (PFTBA); however, higher m/z ions from PFTBA did not suffer any appreciable effects (Jon A. Jones, private communication). Valuable information could be obtained by decoupling the relationship between higher resonance effects and injected m/z ion from that of higher resonance effects and chemical structure of the injected ion.

Quadrupolar Resonance Excitation

Further investigations employing quadrupolar resonance excitation would be of interest. Since this mode traditionally has not been employed routinely, a thorough characterization would be useful. Excitation at q_z points corresponding to overlapping absorption bands (i.e. $q_z=0.65$ and 0.79) may prove to be advantageous for a number of experiments. The power absorption displayed at these points may provide a more efficient means of ion ejection or dissociation. Application of a high voltage excitation at these points may offer an alternative to the dipolar resonance excitation employed for axial modulation. Quadrupolar excitation for axial modulation may be comparable to dipolar, except that the lower q_z values could offer an efficient enhancement of the working mass range.

Endcap Electrode Spacing

Of particular interest to this researcher would be the continued characterization of the asymmetric quadrupole ion trap described in Chapter 3. A quantitative comparison of the three different electrode spacings with regard to resolution and peak shape would offer insight into the influence of higher-order fields on mass-selective instability. A comparison with regard to storage efficiency and detection efficiency for a number of ion populations would be useful. Of particular interest with the asymmetric geometry would be the comparison of the displacement of the exit endcap to that of the entrance endcap. This study could provide insight into fundamental aspects as storage and detection efficiency.

REFERENCE LIST

- Alfred, R.L.; Londry, F.A.; March, R.E. "Resonance Excitation of Ions Stored in a Quadrupole Ion Trap. Part IV. Theory of Quadrupolar Excitation," *Int. J. Mass Spectrom. Ion Processes*, 1993, 125, 171-185.
- Armitage, M.A.; Fulford, J.E.; Hoa, D.-N.; Hughes, R.J.; March, R.E. "The Application of Resonant Ion Ejection to Quadrupole Ion Storage Mass Spectrometry: a Study of Ion/Molecule Reactions in the QUISTOR," *Can. J. Chem.*, 1979, 57, 2108-2113.
- Basic, C. "Probing Trapped Ion Energies in a Quadrupole Ion Trap Mass Spectrometer," Ph.D. Dissertation, University of Florida, 1992.
- Beaty, E.C. "Calculated Electrostatic Properties of Ion Traps," *Phys. Rev. A*, 1986, 33(6), 3645-3656.
- Berberich, D.W.; Hail, M.E.; Johnson, J.V.; Yost, R.A. "Mass-selection of Reactant Ions for Chemical Ionization in Quadrupole Ion Trap and Triple Quadrupole Mass Spectrometers," *Int. J. Mass Spectrom. Ion Processes*, 1989, 94, 115-147.
- Bonner, R.F. "A Study of the Quadrupole Ion Storage Source," Ph.D. Dissertation, University of Kent, Canterbury-Kent, England, 1974.
- Bonner, R.F.; Lawson, G.; Todd, J.F.J. "Ion-Molecule Reaction Studies with a Quadrupole Ion Storage Trap," *Int. J. Mass Spectrom. Ion Phys.*, 1972, 10, 197-203.
- Bonner, R.F.; Lawson, G.; Todd, J.F.J.; March, R.E. "Ion Storage Mass Spectrometry: Applications in the Study of Ionic Processes and Chemical Ionization Reactions," *Adv. Mass Spectrom.*, 1974, 6, 377-384.
- Bonner, R.F.; March, R.E.; Durup, J. "Effect of Charge Exchange Reactions on the Motion of Ions in Three-Dimensional Quadrupole Electric Fields," *Int. J. Mass Spectrom. Ion Phys.*, 1976, 22, 17-34.
- Brodbelt, J.S.; Louris, J.N.; Cooks, R.G. "Chemical Ionization in an Ion Trap Mass Spectrometer," *Anal. Chem.*, 1987, 59, 1278-1285.

- Cameron, D.; Hemberger, P.H. "Ionization and Matrix Gas Effects Observed in High Pressure Analysis with an Ion Trap Mass Spectrometer," *Proceedings of the 38th ASMS Conference on Mass Spectrometry and Allied Topics*, Tucson, AZ, 1990, 61-62.
- Carrico, J.P. "Applications of Inhomogeneous Oscillatory Electric Fields in Ion Physics," *Dyn. Mass Spectrom.*, 1972, 3, 1-65.
- Cooks, R.G.; Kaiser, R.E. "Quadrupole Ion Trap Mass Spectrometry," *Acc. Chem. Res.*, 1990, 23, 213-219.
- Cooks, R.G.; Glush, G.L.; McLuckey, S.A.; Kaiser, R.E., Jr. "Ion Trap Mass Spectrometry," *Chem. Eng. News*, 1991, 69, 26-41.
- Dawson, P.H. *Quadrupole Mass Spectrometry and Its Applications*, Elsevier Scientific Publishing Co., Amsterdam, 1976.
- Dawson, P.H.; Hedman, J.; Whetten, N.R. "A Simple Mass Spectrometer," *Rev. Sci. Instrum.*, 1969, 40, 1444-1450.
- Dawson, P.H.; Whetten, N.R. "Ion Storage in Three-Dimensional, Rotationally Symmetric, Quadrupole Fields. I. Theoretical Treatment," *J. Vac. Sci. Technol.*, 1968a, 5(1), 1-10.
- Dawson, P.H.; Whetten, N.R. "Ion Storage in Three-Dimensional, Rotationally Symmetric, Quadrupole Fields. II. A Sensitive Mass Spectrometer," *J. Vac. Sci. Technol.*, 1968b, 5(1), 11-18.
- Dawson, P.H.; Whetten, N.R. "Some Causes of Poor Peak Shapes in Quadrupole Field Mass Analyzers," *J. Vac. Sci. Technol.*, 1969a, 6(1), 100-103.
- Dawson, P.H.; Whetten, N.R. "Non-Linear Resonances in Quadrupole Mass Spectrometers Due to Imperfect Fields I. The Quadrupole Ion Trap," *Int. J. Mass Spectrom. Ion Phys.*, 1969b, 2, 45-59.
- Dawson, P.H.; Whetten, N.R. "Three-dimensional Mass Spectrometer and Gauge," *British Patent*, 1971, 1225272.
- Dehmelt, H.G. "Radiofrequency Spectroscopy of Stored Ions I: Storage," *Adv. At. Mol. Phys.*, 1967, 3, 53-72.
- Dehmelt, H.G. "Radiofrequency Spectroscopy of Stored Ions II: Spectroscopy," *Adv. At. Mol. Phys.*, 1969, 5, 109-154.

- Eades, D.M.; Yates, N.A.; Yost, R.A. "Mass-Selective Ion Accumulation in a Quadrupole Ion Trap," *Proceedings of the 39th ASMS Conference On Mass Spectrometry and Allied Topics*, Nashville, TN, 1991, 1491-1492.
- Fischer, E. "Three-dimensional Stabilization of Charge Carriers in a Quadrupole Field," *Z. Phys.*, 1959, 156, 1-26.
- Franzen, J. "Simulation Study of an Ion Cage with Superimposed Multipole Fields," *Int. J. Mass Spectrom. Ion Processes*, 1991, 106, 63-78.
- Franzen, J. "The Non-linear Ion Trap. Part 4. Mass Selective Instability Scan With Multipole Superposition," *Int. J. Mass Spectrom. Ion Processes*, 1993, 125, 165-170.
- Franzen, J. "The Non-Linear Ion Trap (V) Nature of Non-Linear Resonances and Resonant Ion Ejection," *Int. J. Mass Spectrom. Ion Processes*, 1994, (in press).
- Franzen, J.; Gagling, R.-H.; Heinen, G.; Weiss, G. "Method of Mass Analyzing a Sample by Use of a Quistor," *United States Patent*, 1989, 4882484.
- Fulford, J.E.; Hoa, D.-N.; Hughes, R.J.; March, R.E.; Bonner, R.F.; Wong, G.J. "Radio-Frequency Mass Selective Excitation and Resonant Ejection of Ions in a Three-Dimensional Quadrupole Ion Trap," *J. Vac. Sci. Technol.*, 1980, 17, 829-835.
- Fulford, J.E.; March, R.E. "A New Mode of Operation for the Three-Dimensional Quadrupole Ion Store (QUISTOR): The Selective Ion Reactor," *Int. J. Mass Spectrom. Ion Phys.*, 1978, 26, 155-162.
- Griffiths, I.W.; Heesterman, P.J.L. "Quadrupole Ion Store (QUISTOR) Mass Spectrometry," *Int. J. Mass Spectrom. Ion Processes*, 1990, 99, 79-98.
- Gronowska, J.; Paradisi, C.; Traldi, P.; Vettori, U. "A Study of Relevant Parameters in Collisional-activation of Ions in the Ion-trap Mass Spectrometer," *Rapid Commun. Mass Spectrom.*, 1990, 4, 306-313.
- Guidugli, F.; Traldi, P. "A Phenomenological Description of a Black Hole for Collisionally Induced Decomposition Products in Ion-trap Mass Spectrometry," *Rapid Commun. Mass Spectrom.*, 1991, 5, 343-348.
- Guidugli, F.; Traldi, P.; Franklin, A.M.; Langford, M.L.; Murrell, J.; Todd, J.F.J. "Further Thoughts on the Occurrence of 'Black Holes' in Ion-trap Mass Spectrometry," *Rapid Commun. Mass Spectrom.*, 1992, 6, 229-231.

- Harrison, A.G. *Chemical Ionization Mass Spectrometry*, CRC Press, Boca Raton, 1992, Ed. 2.
- Harrison, A.G.; Lin, M.S. "Energy Dependence of the Fragmentation of the n-Butylbenzene Molecular Ion," *Int. J. Mass Spectrom. Ion Phys.*, 1983, 51, 353-356.
- Johnson, J.V.; Pedder, R.E.; Kleintop, B.L.; Yost, R.A. "Resonant Excitation for CID in the Quadrupole Ion Trap: Energetics and Efficiencies," *Proceedings of the 38th ASMS Conference on Mass Spectrometry and Allied Topics*, Tucson, AZ, 1990a, 1130-1131.
- Johnson, J.V.; Pedder, R.E.; Yost, R.A. "The Stretched Quadrupole Ion Trap: Implications for the Mathieu a_n and q_n Parameters and Experimental Mapping of the Stability Diagram," *Rapid Commun. Mass Spectrom.*, 1992, 6, 760-764.
- Johnson, J.V.; Yost, R.A.; Kelley, P.E.; Bradford, D.C. "Tandem-in-space and Tandem-in-time Mass Spectrometry: Triple Quadrupoles and Quadrupole Ion Traps," *Anal. Chem.*, 1990b, 62, 2162-2172.
- Julian, R.K.; Cooks, R.G. "Broad-Band Excitation in the Quadrupole Ion Trap Mass Spectrometer Using Shaped Pulses Created with the Inverse Fourier Transform," *Anal. Chem.*, 1993, 65, 1827-1833.
- Julian, R.K.; Reiser, H.-P.; Cooks, R.G. "Large Scale Simulation of Resonant Ejection in the Quadrupole Ion Trap Mass Spectrometer," *Proceedings of the 40th ASMS Conference on Mass Spectrometry and Allied Topics*, Washington, DC, 1992, 1777-1778.
- Jungmann, K.; Hoffnagle, J.; DeVoe, R.G.; Brewer, R.G. "Collective Oscillations of Stored Ions," *Physical Review A*, 1987, 36, 3451-3454.
- Kaiser, R.E., Jr.; Cooks, R.G.; Stafford, G.C., Jr.; Syka, J.E.P.; Hemberger, P.H. "Operation of a Quadrupole Ion Trap to Achieve High Mass/Charge Ratios," *Int. J. Mass Spectrom. Ion Processes*, 1991, 106, 79-115.
- Kelley, P.E.; Hoekman, D.J.; Bradshaw, S.C. "A New Method of Operation for the Quadrupole Ion Trap," *Proceedings of the 41st ASMS Conference on Mass Spectrometry and Allied Topics*, San Francisco, CA, 1993, 453a-453b.
- Kelley, P.E.; Stafford, G.C.; Syka, J.E.P.; Reynolds, W.E.; Louris, J.N.; Amy, J.W.; Todd, J.F.J. "New Advances in the Operation of the Ion Trap Mass Spectrometer," *Proceedings of the 33rd ASMS Conference on Mass Spectrometry and Allied Topics*, San Diego, CA, 1985, 707-708.

- Kelley, P.E.; Stafford, G.C.; Syka, J.E.P.; Reynolds, W.E.; Louris, J.N.; Todd, J.F.J. "New Advances in the Operation of the Ion Trap Mass Spectrometer," *Adv. Mass Spectrom.*, **1986a**, 869-870.
- Kelley, P.E.; Syka, J.E.P.; Ceja, P.C.; Stafford, G.C.; Louris, J.N.; Grutzmacher, H.F.; Kuck, D.; Todd, J.F.J. "Continuing Developments of Advanced Ion Trap Instrumentation," *Proceedings of the 34th ASMS Conference on Mass Spectrometry and Allied Topics*, Cincinnati, OH, **1986b**, 963-964.
- Knight, R.D. "The General Form of the Quadrupole Ion Trap Potential," *Int. J. Mass Spectrom. Ion Phys.*, **1983**, 51, 127-131.
- Lammert, S.A.; Clevon, C.D.; Cooks, R.G. "Evidence for 'Black Holes' During EI in a Quadrupole Ion Trap Mass Spectrometer," *Proceedings of the 41st ASMS Conference on Mass Spectrometry and Allied Topics*, San Francisco, CA, **1993**, 473a-473b.
- Lawson, G.; Bonner, R.F.; Mather, R.E.; Todd, J.F.J.; March, R.E. "Quadrupole Ion Store (QUISTOR). Part I. Ion-Molecule Reactions in Methane, Water, and Ammonia," *J. Chem. Soc., Faraday Trans. I*, **1976**, 73, 545-557.
- Louris, J.N.; Amy, J.W.; Ridley, T.Y.; Cooks, R.G. "Injection of Ions Into a Quadrupole Ion Trap Mass Spectrometer," *Int. J. Mass Spectrom. Ion Processes*, **1989**, 88, 97-111.
- Louris, J.N.; Cooks, R.G.; Syka, J.E.P.; Kelley, P.E.; Stafford, G.C., Jr.; Todd, J.F.J. "Instrumentation, Applications, and Energy Deposition in Quadrupole Ion-Trap Tandem Mass Spectrometry," *Anal. Chem.*, **1987**, 59, 1677-1685.
- Louris, J.; Schwartz, J.C.; Stafford, G.C.; Syka, J.E.P.; Taylor, D. "The Paul Ion Trap Mass Selective Instability Scan: Trap Geometry and Resolution," *Proceedings of the 40th ASMS Conference on Mass Spectrometry and Allied Topics*, Washington, DC, **1992**, 1003-1004.
- March, R.E. "Ion Trap Mass Spectrometry," *Int. J. Mass Spectrom. Ion Processes*, **1992**, 118/119, 71-135.
- March, R.E.; Hughes, R.J. *Quadrupole Storage Mass Spectrometry*, John Wiley & Sons, New York, **1989**.
- March, R.E.; Londry, F.A.; Alfred, R.L.; Franklin, A.M.; Todd, J.F.J. "Mass-Selective Isolation of Ions Stored in a Quadrupole Ion Trap. A Simulation Study," *Int. J. Mass Spectrom. Ion Processes*, **1992**, 112, 247-271.

- March, R.E.; Londry, F.A.; Alfred, R.L.; Todd, J.F.J.; Penman, A.D.; Vedel, F.; Vedel, M. "Resonance Excitation of Ions Stored in a Quadrupole Ion Trap. Part 3. Introduction to the Field Interpolation Simulation Method," *Int. J. Mass Spectrom. Ion Processes*, **1991**, 110, 159-178.
- March, R.E.; McMahon, A.W.; Allinson, E.T.; Londry, F.A.; Alfred, R.L.; Todd, J.F.J.; Vedel, F. "Resonance Excitation of Ions Stored in a Quadrupole Ion Trap. Part 2. Further Simulation Studies," *Int. J. Mass Spectrom. Ion Processes*, **1990**, 99, 109-124.
- March, R.E.; McMahon, A.W.; Londry, F.A.; Alfred, R.L.; Todd, J.F.J.; Vedel, F. "Resonance Excitation of Ions Stored in a Quadrupole Ion Trap. Part 1. A Simulation Study," *Int. J. Mass Spectrom. Ion Processes*, **1989**, 95, 119-156.
- March, R.E.; Todd, J.F.J. *Applications of Quadrupole Ion Trap Mass Spectrometry*, **1994**, in press.
- Mather, R.E.; Todd, J.F.J.; Lawson, G.; Bakker, J.M.B. "The Quadrupole Ion Storage Trap (QUISTOR) as a Low Pressure Chemical Ionization Source for a Magnetic Sector Mass Spectrometer," *Int. J. Mass Spectrom. Ion Phys.*, **1978**, 28, 347-364.
- McLachlan, N.W. *Theory and Applications of Mathieu Functions*, Clarendon, Oxford, **1947**.
- McLuckey, S.A.; Goeringer, D.E.; Glish, G.L. "Collisional Activation with Random Noise in Ion Trap Mass Spectrometry," *Anal. Chem.*, **1992**, 64, 1455-1460.
- Morand, K.L.; Lammert, S.A.; Cooks, R.G. "Concerning 'Black Holes' in Ion-trap Mass Spectrometry," *Rapid Commun. Mass Spectrom.*, **1991**, 5, 491.
- Nourse, B.D.; Cooks, R.G. "Aspects of Recent Developments in Ion-trap Mass Spectrometry," *Anal. Chim. Acta*, **1990**, 228, 1-21.
- Paradisi, C.; Todd, J.F.J.; Traldi, P.; Vettori, U. "Boundary Effects and Collisional Activation in a Quadrupole Ion Trap," *Org. Mass Spectrom.*, **1992**, 27, 251-254.
- Paul, W.; Reinhard, H.P.; Zahn, U. "The Electric Mass Filter as a Mass Spectrometer and Isotopic Separator," *Z. Phys.*, **1958**, 152(2), 143-182.
- Paul, W.; Steinwedel, H. "A New Mass Spectrometer Without a Magnetic Field," *Z. Naturforsch.*, **1953**, 8, 448-450.

- Paul, W.; Steinwedel, H. "Apparatus for Separating Charged Particles of Different Specific Charges," *German Patent*, 1956, 944900.
- Pedder, R.E.; "Fundamental Studies in Quadrupole Ion Trap Mass Spectrometry," PH.D. Dissertation, University of Florida, 1992.
- Pedder, R.E.; Yost, R.A. "Computer Simulation of Ion Trajectories in a Quadrupole Ion Trap Mass Spectrometer," *Proceedings of the 36th ASMS Conference on Mass Spectrometry and Allied Topics*, San Francisco, CA, 1988, 632-633.
- Pedder, R.E.; Yost, R.A.; Weber-Grabau, M. "Injection of Ions into a Quadrupole Ion Trap from a Chemical Ionization Source using a DC Quadrupole Deflector," *Proceedings of the 37th ASMS Conference on Mass Spectrometry and Allied Topics*, Miami Beach, FL, 1989, 468-469.
- Post, R.F.; Henrich, L., *Univ. California Rad. Lab. Report*, Berkeley, CA, 1953, UCRL-2209.
- Reiser, H.-P.; Julian Jr., R.K.; Cooks, R.G. "A Versatile Method of Simulation of the Operation of Ion Trap Mass Spectrometers," *Int. J. Mass Spectrom. Ion Processes*, 1992, 121, 49-63.
- Resnick, R.; Halliday, D. *Physics, Part I*, John Wiley & Sons, Inc., New York, 1966.
- Rettinghaus, V., von G. "The Detection of Low Partial Pressures by Means of the Ion Cage," *Z. Angew. Phys.*, 1967, 22, 321-326.
- Schwartz, J.C.; Cooks, R.G. "Quantitative Evaluation of Ion Injection into a Quadrupole Ion Trap," *Proceedings of the 36th ASMS Conference on Mass Spectrometry and Allied Topics*, San Francisco, CA, 1988, 634-635.
- Schwartz, J.C.; Jardine, I. "High Resolution Parent-ion Selection/Isolation Using a Quadrupole Ion-trap Mass Spectrometer," *Rapid Commun. Mass Spectrom.*, 1992, 6, 313-317.
- Schwartz, J.C.; Syka, J.E.P.; Jardine, I. "High Resolution on a Quadrupole Ion Trap Mass Spectrometer," *J. Am. Soc. Mass Spectrom.*, 1991, 2, 198-204.
- Sheretov, E.P.; Zenkin, V.A.; Samodurov, V.F. "Effect of Space Charge on a Three-Dimensional Storage Quadrupole Mass Spectrometer," *Sov. Phys. Tech. Phys.*, 1973, 18, 282-283.
- Stafford, G.C.; Kelley, P.E.; Bradford, D.C. "Advanced Ion Trap Technology in an Economical Detector for GC," *Am. Lab.*, 1983a, 51-57.

- Stafford, G.C.; Kelley, P.E.; Reynolds, W.E.; Syka, J.E.P. "Recent Improvements in Ion Trap Technology," *Proceedings of the 31st ASMS Conference on Mass Spectrometry and Allied Topics*, Boston, MA, 1983b, 48-49.
- Stafford, G.C.; Kelley, P.E.; Syka, J.E.P.; Reynolds, W.E.; Todd, J.F.J. "Recent Improvements in and Analytical Applications of Advanced Ion-trap Technology," *Int. J. Mass Spectrom. Ion Processes*, 1984, 60, 85-98.
- Strife, R.J.; Simms, J.R.; Lacey, M.P. "Combined Capillary Gas Chromatography/Ion Trap Mass Spectrometry Quantitative Methods Using Labeled or Unlabeled Internal Standards," *J. Am. Soc. Mass Spectrom.*, 1990, 1, 265-271.
- Todd, J.F.J. "Ion Trap Mass Spectrometer - Past, Present, and Future (?)," *Mass. Spectrom. Rev.*, 1991, 10, 3-52.
- Todd, J.F.J.; Bexon, J.J.; Smith, R.D.; Weber-Grabau, M.; Kelley, P.E.; Syka, J.E.P.; Stafford, G.C.; Bradshaw, S.C. "The Use of DC Fields to Enhance the Performance of the Ion Trap Mass Spectrometer," *Proceedings of the 16th Meeting of the British Mass Spectrometry Society*, York, U.K., 1987, 206-209.
- Todd, J.F.J.; Bonner, R.F.; Lawson, G. "A Low-pressure Chemical Ionization Source: An Application of a Novel Type of Ion Storage Mass Spectrometer," *J. Chem. Soc. Chem. Commun.*, 1972, 1179-1180.
- Todd, J.F.J.; Penman, A.D.; Smith, R.D. "Some Alternative Scanning Methods for the Ion Trap Mass Spectrometer," *Int. J. Mass Spectrom. Ion Processes*, 1991, 106, 117-135.
- Todd, J.F.J.; Waldren, R.M.; Mather, R.E.; Lawson, G. "On The Relative Efficiencies of Confinement of Ar^+ and Ar^{+2} Ions in a Quadrupole Ion Storage Trap (Quistor)," *Int. J. Mass Spectrom. Ion Phys.*, 1978, 28, 141-151.
- Tucker, D.B.; Hameister, C.H.; Bradshaw, S.C.; Hoekman, D.J.; Weber-Grabau, M. "The Application of Novel Ion Trap Scan Modes for High Sensitivity GC/MS," *Proceedings of the 36th ASMS Conference on Mass Spectrometry and Allied Topics*, San Francisco, CA, 1988, 628-629.
- Vedel, F. "On the Dynamics and Energy of Ion Clouds Stored in an R.F. Quadrupole Trap," *Int. J. Mass Spectrom. Ion Processes*, 1991, 106, 33-61.
- Vedel, F.; Vedel, M.; March, R.E. "New Schemes for Resonant Ejection in R.F. Quadrupolar Ion Traps," *Int. J. Mass Spectrom. Ion Processes*, 1990, 99, 125-138.

- Vedel, F.; Vedel, M.; March, R.E. "A Sensitive Method for the Detection of Stored Ions by Resonant Ejection Using a Wide-Band Signal," *Int. J. Mass Spectrom. Ion Processes*, **1991**, 108, R11-R20.
- von Busch, F.; Paul, W. "Uber nichtlineare Resonanzen in elektrischen Massenfilter als folge Feldfehlern," *Z. Physik*, **1961**, 164, 588-595.
- Wang, Y. "A Fundamental Study of Magnetical and Electrical Ion Traps," Ph.D. Dissertation, Bremen, **1992**.
- Wang, Y.; Franzen, J.; Wanczek, K.P. "The Non-Linear Resonance Ion Trap. Part 2. A General Theoretical Analysis," *Int. J. Mass Spectrom. Ion Processes*, **1993**, 124, 125-144.
- Wang, Y.; Wanczek, K.P. "Generation of an Exact Three-dimensional Quadrupole Electric Field and Superposition of a Homogeneous Electric Field Within a Common Closed Boundary with Application to Mass Spectrometry," *J. Chem. Phys.*, **1993**, 98, 2647-2652.
- Weber-Grabau, M.; Kelley, P.E.; Bradshaw, S.C.; Hoekman, D.J. "Advances in MS/MS Analysis with the Ion Trap Mass Spectrometer," *Proceedings of the 36th ASMS Conference on Mass Spectrometry and Allied Topics*, San Francisco, CA, **1988**, 1106-1107.
- Weber-Grabau, M.; Kelley, P.E.; Syka, J.E.P.; Bradshaw, S.C.; Brodbelt, J.S. "Improved Ion Trap Performance With New CI and MS/MS Scan Functions," *Proceedings of the 35th ASMS Conference on Mass Spectrometry and Allied Topics*, Denver, CO, **1987**, 773-774.
- Williams, J.D.; Cox, K.; Morand, K.L.; Cooks, R.G.; Julian, R.K., Jr. "High Mass-Resolution using a Quadrupole Ion Trap Mass Spectrometer," *Proceedings of the 39th ASMS Conference On Mass Spectrometry and Allied Topics*, Nashville, TN, **1991a**, 1481-1482.
- Williams, J.D.; Reiser, H.-P.; Kaiser, R.E.; Cooks, R.G. "Resonance effects during ion injection into an ion trap mass spectrometer," *Int. J. Mass Spectrom. Ion Processes*, **1991b**, 108, 199-219.
- Wuerker, R.F.; Shelton, H.; Langmuir, R.V. "Electrodynamic Containment of Charged Particles," *J. Appl. Physics*, **1959**, 30(3), 342-349.
- Yates, N.A.; Griffin, T.P.; Yost, R.A.; Borum, P.R. "A Novel Benchtop Ion Trap Mass Spectrometer for GC/MS/MS," *Proceedings of the 41st ASMS Conference on Mass Spectrometry and Allied Topics*, San Francisco, CA, **1993**, 444a-444b.


- Yates, N.A.; Yost, R.A.; Bradshaw, S.C.; Tucker, D.B. "A Comparative Study of Selective Mass Storage and Two-step Isolation in the Quadrupole Ion Trap," *Proceedings of the 39th ASMS Conference On Mass Spectrometry and Allied Topics*, Nashville, TN, **1991a**, 1489-1490.
- Yates, N.A.; Yost, R.A.; Bradshaw, S.C.; Tucker, D.B. "Resonant Excitation for GC/MS/MS in the Quadrupole Ion Trap via Frequency Assignment Pre-scans and Broadband Excitation," *Proceedings of the 39th ASMS Conference On Mass Spectrometry and Allied Topics*, Nashville, TN, **1991b**, 132-133.

BIOGRAPHICAL SKETCH


Donald M. Eades was born in Springfield, Illinois, on November 10, 1963, to Richard E. and Mary P. Eades. After graduating from Buffalo Tri-City High School in 1981, he attended Lincoln Land Community College and then went on to Sangamon State University in Springfield, Illinois, where he completed his Bachelor of Science degree in May 1986. During the following three years, he worked as a medical research technician at Washington University Medical School in St. Louis, Missouri.

In August 1989 he moved to Gainesville, Florida, to pursue his doctoral studies in chemistry with the emphasis on analytical mass spectrometry at the University of Florida under the supervision of Dr. Richard A. Yost. Upon completion of his graduate work, he will begin working somewhere on the west coast.

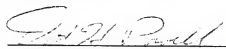
I certify that I have read this study and that in my opinion it conforms to acceptable standards of scholarly presentation and is fully adequate, in scope and quality, as a dissertation for the degree of Doctor of Philosophy.


Richard A. Yost, Chair
Professor of Chemistry

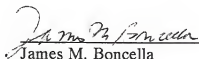
I certify that I have read this study and that in my opinion it conforms to acceptable standards of scholarly presentation and is fully adequate, in scope and quality, as a dissertation for the degree of Doctor of Philosophy.


Willard W. Harrison
Professor of Chemistry

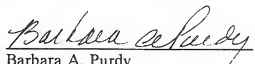
I certify that I have read this study and that in my opinion it conforms to acceptable standards of scholarly presentation and is fully adequate, in scope and quality, as a dissertation for the degree of Doctor of Philosophy.


David H. Powell
Associate Scientist of Chemistry

I certify that I have read this study and that in my opinion it conforms to acceptable standards of scholarly presentation and is fully adequate, in scope and quality, as a dissertation for the degree of Doctor of Philosophy.


James M. Boncella
Associate Professor of Chemistry

I certify that I have read this study and that in my opinion it conforms to acceptable standards of scholarly presentation and is fully adequate, in scope and quality, as a dissertation for the degree of Doctor of Philosophy.


Barbara A. Purdy
Professor Emerita of Anthropology

This dissertation was submitted to the Graduate Faculty of the Department of Chemistry in the College of Liberal Arts and Sciences and to the Graduate School and was accepted as partial fulfillment of the requirements for the degree of Doctor of Philosophy.

April 1994

Dean, Graduate School